Hfq CLASH uncovers sRNA-target interaction networks linked to nutrient availability adaptation

Hfq CLASH uncovers sRNA-target interaction networks linked to nutrient availability adaptation

Ira A. Iosub[1], Rob W. van Nues[2], Stuart McKellar[1], Karen J. Nieken[2], Marta Marchioretto[3], Brandon Sy[4], Jai J. Tree[4], Gabriella Viero[3] and Sander Granneman[1*]

Affiliations:

[1]Centre for Synthetic and Systems Biology, University of Edinburgh, Edinburgh EH9 3BF, UK.

[2]Institute of Cell Biology, University of Edinburgh, Edinburgh EH9 3FF, UK.

[3]Institute of Biophysics, CNR Unit at Trento, Italy.

[4]School of Biotechnology and Biomolecular Sciences, University of New South Wales, Sydney 2052, NSW, Australia.

*To whom correspondence should be addressed:
Sander Granneman
e-mail: Sander.Granneman@ed.ac.uk
Tel: +44 131 6519082

Abstract

By shaping gene expression profiles, small RNAs (sRNAs) enable bacteria to efficiently adapt to changes in their environment. To better understand how *Escherichia coli* acclimatizes to nutrient availability, we performed UV cross-linking, ligation and sequencing of hybrids (CLASH) to uncover Hfq-associated RNA-RNA interactions at specific growth stages. We demonstrate that Hfq CLASH robustly captures *bona fide* RNA-RNA interactions identified hundreds of novel sRNA base-pairing interactions, including many sRNA-sRNA interactions and involving 3'UTR-derived sRNAs. We rediscovered known and identified novel sRNA seed sequences. The sRNA-mRNA interactions identified by CLASH have strong base-pairing potential and are highly enriched for complementary sequence motifs, even those supported by only a few reads. Yet, steady state levels of most mRNA targets were not significantly affected upon over-expression of the sRNA regulator. Our results reinforce the idea that the reproducibility of the interaction, not base-pairing potential, is a stronger predictor for a regulatory outcome.

Microorganisms are renowned for their ability to adapt to environmental changes by rapidly rewiring their gene expression program. These responses are mediated through integrated transcriptional and post-transcriptional networks. Transcriptional control dictates which genes are expressed (Balleza et al., 2009; Martínez-Antonio et al., 2008) and is well-characterised in *Escherichia coli*. Post-transcriptional regulation is key for controlling adaptive responses. By using riboregulators and RNA-binding proteins (RBPs), cells can efficiently integrate multiple pathways and incorporate additional signals into regulatory circuits. *E. coli* employs many post-transcriptional regulators, including small regulatory RNAs (sRNAs (Waters and Storz, 2009)), *cis*-acting RNAs (Kortmann and Narberhaus, 2012), and RNA binding proteins (RBPs) (Holmqvist and Vogel, 2018). The sRNAs are the largest class of bacterial regulators, working in tandem with RBPs to regulate their RNA targets (Storz et al., 2011; Waters and Storz, 2009). By base-pairing with their targets, small RNAs can repress or stimulate translation and transcription elongation and control the stability of transcripts (Sedlyarova et al., 2016; Updegrove et al., 2016; Vogel and Luisi, 2011; Waters and Storz, 2009)

Base-pairing interactions are often mediated by RNA chaperones such as Hfq and ProQ, which help to anneal or stabilize the sRNA and sRNA-target duplex (Melamed et al., 2020, 2016; Smirnov et al., 2017, 2016; Updegrove et al., 2016). Although Hfq is most frequently mentioned in association with sRNA-mediated regulation, it can also control gene expression independently of sRNAs in response to environmental changes (Salvail et al., 2013; Sonnleitner and Bläsi, 2014). In *Pseudomonas aeruginosa,* Hfq directly binds to mRNAs to repress translation in response to changes in nutrient availability, which relies on a protein co-factor Crc that acts cooperatively with Hfq to inhibit translation (Pei et al., 2019; Sonnleitner and Bläsi, 2014).

During growth in rich media, *E. coli* are exposed to continuously changing conditions, such as fluctuations in nutrient availability, pH and osmolarity. Consequently, *E. coli* elicit complex responses that result in physiological and behavioural changes such as envelope composition remodelling, quorum sensing, nutrient scavenging, swarming and biofilm formation. Even subtle changes in the growth conditions can trigger rapid adaptive responses.

Accordingly, each stage of the growth curve is characterised by different physiological states driven by the activation of different transcriptional and post-transcriptional networks. Moreover, growth phase dependency of virulence and pathogenic behaviour has been demonstrated in both Gram-positive and Gram-negative bacteria. In some cases a particular growth stage is non-permissive for the induction of virulence (Mäder et al., 2016; Mouali et al., 2018). Although the exponential and stationary phases have been characterised in detail (Navarro Llorens et al., 2010; Pletnev et al., 2015), little is known about the transition

between these two phases. During this transition, the cell population starts to scavenge alternative carbon sources, which requires rapid remodelling of their transcriptome (Baev et al., 2006a, 2006b; Sezonov et al., 2007).

To understand sRNA-mediated adaptive responses, detailed knowledge of the underlying post-transcriptional circuits is required. In *E. coli*, hundreds of sRNAs have been discovered, and only a small fraction of these have been characterised. A key step to unravel the roles of sRNAs in regulating adaptive responses is to identify their target mRNAs. To tackle this at genome-wide level, high-throughput methods have been developed to uncover sRNA base-pairing interactions (Han et al., 2016; Hör et al., 2018; Hör and Vogel, 2017; Lalaouna et al., 2015a; Melamed et al., 2016; Waters et al., 2017).

To unravel sRNA base-pairing interactions taking place during the entry into stationary phase, we applied UV cross-linking, ligation and sequencing of hybrids (CLASH) (Helwak et al., 2013; Kudla et al., 2011) to *E. coli*. Firstly, we demonstrate that the highly stringent purification steps make CLASH a robust method for direct mapping of Hfq-mediated sRNA base-pairing interactions in *E. coli*. This enabled us to significantly expand on the sRNA base-pairing interactions found by RNase E CLASH (Waters et al., 2017) and RIL-seq (Melamed et al., 2016). Additionally, we identified a plethora of sRNA-sRNA interactions and potentially novel 3'UTR-derived sRNAs, confirming that this class of sRNAs is highly prevalent (Chao et al., 2012, 2017; Chao and Vogel, 2016; Miyakoshi et al., 2015a). The sRNA-mRNA interactions identified by CLASH have a high base-pairing potential and are strongly enriched for complementary sequence motifs, even those supported by only a few chimeric reads. We rediscovered known and identified novel sRNA seed sequences, implying they represent genuine *in vivo* interactions. However, in many cases, over-expression of the sRNA did not significantly impact the steady state levels of putative mRNA targets. Although base-pairing potential is important, our results reinforce the notion that reproducibly detected interactions, are more likely to impact target steady-state levels (Faigenbaum-Romm et al., 2020).

Results

Hfq CLASH in *E. coli.*

To unravel the post-transcriptional networks that underlie the transition between exponential and stationary growth phases in *E. coli*, we performed CLASH (Helwak et al., 2013; Kudla et al., 2011) using Hfq as bait (Figure 1A). To generate high quality Hfq CLASH data, we made a number of improvements to the original protocol used for RNase E CLASH (Waters et al., 2017). Our Hfq CLASH protocol has several advantages over the related RIL-seq method (see Materials and Methods and Discussion). As negative controls, replicate

CLASH experiments were performed on the untagged parental strain. When combined, the control samples had ~10 times less single-mapping reads and contained only 297 unique chimeric reads, compared to the over 50,000 chimeras identified in the tagged Hfq data. This result demonstrates that the CLASH purification method produced very low background levels.

Cell samples from seven different optical densities were subjected to Hfq CLASH. Based on the growth curve analysis shown in Figure 1B, we categorized OD_{600} densities 0.4 and 0.8 as exponential growth phase, 1.2, 1.8, 2.4 as the transition phase from exponential to stationary, and 3.0 and 4.0 as early stationary phase. To complement the CLASH data, RNA-seq and Western blot analyses were performed on UV-irradiated cells to quantify steady state RNA and Hfq protein levels, respectively (Figure 1C, Figure 1 - figure supplement 1). Western blot analyses revealed that Hfq levels were very modestly increased during growth (Figure 1 - figure supplement 1A-B). To determine the cross-linking efficiency, Hfq-RNA complexes immobilized on nickel beads were radiolabelled, resolved on NuPAGE gels and analysed by autoradiography. The data show that the recovery of Hfq and radioactive signal was comparable at each optical density studied (Figure 1 - figure supplement 1C). Comparison of normalized read counts of replicate CLASH and RNA-seq experiments showed that the results were highly reproducible (Figure 1 - figure supplement 2). Meta-analyses of the Hfq CLASH sequencing data revealed that the distribution of Hfq binding across mRNAs was very similar at each growth stage. We observed the expected Hfq enrichment at the 5'UTRs and at the 3'UTRs at each growth stage (Figure 1 - figure supplement 3A and 3B for examples). After identifying significantly enriched Hfq binding peaks (FDR <= 0.05; see Methods for details) we used the genomic coordinates of these peaks to search for Hfq binding motifs in mRNAs. The most enriched k-mer included poly-U stretches (Figure 1 - figure supplement 3C) that resemble the poly-U tracts characteristic to Rho-independent terminators found at the end of many bacterial transcripts (Wilson and Hippel, 1995), and confirms the motif uncovered in CLIP-seq studies in *Salmonella* (Holmqvist et al., 2016).

Hfq CLASH robustly detects RNA-RNA interactions.

To get the complete catalogue of the RNA-RNA interactions captured by Hfq CLASH, we merged the data from the two biological replicates of CLASH growth phase experiments (Supplementary File 1). Overlapping paired-end reads were merged and unique chimeric reads were identified using the hyb pipeline (Travis et al., 2013). To select RNA-RNA interactions for further studies, we applied a probabilistic analysis pipeline previously used for detecting RNA-RNA interactions in human cells (Sharma et al., 2016) and adapted for the analyses of RNase E CLASH data (Waters et al., 2017). This pipeline tests the likelihood

that observed chimeras could have formed spuriously. Strikingly, 87% of the chimeric reads had a Benjamini-Hochberg adjusted p-value of 0.05 or less, indicating that it is highly unlikely that these chimeras were generated by random ligation of RNA molecules. A complete overview of statistically significantly enriched chimeras is provided in Supplementary File 2.

We next analysed the distribution of combinations of transcript classes found in the statistically filtered chimeric reads. Hfq CLASH identified over unique 2000 sRNA-mRNA target interactions represented by 18783 chimeras (Figure 2A; Supplementary File 3). These chimeras included sRNAs derived from 3'-UTRs and were the most frequently recovered Hfq-mediated interaction type (65.7%; Figure 2A). We suspect that this number might be higher, as 1.7% of the chimeras contained fragments of sRNAs fused to short sequences from intergenic regions (Figure 2A). Manual inspection of several of these indicated that some of the intergenic sequences were located near genes for which the UTRs were either unannotated or too short. Interestingly, 10.5% of the intermolecular chimeras contained fragments from two different mRNAs (Figure 2A). Based on analyses presented below, we speculate that many of these could be interactions between novel 3'UTR-derived sRNAs and mRNA substrates. Around 1% of the chimeras represented sRNA-tRNA interactions. In *E. coli* external transcribed spacers of tRNAs can base-pair with sRNAs to absorb transcriptional noise (Lalaouna et al., 2015a). In many cases the predicted base-pairing interactions between the tRNA and sRNA halves in chimeras are quite extensive (Supplementary File 2). Hence, it is possible that this group contains biologically relevant interactions.

Most of the interactions, including sRNA-mRNA interactions, were identified in the transition phase (Figure 2C-D). The mRNA fragments found in chimeric reads were strongly enriched in 5'UTRs peaking near the translational start codon (Figure 2E-F), consistent with the canonical mode of translational inhibition by sRNAs (Bouvier et al., 2008). Enrichment was also found in 3'UTRs of mRNAs, although to a lesser extent compared to 5'UTRs (Figure 2E). Motif analyses revealed a distinct sequence preference in 5'UTR and 3'UTR binding sites (Figure 2G-H, Supplementary Files 8-9). The motifs enriched in the 5'UTR chimeric fragments are more consistent with Hfq binding to Shine Dalgarno-like $(ARN)_n$ sequences (Tree et al., 2014; Supplementary File 8) and U-tracts, whereas the 3'UTR-containing chimera consensus motif corresponds to poly-U transcription termination sites (Figure 2G-H and Supplementary File 9).

To further test the quality of our CLASH data, we focussed on the 24 experimentally verified sRNA-mRNA interactions recovered in our data, which we used as a "ground truth" for known interactions. Strikingly, 92% of the sRNAs in our chimeras with experimentally

verified interactions were fused to the cognate mRNA fragments (Figure 2 - figure supplement 1A). *Vice versa*, ~87% of the mRNAs in our chimeras known to be regulated by sRNAs, were fused to cognate sRNA fragments (Figure 2 - figure supplement 1B). Except for the GcvB-*sstT*, all of the experimentally verified interactions in our data had the known mRNA and sRNA seeds (Figure 2 - figure supplement 1C-D). This implies that the false negative rate in our data is very low. When we extended these analyses to *all* sRNAs and mRNAs identified in our data, we obtained very similar results (Figure 2 - figure supplement 2A-B). Only the known MicC seed sequence was absent in MicC chimeras (Figure 2 - figure supplement 2C).

As a proxy for noise we quantified intermolecular chimeras containing rRNA sequences. Ribosomal RNA represents up to 80% of total cellular RNA and therefore often contributes significantly to noise in sequencing data. Although Hfq is known to interact with rRNA, this interaction appears to be sRNA independent (Andrade et al., 2018). Therefore, chimeras containing rRNA fragments likely represent background. In less than 4% of the chimeras were sRNAs or mRNAs fused to rRNA sequences, suggesting that the CLASH data has low background (Figure 2 - figure supplements 1-2).

We recovered around 20% of the sRNA-mRNA networks found with RIL-seq (Figure 2B) and 37 experimentally verified interactions (Supplementary File 7). These results suggest that while the CLASH data contained many known interactions, the analyses were clearly not exhaustive (also see Discussion). A large number of sRNA-mRNA interactions (~1700) were uniquely found in the CLASH data (Figure 2B) and many were supported by a relatively low number of reads compared to those found both in RIL-seq and CLASH (Supplementary File 2; Figure 2 - figure supplement 3). This raises the question whether these chimeras represent *bona fide* interactions or were merely generated through random/stochastic ligation events. To address this, we repeated the previous bioinformatics analyses on the chimeras unique to the CLASH data. This gave almost identical results. The vast majority of the chimeras were fusions between sRNA and mRNA fragments (Figure 2 - figure supplement 4A-B) and again in almost all cases the experimentally verified sRNA seeds were recovered (Figure 2 - figure supplement 4B). Next, we analysed the chimeras unique to the CLASH data that were supported by less than 4 reads. (Figure 2 - figure supplement 5). The majority of these chimeras in this group represented sRNA-mRNA and mRNA-mRNA interactions (Figure 2 - figure supplement 5A-B) and again in almost all cases the known sRNA seed sequences were recovered (Figure 2 - figure supplement 5C). We do note the slightly higher percentage of sRNA-rRNA and mRNA-rRNA chimeras (12-13%) in this group, suggesting higher background levels (Figure 2 - figure supplement 5A-B).

However, considering again the sheer abundance of rRNA in bacterial cells, we argue that also the background in this group of low abundance chimeras is remarkably low.

To provide additional evidence that the low abundant interactions identified with CLASH represent genuine interactions and not weak or stochastic interactions, we calculated the base-pairing potential between the two halves of the chimeras. For this purpose, we used RNAduplex (Lorenz et al., 2011) to compute the hybridization potential (in kcal/mol) of the two halves in each chimera. We focussed on sRNA-mRNA chimeras as this group represented the largest number of interactions (Figure 3). These analyses revealed that the chimeras in the CLASH data, even those supported by only a few reads (Figure 3D), had a significantly higher propensity to form stable duplexes when compared to *in silico* shuffled chimeric reads (p-value < $6*10^{-16}$). These data imply that a large fraction of the chimeras represent genuine base-pairing interactions and not random ligation events.

If the recovered interactions indeed represent *bona fide* interactions, then it may be expected that the putative mRNA targets found in CLASH chimeras are enriched for sequence motifs complementary to the sRNA seed sequences. To test this, we performed motif analyses on targets of 38 sRNAs that showed at least five unique interactions with different mRNAs (Figure 4A). Some sRNAs appeared to utilize multiple and independent seed sequences to base-pair with mRNAs. In these cases, we first performed a K-means clustering analysis to group those chimeras that contained similar sRNA sequences. For each of the resulting clusters (usually 4-5), we subsequently extracted the corresponding mRNA fragments and performed motif analyses using the MEME tool suite (Bailey et al., 2009). This enabled us to detect mRNA sequence motifs that are associated with specific sRNA seed sequences. The results are shown in Figure 4 - figure supplements 1-12. The motif analyses were performed for all the mRNA fragments found in sRNA-mRNA chimeras, mRNA fragments from sRNA-mRNA interactions uniquely identified by CLASH, and mRNA fragments found in sRNA-mRNA interactions supported by less than four reads. In the majority of cases we recovered previously identified mRNA sequence motifs (Faigenbaum-Romm et al., 2020; Melamed et al., 2016; Waters et al., 2017). The majority of the sRNA-mRNA interactions involving RyjB , ChiX, SdsR and GadY were supported by less than four reads and only found in our CLASH data. Regardless, the mRNA fragments in these chimeras were significantly enriched for sequence motifs complementary to the sRNA including known seed sequences (Figure 4B, Figure 4 - figure supplements 1-3). We also identified novel mRNA sequence motifs for RyjB, GadY, ArcZ, CyaR and GcvB (Figure 4B, Figure 4 – figure supplements 3-6). GcvB was previously reported to recognize the consensus motif CACAaCAY in mRNAs through interactions with the GU-rich R1 seed region located at bases 66–89 (Gulliver et al., 2018; Sharma et al., 2011). Consistent with this, we found a similar motif in cluster 2 chimeras, although these less frequently recovered

in the interactions only identified by CLASH and chimeras supported by less than four reads. Our analyses also identified a well-defined sequence motif in putative mRNA targets that is highly complementary to the R3 seed, consistent with the idea that this seed is also very frequently used to regulate mRNAs (Lalaouna et al., 2019). The R3 complementary sequence motif was most highly enriched in the interactions uniquely identified in CLASH (Figure 4 - figure supplement 6B). In all but one case (CyaR motif in cluster 3; Figure 4 - figure supplement 5B) did the mRNA sequence motifs show significant complementarity to known seed sequences (Figure 4 - figure supplements 1-12). In addition, these analyses indicated that sequences in the 3' ends of ArcZ and CyaR can also function as seeds (Figure 4 - figure supplements 4-5). Certain motifs were more frequently found in sRNA-mRNA interactions uniquely identified by CLASH: The MgrR mRNA motif found in the RIL-seq data was not frequently detected in our data, but the novel MgrR interactions recovered by CLASH showed a significant enrichment of G-rich motifs in mRNA fragments (Figure 4 - figure supplement 7).

We also reasoned that genuine interactions should be enriched in RNA-RNA interaction data generated by alternative experimental approaches. To test this, we compared our data to recent GcvB and CyaR MS2 Affinity Purification coupled with RNA Sequencing (MAPS) datasets (Lalaouna et al., 2019, 2018) (Figure 4 - figure supplements 13A and B). The CyaR and GcvB datasets were chosen as we had a large number of different mRNA interactions with these sRNAs (> 200), which enabled us to do a statistically meaningful comparison of the datasets. Indeed, the results show that CLASH mRNA targets were significantly more highly enriched compared to the other genes in the MAPS datasets. This was even the case for those interactions supported by a relatively low number of chimeric reads, including many interactions uniquely found in our CLASH data.

Collectively, these analyses strongly suggest that the predicted interactions found in our CLASH data, even those supported by a relatively low number of chimeras, are highly enriched for *bona fide* sRNA-mRNA interactions and less likely to be formed by random/stochastic events.

What is the biological significance of these interactions? Because sRNAs can influence the stability of their mRNA targets, we asked how many of the putative mRNA targets showed changes in gene expression in existing sRNA over-expression datasets (Figure 5, Figure 5 -figure supplements 1-4). We initially analysed previously published *E. coli* microarray datasets (Beisel and Storz, 2011; De Lay and Gottesman, 2009; Sharma et al., 2011) similar to what was performed to validate RIL-seq interactions (Melamed et al., 2016). For these analyses we also focussed our analyses on sRNAs that had a very high number of different mRNA interactions (>200) in our CLASH data (ArcZ, GcvB, CyaR and

Spot42; Figure 5 - figure supplements 1-4). While this work was under revision, RNA-seq data from several sRNA over-expression analyses in *E. coli* became available (Faigenbaum-Romm et al., 2020), which we subsequently included in our analyses (Figure 5A). Only a subset of the predicted sRNA targets showed significant changes in gene expression. GcvB CLASH mRNA targets were most highly enriched for differentially expressed genes, although this was lower for the less abundant interactions uniquely found in the CLASH data (Figure 5A, Figure 5 – figure supplement 1). Surprisingly, although the CyaR targets were highly enriched in the MAPS data, only a few of the mRNAs were significantly differentially expressed in the CyaR over-expression data (Figure 5A, Figure 5 - figure supplement 2). The Spot42 mRNA targets predicted by CLASH showed larger (albeit modest) changes in gene expression compared to the other genes in the dataset (Figure 5 - figure supplement 3).

Previous work implied that those interactions that impact mRNA steady-state levels are mostly found in multiple replicate RIL-seq experiments and are generally more abundant (Faigenbaum-Romm et al., 2020). The interactions recovered by both RIL-seq and CLASH were supported by a significantly higher number of chimeras compared to those uniquely identified in the CLASH data (Figure 2 – figure supplement 3). Therefore, we asked if this group of interactions was more likely to alter mRNA levels. This was the case for the GcvB and MicA mRNA interactions but not ArcZ and CyaR interactions (Figure 5B).

In conclusion, similar to what was observed for RIL-seq mRNA targets (Faigenbaum-Romm et al., 2020), many of the sRNA-mRNA interactions do not appear to significantly affect mRNA steady-state levels and for some sRNAs reproducible interactions have a higher likelihood impacting mRNA target levels (also see Discussion).

Hfq CLASH predicts sRNA-sRNA interactions as a widespread layer of post-transcriptional regulation.

Surprisingly, we uncovered a large number of sRNA-sRNA chimeras, representing 200 unique interactions (Figure 2A; 2.1%; Supplementary File 4). Many of the sRNA-sRNA interactions were uniquely found in our Hfq CLASH data (Figure 6A), were growth-stage specific and the sRNA-sRNA networks show extensive rewiring across the exponential, transition and stationary phases (Figure 6 - figure supplement 1). The sRNA-sRNA network is dominated by several abundant sRNAs that appear to act as hubs with many interacting partners: ChiX, Spot42 (spf), ArcZ and GcvB. Again, in many cases the experimentally validated sRNA seed sequences were found in the chimeric reads, for both established and novel interactions. For example, the majority of ArcZ sRNA-sRNA chimeras contained the known and well conserved seed sequence (Figure 6B, Figure 6 - figure supplement 2).

The sRNA-sRNA chimeras containing CyaR fragments were of particular interest, as the sRNA is primarily expressed during the transition from late exponential to stationary phase (De Lay and Gottesman, 2009). While 30% of the CyaR chimeras contained the known seed sequence (De Lay and Gottesman, 2009; Papenfort et al., 2008), the majority of the chimeras contained a ~25 nt fragment in the 5' region of CyaR, which was also frequently recovered in RNase E CLASH data (Waters et al., 2017) (Figure 6B; Figure 6 - figure supplement 2), suggesting that this region represents a *bona fide* interaction site. Notably, the ArcZ-CyaR chimeras contained the seed sequences from both sRNAs (Figure 6 - figure supplement 2) and these were detected specifically in the transition phase (Figure 6A; Figure 6 - figure supplement 1).

To validate the predicted *in vivo* interaction between ArcZ and CyaR (Figure 7A), we used an *E. coli* plasmid-based assay that is routinely used to monitor sRNA-sRNA interactions and expression of their target mRNAs (Melamed et al., 2016; Miyakoshi et al., 2015b; Tree et al., 2014). An advantage of this system is that each sRNA would be uncoupled from the chromosomally encoded regulatory networks (that were thought to act largely in a 1:1 stoichiometry) and to allow the specific effects of the sRNA-target RNA to be assessed (Miyakoshi et al., 2015b). Importantly, these sRNAs were induced during early exponential growth phase when the endogenous (processed) ArcZ and CyaR sRNAs are detectable at only very low levels (Figure 7B, lanes 1, 2, 5, 7). The qPCR data were subsequently normalized to the results obtained with the pJV300 control to calculate fold changes in expression levels. It has recently been shown that sRNAs can also function as "decoys" or "sponges" that can divert other sRNA away from its mRNA targets (Azam and Vanderpool, 2015; Figueroa-Bossi and Bossi, 2018; Kavita et al., 2018). This mode of "regulating the regulator" often results in cross-talk between pathways (reviewed in (Figueroa-Bossi and Bossi, 2018)). We hypothesized that the ArcZ-CyaR interaction may represent such a sponging activity. However, since it is difficult to predict directly from the CLASH data which sRNA in each pair acts as the decoy/sponge, we tested both directions. ArcZ over-expression not only decreased the expression of its mRNA targets (*tpx*, *sdaC*) by more than 50%, but also that of CyaR (Figure 7C, panel I; Figure 7D, panel I). Concomitantly, we observed a substantial increase in CyaR targets *nadE* and *yqaE* (Figure 7C, panel I). CyaR over-expression reduced the level of a direct mRNA target (*nadE*) by ~40% but it did not significantly alter the level of ArcZ or ArcZ mRNA targets (*tpx* and *sdaC*; Figure 7C, panel II). Notably, in this two-plasmid assay CyaR was not expressed at levels higher than ArcZ (Figure 7D, panel II). Therefore, it is plausible that under the tested conditions the CyaR over-expression was not sufficient to see an effect on ArcZ. We find this unlikely as over-expression of CyaR also did not significantly affect endogenous ArcZ levels, which was ~80-fold less abundant than CyaR in this experiment (Figure 7D, panel III). The

qPCR results were also confirmed by Northern blot analyses (Figure 3 - figure supplement 3B, lanes 1-8), which confirmed the reduction in CyaR levels upon ArcZ over expression and demonstrated that ArcZ processing was not affected upon CyaR over-expression. These results suggest that the regulation is unidirectional, reminiscent of what has been described for Qrr3 in *Vibrio harveyi* (Feng et al., 2015).

To provide additional support for direct interactions between these sRNAs, we generated mutations in the seed sequences of the sRNAs analysed here (Figure 7A). We found that two G to C nucleotide substitutions in ArcZ was sufficient to disrupt ArcZ regulation of CyaR (Figure 7C panel III; ArcZ 70-71 + CyaR). Unexpectedly, the wild-type ArcZ was also able to effectively suppress the CyaR seed mutant (Figure 7C panel III; ArcZ + CyaR 38-39). We predict that the wild-type ArcZ can still form stable base-pairing interactions with the CyaR mutant. Nevertheless, regulation by the ArcZ 70-71 mutant was almost fully restored when complementary mutations were introduced in the CyaR region (Figure 7C panel III; ArcZ 70-71 + CyaR 38-39), providing additional evidence that these sRNAs base-pair *in vivo*. Furthermore, the data also demonstrate that it is very unlikely that the observed changes in CyaR levels were the result of Hfq redistribution due to over-expression of ArcZ (Moon and Gottesman, 2011; Papenfort et al., 2009), as the ArcZ seed mutant stably accumulated (and therefore effectively binds Hfq), but did not affect CyaR levels (Figure 7C panel III).

These results, together with the CLASH data, imply that ArcZ and CyaR base-pair *in vivo*, and that this interaction could lead to a reduction in CyaR levels but not *vice versa*.

Hfq CLASH identifies novel sRNAs in untranslated regions

Two lines of evidence from our data indicate that many other mRNAs may be harbouring sRNAs in their UTRs or be involved in base-pairing among themselves. First, around 10% of the unique intermolecular chimeras mapped to mRNA-mRNA interactions (Figure 2A). Secondly, we observed extensive binding of Hfq in 3'UTRs near transcriptional terminators (Figure 1 - figure supplement 3A-B), indicating that like in *Salmonella*, the *E. coli* 3'UTRs may harbour many functional sRNAs (Chao et al., 2017). We identified 116 3'UTR-containing mRNA fragments that were involved in 507 interactions (represented by a total of 3149 unique chimeras). Eighteen of these 3'UTR fragments were also identified in 3'UTR-mRNA chimeric reads in the RIL-seq S-chimeras data (Melamed et al., 2016) and 10 appeared stabilised upon transient inactivation of RNase E performed in *Salmonella* (TIER-seq data (Chao et al., 2017)); Figure 8A, Supplementary Files 5 and 6). For several of the putative 3'-UTR derived sRNAs, complementary sequence motifs in the mRNA fragments were identified, including motifs for the putative sRNA derived from the 3'UTR of *ahpF* (Figure 4C-D; Figure 8 - figure supplements 1-3). Out of the 507 3'UTR-mRNA interactions,

75 were 3'UTRs fused to 5'UTRs of mRNAs, suggesting that these may represent 3'UTR-derived sRNAs that base-pair with 5'UTRs of mRNAs, a region frequently targeted by sRNAs (Supplementary Files 5 and 6). Strikingly, 233 interactions (2094 unique chimeras) contained the 3'UTR fragment of *cpxP*, 51 (812 chimeras) of which were also found in the RIL-Seq data (Supplementary File 6). In *Salmonella cpxP* harbours the CpxQ sRNA (Chao and Vogel, 2016). Our analyses greatly increased the number of potential CpxQ mRNA targets and show that the vast majority of CpxQ interactions take place during the transition and stationary phases (Supplementary File 6). Motif analyses of the putative CpxQ mRNA targets, including those identified in the interactions unique to CLASH, revealed two highly enriched G-rich sequence motifs that showed strong sequence complementarity to the known seed sequences (Figure 8 - figure supplement 2).

We identified six mRNA 3'UTRs that were uncovered in all three (Hfq CLASH, RIL-seq and TIER-seq) datasets (Figure 8A), suggesting they likely contain sRNAs released from 3'UTRs by RNase E processing. Northern blot analyses confirmed the presence of sRNAs in *malG*, *ygaM* and *gadE* 3'UTRs (Figure 8B, Figure 8 - figure supplement 4). We predict that the 3'UTR of *ygaM* harbours a ~100 nt sRNA (hereafter referred to as YgaN; Figure 8 - figure supplement 4) and robust Hfq cross-linking could be detected in this region (Figure 8C).

The *gadE* 3'UTR was also detected in the RIL-seq data and experimentally confirmed and annotated as GadF (Melamed et al., 2016). Remarkably, even though we only recovered 23 unique GadF-mRNA interactions, two distinct complementary sequence motifs (CCAGGGG and CUGGUG) were identified in mRNA fragments of these chimeras, the former of which was not previously detected (Figure 8 - figure supplement 3). Again, these complementary mRNA motifs were also enriched in interactions uniquely identified by CLASH (Figure 8 - figure supplement 3). For two other 3'UTR-derived sRNAs (MicL and SdhX), we recovered 13 and 9 interactions with mRNAs, respectively (Figure 8 - figure supplement 5). MicL was previously shown to repress the synthesis of the Lpp outer membrane protein (Guo et al., 2014). *Lpp* mRNA fragments were most frequently found in MicL chimeras (15; Figure 8 - figure supplement 5A). The *in silico* folded structure of the MicL-*lpp* chimeras is in excellent agreement with the previously proposed interaction between MicL and *lpp* (Figure 8 - figure supplement 5B) (Guo et al., 2014). SdhX is involved in linking acetate metabolism with the TCA cycle (De Mets et al., 2018; Miyakoshi et al., 2018). Our data predict over a dozen SdhX interactions, several of which had not been previously described (Figure 8 - figure supplement 5C). We recovered two SdhX interactions with known mRNAs targets (*ackA* and *katG*; Figure 8 - figure supplement 5D) (De Mets et al., 2018; Miyakoshi et al., 2018). Interestingly, the SdhX-*ackA* interaction was detected in the exponential phase, whereas the SdhX-*katG* interaction appeared specifically during

stationary phase. Although the number of chimeras supporting these interactions were relatively low (*katG*; 2 chimeras; *ackA*; 3 chimeras), the *in silico* predicted interactions between the two halves of these chimeras are fully consistent with previously published work (De Mets et al., 2018; Miyakoshi et al., 2018). These results reinforce the idea that Hfq CLASH recovers genuine interactions.

To substantiate our 3'UTR-derived sRNA candidate prediction, we analysed RNA-seq data from a study that used Terminator 5'-Phosphate Dependent Exonuclease (TEX) to map transcription start sites (TSS) of coding and non-coding RNAs in *E. coli* (Thomason et al., 2015). TEX degrades processed transcripts that have 5' monophosphates, but not primary transcripts with 5' triphosphates. Therefore, these data enabled us to determine whether (a) a short RNA was detected in the 3'UTR and whether these were generated by RNase-dependent processing (TEX sensitive) or originated from an independent promoter (TEX insensitive). In 47 of the 126 predicted 3'UTR-derived sRNAs in the TEX data we found strong evidence for the presence of sRNAs (Figure 8 - figure supplement 6, Supplementary File 5 and see Data and Code availability). The TEX data indicate that *ygaM* has (at least) two promoters, one of which is located near the 3' end of the gene that we predict is the TSS for YgaN (Figure 8 - figure supplement 6A). Furthermore, we speculate that YgaN is processed by RNases. This is based on the observation that multiple YgaN species were detected in the Northern blot analyses (Figure 8 - figure supplement 4) and the TEX data indicate that shorter YgaN RNAs are sensitive to TEX treatment (Figure 8 - figure supplement 6A).

The majority of the sRNAs we analysed are more abundant at higher cell densities (including GadF, YgaN and RybB; see Figure 8B). In sharp contrast, the sRNA derived from the 3'-UTR of the *malG* mRNA (MalH) was expressed very transiently and peaked at an OD_{600} of 1.8 (Figure 8B). We envisage that the particularly transient expression of this sRNA may be associated with a role in the adaptive responses triggered during transition from exponential to stationary phases of growth.

Discussion

Microorganisms need to constantly adapt their transcriptional program to meet changes in their environment, such as changes in temperature, cell density and nutrient availability. In bacteria, small RNAs (sRNAs) and their associated RNA-binding proteins play a key role in this process. By controlling translation and degradation rates of mRNAs in response to stress (Holmqvist and Wagner, 2017; Nitzan et al., 2017; Shimoni et al., 2007), they can regulate the kinetics of gene expression as well as suppress noisy signals (Beisel and Storz, 2011), enabling organisms to more efficiently adapt to environmental changes. A

major challenge for bacteria is the transition from exponential growth to stationary phase, when the most favourable nutrients become limiting. To counteract this challenge, cells need to rapidly remodel their transcriptome to efficiently metabolize alternative carbon sources. This transition is highly dynamic and involves both activation and repression of diverse metabolic pathways. However, it is unclear to what degree sRNAs contribute to this transition. The most useful piece of information would be to know what sRNAs are upregulated during this transition phase and to identify their RNA targets. This would help to uncover the regulatory networks that govern this adaptation, as well as provide a starting point for more detailed functional analyses on sRNAs predicted to play a key role in this process. For this purpose, we performed UV cross-linking, ligation and sequencing of hybrids (CLASH (Kudla et al., 2011)) to unravel the sRNA base-pairing interactions during this transition. Using Hfq as a bait we uncovered thousands of unique sRNA base-pairing interactions. We identified almost 1700 novel sRNA-mRNA interactions represented by over 18000 unique chimeras, and 200 novel sRNA-sRNA interactions, compared to previously published work (Melamed et al., 2016; Waters et al., 2017). We experimentally validated several of the interactions found in our CLASH findings. We identified a functional sRNA-sRNA interactions and describe a novel 3'UTR-derived sRNA that we propose plays a role in enhancing uptake of an alternative carbon source during the transition to stationary phase.

Hfq CLASH

Our earlier *S. cerevisiae* Cross-linking and cDNA analysis data (CRAC; (Granneman et al., 2009)) showed that a percentage of the cDNAs were formed by intermolecular ligations of two RNA fragments (chimeras) known to base pair *in vivo* (Kudla et al., 2011). These findings prompted us to develop a refined protocol to enrich for sRNA-target chimeric reads using Hfq as an obvious bait. The initial Hfq UV cross-linking data (CRAC; (Tree et al., 2014)) did not yield sufficiently high numbers of chimeric reads to extract new biological insights. In line with observations from other groups (Bandyra et al., 2012; Bruce et al., 2018; Morita et al., 2005), it was proposed that duplexes formed by Hfq are rapidly transferred to the RNA degradosome. This can cause an extensive reduction in the likelihood of capturing sRNA-target interactions with Hfq using CLASH (Waters et al., 2017). However, a recent study demonstrated that Hfq can be used effectively as a bait to enrich for sRNA-target duplexes under lower-stringency purification conditions suggesting that sRNA-mRNA duplexes are sufficiently stable on Hfq during purification (Melamed et al., 2016). This encouraged us to further optimize the CLASH method. We made a number of changes to the protocol that enabled us to recover a large number of chimeric reads, many of which represented sRNAs base-paired to potential targets (detailed in Materials and Methods). We shortened various incubation steps to minimize RNA degradation and

performed very long and stringent washes after bead incubation steps to remove any background binding of non-specific proteins and RNAs. Crucially, we very carefully controlled the RNase digestion step that is used to trim the cross-linked RNAs prior to making cDNA libraries, ensuring the recovery of longer chimeric RNA fragments. The resulting cDNA libraries were paired-end sequenced to increase the recovery of chimeric reads with high mapping scores from the raw sequencing data. These modifications led to a substantial improvement in the recovery of chimeric reads (8.6% compared to 0.001%. 0.47% were intermolecular chimeras).

Both RIL-seq and Hfq CLASH have advantages and disadvantages and are highly complementary. A major strength of CLASH, however, is that the purification steps are performed under highly stringent and denaturing conditions. During the first FLAG affinity purification steps the beads are extensively washed with high salt buffers and the second Nickel affinity purification step is done under denaturing conditions (6M guanidium hydrochloride). These stringent purification steps can significantly reduce noise by strongly enriching for RNAs covalently cross-linked to the bait protein (Granneman et al., 2009). Indeed, we show that Hfq CLASH can generate high quality RNA-RNA interaction data with low background: only a few hundred chimeric reads were found in the control datasets, compared to the over 50,000 chimeras that co-purified with Hfq. The RIL-seq library preparation protocol uses an rRNA depletion step to remove contaminating ribosomal RNA. For Hfq CLASH this is not necessary, and we show that chimeras containing rRNA fragments, which presumably represent noise, are not very abundant in our data (Figure 2 - figure supplements 1, 2, 4, 5). Our library preparation protocol also includes the use of random nucleotides in adapter sequences to remove potential PCR duplicates (“collapsing”) from the data.

The very stringent purification conditions used in CLASH could, in some cases, also be a disadvantage as it completely relies on UV cross-linking to isolate directly bound RNAs. In cases where the efficiencies of protein-RNA cross-linking are low (for example, in the case of proteins that only recognize double-stranded RNA), RIL-seq may be a better approach as it does not completely rely on UV cross-linking (Melamed et al., 2016).

A large number of interactions were unique to both RIL-seq and Hfq CLASH datasets, which we believe can be explained by a number of technical and experimental factors. The denaturing purification conditions used with CLASH completely disrupts the Hfq hexamer ((Tree et al., 2014) and this work). Therefore, during the adapter ligation reactions the RNA ends are likely more accessible for ligation. In support of this, in the RIL-Seq data, the sRNAs are mostly found in the second half of the chimeras (Melamed et al., 2016), whilst in the Hfq CLASH data we observe sRNAs fragments with almost equal distributed in both sides (45% in left fragment and 55% in right fragment). Indeed, it was proposed that in

RIL-seq the 3' end of the sRNA is buried in the hexamer and therefore not always accessible for ligation (Melamed et al., 2016).

For the RIL-seq experiments, the authors harvested the cells at 4ºC and they resuspended them in ice-cold PBS prior to UV irradiation (Melamed et al., 2018, 2016). This procedure results in a cold-shock that can affect the sRNA-interactome as well as sRNA stability. We cross-link actively growing cells in their growth medium and we UV irradiate our cells within seconds using the Vari-X-linker we recently developed (van Nues et al., 2017). We use filtration devices to rapidly harvest our cells (less than 30 seconds) and the filtered cells are subsequently stored at -80ºC. We previously showed that filtration combined with short UV cross-linking times dramatically reduces noise introduced by the activation of the DNA damage response and significantly increased the recovery of short-lived RNA species (van Nues et al., 2017). We speculate that many of the interactions that are unique to our Hfq CLASH data represent short-lived RNA duplexes that are preferentially captured with our UV cross-linking and rapid cell filtration setup.

Biological significance of the interactions

One important question that needs to be addressed in the field is how many of the interactions that are recovered by high-throughput RNA-RNA interactome methodologies represent physiologically or biologically relevant base-pairing interactions. The analysis of the RIL-seq (Melamed et al., 2016) and our CLASH data showed that the predicted mRNA targets did not frequently show significant changes in gene expression upon over-expression of the sRNA. It is, of course, possible that sRNA base-pairing mostly affects mRNA translation and mRNA stability to a lesser extent. Hence, approaches other than over-expression analyses may need to be included to verify the interaction networks. Ribosome profiling analyses on mutant strains should be helpful in determining whether the absence of the sRNA alters the association of mRNA targets with ribosomes (Guo et al., 2014; Wang et al., 2015), however, this is also a method not without challenges (Mohammad et al., 2019). Whilst this work was in progress, the Margalit group presented compelling evidence suggesting that many mRNA targets compete for Hfq and that the binding efficiency of Hfq to the targets primarily determines the regulatory outcome (Faigenbaum-Romm et al., 2020). Those mRNAs that were significantly affected by sRNA over-expression were also more frequently and reproducibly found in chimeras with the sRNA. This offers a plausible explanation for why we did not always observe enrichment of differentially expressed genes in putative mRNA targets recovered in a relatively low number of chimeras. Another aspect to consider is that over-expression of sRNAs will not only impact the direct targets. For example, over-expression of ArcZ in *Salmonella* revealed widespread changes in gene expression, presumably as a result of redistribution of Hfq over the transcriptome (Papenfort

et al., 2009). As a result, a relatively small fraction of the differentially expressed genes will be represented in the CLASH/RIL-seq data, resulting in poor p-values.

One could argue that some of the interactions we present here may represent weak or stochastic interactions that do not have a biological function. For example, sRNAs can cycle on Hfq (reviewed in (Santiago-Frangos and Woodson, 2018)) and it is therefore conceivable that some of the sRNA-sRNA chimeras detected in our CLASH data happen to be two sRNAs that were in close proximity during their exchange on Hfq. Although it is not possible to quantify the number of such interactions, we would argue they are not very abundant in our data. We purified Hfq and cross-linked RNAs under very stringent and completely denaturing conditions before we do the intermolecular ligation reactions. Because our purification conditions completely disrupt the Hfq hexamer (this work and (Tree et al., 2014)), transient interactions that do not involve (significant) base-pairing would only be detected if an Hfq *monomer* was UV cross-linked to both sRNAs simultaneously and if the available 5' and 3' ends are in close proximity. Considering the poor efficiency of UV cross-linking, the likelihood of this happening is very low. Secondly, we show that our chimeras, including those that are supported by only a few reads, have a high propensity to form stable duplexes *in silico* (Figure 3). Finally, for many sRNAs we identified enriched sequence motifs in predicted mRNA targets that have significant sequence complementarity to sRNA seeds (Figure 4, Figure 4 - figure supplements 1-12, Figure 8 - figure supplements 1-3). Thus, we conclude that with the CLASH protocol weaker or stochastic interactions are not easily recovered. While the CLASH and the RIL-seq analyses agree that for some sRNAs the more frequent interactions are more likely to affect target mRNA stability, they also highlight that low-abundance interactions have strong complementarity and base-pairing potential, thus are genuine. The biological significance of these is yet to be determined, but one possibility is that many low-frequency interactions occur to confer robustness to the regulation of a few principal targets (Jost et al., 2013) and we speculate that these principal targets are condition-specific.

Surprisingly, for ArcZ and CyaR, even some of the mRNA targets found in a larger number of chimeric fragments were not differentially expressed. Possible explanations include their regulation at the protein synthesis level, but not at the RNA level, or control by fine-tuning, which would result in modest or undetectable changes in transcript levels.

sRNA-sRNA interactions; ArcZ regulation of CyaR

One of the most striking observation of our global study was the abundance of sRNA-sRNA interactions *in E. coli*, many of which were growth-stage dependent. We experimentally validated the ArcZ-CyaR interaction, which involves the known seed sequence of ArcZ and the 5'end of CyaR. We demonstrate that ArcZ over-expression can

reduce CyaR steady state levels but not *vice versa*, implying the regulation is unidirectional. Consistent with our findings, in *Salmonella*, over-expression of ArcZ showed a dramatic reduction in CyaR bound to Hfq and upregulation of CyaR targets, such as *nadE* (Papenfort et al., 2009). This suggests that this activity is conserved between these two Gram-negative bacteria. A similar type of unidirectional regulation has also been elegantly demonstrated for the Qrr3 sRNA of *Vibrio cholerae* (Feng et al., 2015). The fate of these sRNA-sRNA duplexes may depend on the position of the interaction; It was shown that if the interaction with Qrr3 involves its stabilizing 5' stem-loop structure, the sRNA will be preferentially degraded (Feng et al., 2015). Consistent with this, folding of the chimeric reads suggests that ArcZ preferentially base-pairs with the 5' end of CyaR (Figure 6C and Figure 7A). This may destabilize secondary structures that normally help to stabilize the sRNA.

The biological significance of ArcZ regulating CyaR remains unclear, however, a possible function could be to reduce noise in CyaR expression by preventing CyaR levels from overshooting during the transition phase. ArcZ and CyaR target mRNAs are associated with many different processes. Thus, these interactions are expected to connect multiple pathways. For example, ArcZ regulation of CyaR may connect adaptation to stationary phase/biofilm development (De Lay and Gottesman, 2009; Monteiro et al., 2012) to quorum sensing and cellular adherence (De Lay and Gottesman, 2009). CyaR expression is controlled by the global regulator Crp. Most of the genes controlled by Crp are involved in transport and/or catabolism of amino acids or sugar. Interestingly, ArcZ downregulates the *sdaCB* dicistron which encodes for proteins involved in serine uptake and metabolism (Papenfort et al., 2009). This operon has been shown to be regulated by Crp as well, suggesting that ArcZ can counteract the activity of Crp.

Materials and Methods

Supplementary File 11: Key Resources Table

Bacterial strains and culture conditions

An overview of the bacterial strains used in this study is provided in the Key Resources Table. The *E. coli* MG1655 and TOP10F' strains served as parental strains. The *E. coli* K12 strain used for CLASH experiments, MG1655 *hfq*::HTF was previously reported (Tree et al., 2014). Cells were grown in Lysogeny Broth (LB) at 37°C under aerobic conditions with shaking at 200 rpm. The media were supplemented with antibiotics where

required at the following concentrations: chloramphenicol (Corning, –S, C239RI) - 25 µg/ml and kanamycin (Gibco, US,–11815-024) - 50 µg/ml. For induction of sRNA expression from plasmids, 1 mM IPTG, or 200 nM anhydrotetracycline hydrochloride (Sigma, 1035708-25MG) were used.

Construction of sRNA expression plasmids

The plasmids used in this study are listed in the Key Resources Table. The gene fragments and primers used for cloning procedures in this work are provided in Supplementary File 10. For the sRNA over-expression constructs, the sRNA gene of interest was cloned at the transcriptional +1 site under P*lacO* control by amplifying the pZE12*luc* plasmid (Expressys) by inverse PCR using Q5 DNA Polymerase (NEB). The sRNA genes and seed mutants were synthesized as ultramers (IDT; Supplementary File 10) which served as the forward primers. The reverse primer (oligo pZE12_5P_rev, Supplementary File 10) bears a monophosphorylated 5' end to allow blunt-end self-ligation. The PCR reaction was digested with 10U DpnI (NEB) for 1h at 37°C and purified by ethanol precipitation. The linear PCR product was circularized by self-ligation, and transformed in *E. coli* TOP10F' competent cells. Positive transformants were screened by Sanger sequencing (Edinburgh Genomics, Edinburgh, UK). Small RNA over-expression constructs derived from the pZA21MCS (Expressys) were generated identically, using the indicated ultramers in Supplementary File 10 as forward primers and oligo pZA21MCS_5P_rev as the reverse primer.

Hfq UV Cross-linking, Ligation and Analysis of Hybrids (Hfq-CLASH)

CLASH was performed essentially as described (Waters et al., 2017), with a number of modifications including changes in incubation steps, cDNA library preparation, reaction volumes and UV cross-linking. *E. coli* expressing the chromosomal Hfq-HTF were grown overnight in LB at 37°C with shaking (200 rpm), diluted to starter OD_{600} 0.05 in fresh LB, and re-grown with shaking at 37°C in 750 ml LB. A volume of culture equivalent to 80 OD_{600} per ml was removed at the following cell-densities (OD_{600}): 0.4, 0.8, 1.2, 1.8, 2.4, 3.0 and 4.0, and immediately subjected to UV (254 nm) irradiation for 22 seconds (~500 mJ/cm2) in the Vari-X-linker (van Nues et al., 2017) (https://www.vari-x-link.com). Cells were harvested using a rapid filtration device (van Nues et al., 2017) (https://www.vari-x-link.com) onto 0.45 µM nitrocellulose filters (Sigma, UK, HAWP14250) and flash-frozen on the membrane in liquid nitrogen. Membranes were washed with ~15 ml ice-cold phosphate-buffered saline (PBS), and cells were harvested by centrifugation. Cell pellets were lysed by bead-beating in 1 volume per weight TN150 buffer (50mM Tris pH 8.0, 150 mM NaCl, 0.1% NP-40, 5 mM β-

mercaptoethanol) in the presence of protease inhibitors (Roche, A32965), and 3 volumes 0.1 mm Zirconia beads (Thistle Scientific, 11079101z), by performing 5 cycles of 1 minute vortexing followed by 1-minute incubation on ice. One additional volume of TN150 buffer was added. To reduce the viscosity of the lysate and remove contaminating DNA the lysate was incubated with RQ1 DNase I (10U/ml Promega, M6101) for 30 minutes on ice. Two-additional volumes of TN150 were added and mixed with the lysates by vortexing. The lysates were centrifuged for 20 minutes at 4000 rpm at 4°C and subsequently clarified by a second centrifugation step at 13.4 krpm, for 20 min at 4°C. Purification of the UV cross-linked Hfq-HTF-RNA complexes and cDNA library preparation was performed as described (Granneman et al., 2009). Cell lysates were incubated with 50 µl of pre-equilibrated M2 anti-FLAG beads (Sigma, M8823-5ML) for 1-2 hours at 4°C. The anti-FLAG beads were washed three times 10 minutes with 2 ml TN1000 (50 mM Tris pH 7.5, 0.1% NP-40, 1M NaCl) and three times 10 minutes with TN150 without protease inhibitors (50 mM Tris pH 7.5, 0.1% NP-40, 150mM NaCl). For TEV cleavage, the beads were resuspended in 250 µl of TN150 buffer (without protease inhibitors) and incubated with home-made GST-TEV protease at room temperature for 1.5 hours. The TEV eluates were then incubated with a fresh 1:100 dilution preparation of RNaceIt (RNase A and T1 mixture; Agilent, 400720) for exactly 5 minutes at 37ºC, after which they were mixed with 0.4g GuHCl (6M, Sigma, G3272-100G), NaCl (300mM), and Imidazole (10mM, I202-25G). Note this needs to be carefully optimized to obtain high-quality cDNA libraries. The samples were then transferred to 50 µl Nickel-NTA agarose beads (Qiagen, 30210), equilibrated with wash buffer 1 (6 M GuHCl, 0.1% NP-40, 300 mM NaCl, 50 mM Tris pH 7.8, 10 mM Imidazole, 5 mM beta-mercaptoethanol). Binding was performed at 4ºC overnight with rotation. The following day, the beads were transferred to Pierce SnapCap spin columns (Thermo Fisher, 69725), washed 3 times with wash buffer 1 and 3 times with 1xPNK buffer (10 mM $MgCl_2$, 50mM Tris pH 7.8, 0.1% NP-40, 5 mM beta-mercaptoethanol). The washes were followed by on-column TSAP incubation (Thermosensitive alkaline phosphatase, Promega, M9910) treatment for 1h at 37°C with 8 U of phosphatase in 60 µl of 1xPNK, in the presence of 80U RNasin (Promega, N2115). The beads were washed once with 500 µl wash buffer 1 and three times with 500 µl 1xPNK buffer. To add 3'-linkers (App-PE – Key Resources Table), the Nickel-NTA beads were incubated in 80 µl 3'-linker ligation mix with (1 X PNK buffer, 1 µM 3'-adapter, 10% PEG8000, 30U Truncated T4 RNA ligase 2 K227Q (NEB, M0351L), 60U RNasin). The samples were incubated for 4 hours at 25°C. The 5' ends of bound RNAs were radiolabelled with 30U T4 PNK (NEB, M0201L) and 3µl ^{32}P-γATP (1.1µCi; Perkin Elmer, NEG502Z-500) in 1xPNK buffer for 40 min at 37°C, after which ATP (Roche, 11140965001) was added to a final concentration of 1mM, and the incubation prolonged for another 20 min to complete 5'

end phosphorylation. The resin was washed three times with 500 µl wash buffer 1 and three times with equal volume of 1xPNK buffer. For on-bead 5'-linker ligation, the beads were incubated 16h at 16°C in 1xPNK buffer with 40U T4 RNA ligase I (NEB, M0204L), and 1 µl 100 µM L5 adapter (Key Resources Table), in the presence of 1mM AtP and 60U RNasin. The Nickel-NTA beads were washed three times with wash buffer 1 and three times with buffer 2 (50 mM Tris–HCl pH 7.8, 50 mM NaCl, 10 mM imidazole, 0.1% NP-40, 5 mM β-mercaptoethanol). The protein-RNA complexes were eluted in two steps in new tubes with 200 µl of elution buffer (wash buffer 2 with 250 mM imidazole). The protein-RNA complexes were precipitated on ice by adding TCA (T0699-100ML) to a final concentration of 20%, followed by a 20-minute centrifugation at 4°C at 13.4 krpm. Pellets were washed with 800 µl acetone, and air dried for a few minutes in the hood. The protein pellet was resuspended and incubated at 65°C in 20 µl 1x NuPage loading buffer (Thermo Scientific, NP0007), resolved on 4–12% NuPAGE gels (Thermo Scientific, NP0323PK2) and visualised by autoradiography. The cross-linked proteins-RNA were cut directly from the gel and incubated with 160 µg of Proteinase K (Roche, 3115801001) in 600 µl wash buffer 2 supplemented with 1% SDS and 5 mM EDTA at 55°C for 2-3 hours with mixing. The RNA was subsequently extracted by phenol-chloroform extraction and ethanol precipitated. The RNA pellet was directly resuspended in RT buffer and was transcribed in a single reaction with the SuperScript IV system (Invitrogen, 18090010) according to manufacturer's instructions using the PE_reverse oligo as primer. The cDNA was purified with the DNA Clean and Concentrator 5 kit (Zymo Research) and eluted in 11 µl DEPC water. Half of the cDNA (5 µl) was amplified by PCR using Pfu Polymerase (Promega, M7745) with the cycling conditions (95°C for 2 min; 20-24 cycles: 95°C for 20s, 52°C for 30s and 72°C for 1 min; final extension of 72°C for 5 min). The PCR primers are listed in the Key Resources Table. PCR products were treated with 40U Exonuclease 1 (NEB, M0293L) for 1 h at 37°C to remove free oligonucleotide and purified by ethanol precipitation/ or the DNA Clean and Concentrator 5 kit (Zymo Research, D4003T). Libraries were resolved on a 2% MetaPhor agarose (Lonza, LZ50181) gel and 175-300bp fragments were gel-extracted with the MinElute kit (Qiagen, 28004) according to manufacturer's instructions. All libraries were quantified on a 2100 Bionalyzer using the High-Sensitivity DNA assay and a Qubit 4 (Thermo Scientific, Q33226). Individual libraries were pooled based on concentration and barcode sequence identity. Paired-end sequencing (75 bp) was performed by Edinburgh Genomics on an Illumina HiSeq 4000 platform.

RNA-seq

E. coli MG1655 was cultured, UV-irradiated and harvested as described for the

CLASH procedure. Total RNA was extracted using the Guanidium thiocyanate phenol method. RNA integrity was assessed with the Prokaryote Total RNA Nano assay on a 2100 Bioanalyzer (Agilent, G2939BA). Sequencing libraries from two biological replicates were prepared by NovoGene using the TruSeq library preparation protocol and 150bp paired-end sequencing was performed on an Illumina NovaSeq 6000 system. This yielded ~7-8 million paired-end reads per sample.

Small RNA over-expression studies

Individual TOP10F' clones carrying pZA21 and pZE12-derived sRNA constructs and control plasmids combinations (Key Resources Table) were cultured to OD_{600} 0.1 and expression of sRNAs was induced with IPTG and anhydrotetracycline hydrochloride (Sigma, I6758-1G and 1035708-25MG) for one hour. Cells were collected by centrifugation for 30 seconds at 14000 rpm, flash-frozen in liquid nitrogen and total RNA was isolated as above. Gene expression was quantified by RT-qPCR (see below) using 10 ng total RNA as template, and expressed as fold change relative to the reference sample containing pJV300 (Sittka et al., 2007) or empty pZA21.

RT-qPCR

Total RNA (10 µg) was treated with 2 U of Turbo DNase (Thermo Scientific, AM2238) for 1 hour at 37°C in a 10 µl reaction in the presence of 2 U superaseIn RNase inhibitor (Thermo Scientific, AM2694). The RNA was purified with RNAClean XP beads (Beckman Coulter, A63987). Quantitative PCR was performed on 10 ng of DNAse I-treated total RNA using the Luna Universal One-Step RT-qPCR Kit (NEB, E3005E) according to manufacturer's instructions. The qPCRs were run on a LightCycler 480 (Roche), and the specificity of the product was assessed by generating melt curves, as follows: 65°C-60s, 95°C (0.11 ramp rate with 5 acquisitions per °C, continuous). The data analyses were performed with the IDEAS2.0 software, at default settings: Absolute Quantification/Fit Points for Cp determination and Melt Curve Genotyping. The RT-qPCR for all samples was performed in technical triplicate. Outliers from the samples with technical triplicate standard deviations of Cp > 0.3 were discarded from the analyses. To calculate the fold-change relative to the control, the 2^{-ddCp} method was employed, using 5S rRNA (*rrfD*) as the reference gene. Experiments were performed for three biological replicates, and the mean fold-change and standard error of the mean were computed. Unless otherwise stated, significance of the fold-change difference compared to the reference sample control (for which fold-change =1 by definition) was tested with a one-sample t-test.

Northern Blot analysis

Total RNA was extracted from cell lysates by GTC-Phenol extraction. 10 µg total RNA was separated on an 8% polyacrylamide TBE-Urea gel and transferred to a nylon membrane (HyBond N+, GEHealthcare, RPN1210B) by electroblotting for four hours at 50 V. Membranes were pre-hybridised in 10 ml of UltraHyb Oligo Hyb (Thermo Scientific, AM8663) for one hour and probed with ^{32}P-labeled DNA oligo at 42°C for 12-18 hours in a hybridization oven. The sequences of the probes used for Northern blot detection are detailed in Supplementary File 10. Membranes were washed twice with 2xSSC + 0.5% SDS solution for 10 minutes and visualized using a Phosphor imaging screen and FujiFilm FLA-5100 Scanner (IP-S mode). For detection of highly abundant species (5S rRNA) autoradiography was used for exposure.

Western blot analyses

E. coli MG1655 Hfq::*htf* lysates using strains cultured, cross-linked, harvested and lysed in identical conditions as the CLASH experiments containing 40 µg protein were resolved on PAGE gels and transferred to a nitrocellulose membrane. The membranes were blocked for one hour in blocking solution (5% non- fat milk in PBST (1X phosphate saline buffer, 0.1% Tween-20). To detect Hfq-HTF protein, the membrane was probed overnight at 4°C with the Rabbit anti-TAP polyclonal primary antibody (Thermo Fisher, 1:5000 dilution in blocking solution), which recognizes an epitope at the region between the TEV-cleavage site and His6. For the loading control we used a rabbit polyclonal to GroEL primary antibody (Abcam, 1:150000 dilution, ab82592), for 2 hours at room temperature. After 3x10 min PBST washes, the membranes were blotted for one hour with a Goat anti-rabbit IgG H&L (IRDye 800) secondary antibody (Abcam, ab216773, 1:10000 in blocking solution) at room temperature. Finally, after three 10-minute PBST washes, the blot was rinsed in PBS, and the proteins were visualised with a LI-COR (Odyssey CLx) using the 800 nm channel and scan intensity 4. Image acquisition and quantifications were performed with the Image Studio Software.

Computational analysis

Pre-processing of the raw sequencing data.

Raw sequencing reads in fastq files were processed using a pipeline developed by Sander Granneman, which uses tools from the pyCRAC package (Webb et al., 2014). The entire pipeline is available at https://bitbucket.org/sgrann/). The CRAC_pipeline_PE.py pipeline first demultiplexes the data using pyBarcodeFilter.py and the in-read barcode sequences found in the L5 5’ adapters. Flexbar then trims the reads to remove 3’-adapter

sequences and poor-quality nucleotides (Phred score <23). Using the random nucleotide information present in the L5 5' adaptor sequences, the reads are then collapsed to remove potential PCR duplicates. The reads were then mapped to the *E. coli* MG1655 genome using Novoalign (www.novocraft.com). To determine to which genes the reads mapped to, we generated an annotation file in the Gene Transfer Format (GTF). This file contains the start and end positions of each gene on the chromosome as well as what genomic features (i.e. sRNA, protein- coding, tRNA) it belongs to. To generate this file, we used the Rockhopper software (Tjaden, 2015) on *E. coli* rRNA-depleted total RNA-seq data (generated by Christel Sirocchi), a minimal GTF file obtained from ENSEMBL (without UTR information). The resulting GTF file contained information not only on the coding sequences, but also complete 5' and 3' UTR coordinates. We then used pyReadCounters.py with Novoalign output files as input and the GTF annotation file to count the total number of unique cDNAs that mapped to each gene.

Normalization steps.

To normalize the read count data generated with pyReadCounters.py and to correct for differences in library depth between time-points, we calculated Transcripts Per Million reads (TPM) for each gene. Briefly, for each time-point the raw counts for each gene was first divided by the gene length and then divided by the sum of all the values for the genes in that time-point to normalize for differences in library depth. The TPM values for each OD_{600} studied were then log_2-normalized.

Hfq-binding coverage plots.

For the analysis of the Hfq binding sites the pyCRAC package (Webb et al., 2014) was used (versions. 1.3.2-1.4.3). The pyBinCollector tool was used to generate Hfq cross-linking distribution plots over genomic features. First, PyCalculateFDRs.py was used to identify the significantly enriched Hfq-binding peaks (minimum 10 reads, minimum 20 nucleotide intervals). Next, pyBinCollector was used to normalize gene lengths by dividing their sequences into 100 bins and calculate nucleotide densities for each bin. To generate the distribution profile for all genes individually, we normalized the total number of read clusters (assemblies of overlapping cDNA sequences) covering each nucleotide position by the total number of clusters that cover the gene. Motif searches were performed with pyMotif.py using the significantly enriched Hfq-binding peaks (FDR intervals). The 4-8 nucleotide k-mers with Z-scores above the indicated threshold were used for making the motif logo with the k-mer probability logo tool (Wu and Bartel, 2017) with the -ranked option (http://kplogo.wi.mit.edu/).

Analysis of chimeric reads.

Chimeric reads were identified using the hyb package using default settings (Travis et al., 2013) and further analysed using the pyCRAC package (Webb et al., 2014). To apply this single-end specific pipeline to our paired-end sequencing data, we joined forward and reverse reads using FLASH (https://github.com/dstreett/FLASH2) (Magoč and Salzberg, 2011), which merges overlapping paired reads into a single read. Paired reads that were not considered overlapping were subsequently concatenated into a single sequence and again filtered for overlapping reads that were missed by FLASH. These were then analysed using hyb. The -anti option for the hyb pipeline was used to be able to use a genomic *E. coli* hyb database, rather than a transcript database. Uniquely annotated hybrids (.ua.hyb) were used in subsequent analyses. To visualise the hybrids in the genome browser, the .ua.hyb output files were converted to the GTF format. To generate distribution plots for the genes to which the chimeric reads mapped, the parts of the chimeras were clustered with pyClusterReads.py and BEDtools (Quinlan and Hall, 2010) (intersectBed) was used to remove clusters that map to multiple regions. To produce the coverage plots with pyBinCollector, each cluster was counted only once, and the number of reads belonging to each cluster was ignored.

Statistical filtering of the data.

The uniquely annotated chimeras from the merged CLASH experiments were statistically scored using available pipelines (Waters et al., 2017). Only chimeras with an Benjamini-Hochberg adjusted p-value lower than 0.05 were considered and referred to as statistically filtered chimeras.

Predicted folding energy analyses.

Cumulative distributions of minimum folding energy were generated using the minimum folding energies predicted with RNADuplex (Lorenz et al., 2011) for all statistically filtered sRNA-mRNA chimeras. To generate the data for the shuffled chimeras, the fragments were randomly shuffled over the same gene, or over genes belonging to the same class of genes (e.g sRNAs or mRNAs), respectively. Significance was tested with Kolmgorov-Smirnov test.

Motif analyses for sRNA targets.

For each sRNA with at least five different putative targets, we clustered those chimeras based on the similarity of sRNA sequences using K-means clustering. The clustering step was skipped for those sRNAs for which almost all chimeric reads overlapped the same region. The sequences of the fused mRNA fragments in each cluster were

extracted and motif searches using MEME (Bailey et al., 2009). To calculate complementarity between the identified motifs in putative mRNA targets and the sRNA we used MAST (Bailey et al., 2009). Only motifs that had a MAST p-value <= 0.001 were considered.

Microarray analyses.

ArcZ, Spot42 and GcvB microarray data were processed by GEO2R using the limma package (Ritchie et al., 2015). The accession numbers for these datasets are GSE17771, GSE24875 and GSE26573. The processed CyaR data were obtained from the Supplementary data provided in the paper describing the CyaR over-expression in *E. coli* (De Lay and Gottesman, 2009). Cumulative distribution plots were generated using the T-statistics calculated by the limma package. Average expression levels were calculated by averaging the expression of genes in the parental and over-expression strain.

sRNA density plots.

To visualize the nucleotide read density of sRNA-target pairs for a given sRNA, the hit counts at each nucleotide position for all statistically filtered chimeras were summed. The count data was $\log_2$-normalized (actually $\log_2$(Chimera count +1) to avoid NaN for nucleotide positions with 0 hits when log-transforming the data).

To make distributions of the chimeric reads around known sRNA and mRNA seeds, we manually retrieved the experimentally validated sRNA and mRNA seed sequences from sRNATarbase 3.0 (Wang et al., 2015) and literature. We converted the FASTA sequences to the genomic coordinates of our reference genome. Next, we normalized the length of all sequences to eight nucleotides with pyNormalizeIntervalLengths.py, then used the pyBinCollector tool to calculate the overlap of the intervals corresponding to statistically filtered chimeric reads with the seed sequence interval of each sRNA and sRNA-mRNA interaction.

sRNA-sRNA network visualization.

Only the sRNA-sRNA chimeric reads representing statistically filtered chimeras in the merged CLASH dataset were considered. For each such interaction, chimera counts corresponding in either orientation were summed, $\log_2$-transformed and visualized with the igraph Python package.

Data and Code availability.

The next generation sequencing data have been deposited on the NCBI Gene Expression Omnibus (GEO) with accession number GSE123050. The python pyCRAC

(Webb et al., 2014), kinetic-CRAC and GenomeBrowser software packages used for analysing the data are available from https://bitbucket.org/sgrann (pyCRAC up to version 1.4.3), https://git.ecdf.ed.ac.uk/sgrannem/ and pypi (https://pypi.org/user/g_ronimo/). The hyb pipeline for identifying chimeric reads is available from https://github.com/gkudla/hyb. The scripts for statistical analysis of hyb data is available from https://bitbucket.org/jaitree/hyb_stats/. The FLASH algorithm for merging paired reads is available from https://github.com/dstreett/FLASH2. Bedgraph and Gene Transfer Format (GTF) generated from the analysis of the Hfq CLASH, RNA-seq and TEX RNA-seq data (Thomason et al., 2015) are available from the Granneman lab DataShare repository (https://datashare.is.ed.ac.uk/handle/10283/2915).

Acknowledgement

We are grateful to Lionello Bossi and Meriem El Karoui for their valuable feedback on the project and fruitful discussions. We thank Jörg Vogel and Yanjie Chao for providing the *Salmonella* CpxQ microarray data, Alasdair Ivens for help with the microarray data analysis, Christel Sirocchi for help with preparing *E. coli* RNA-seq libraries, Erica de Leau for expert technical assistance and the members of the Granneman lab for critically reading the manuscript. This work was supported by grants from the Wellcome Trust (091549 to S.G and 102334 to I.A.I.), the Wellcome Trust Centre for Cell Biology core grant (092076), a Medical Research Council non Clinical Senior Research Fellowship (MR/R008205/1 to S.G.), the Australian National Health and Medical Research Council Project grants (GNT1067241 and GNT1139313 to J.J.T) and the Autonomous Province of Trento (Axonomix to G.V and M.M.). Next Generation Sequencing was in part carried out by Edinburgh Genomics that is supported through core grants from NERC (R8/H10/56), MRC (MR/K001744/1) and BBSRC (BB/J004243/1).

Competing interest.

The authors declare no competing financial interest.

Materials & Correspondence

All requests for code, materials and reagents should be sent to Sander Granneman (Sander.Granneman@ed.ac.uk)

Figure Legends

Figure 1. Hfq CLASH experiments at different growth phases in *E. coli*.

(**A**) Overview of the critical experimental steps for obtaining the Hfq CLASH data. *E. coli* cells expressing an HTF (His6-TEV-3xFLAG)-tagged Hfq (Tree et al., 2014) were grown in LB and an equal number of cells were harvested at different optical densities (OD_{600}). Hfq binds to sRNA-RNA duplexes, and RNA ends that are in close proximity are ligated together. After removal of the protein with Proteinase K, cDNA libraries are prepared and sequenced. The single reads can be used to map Hfq-RNA interactions, whereas the chimeric reads can be traced to sRNA-target interactions. (**B**) A growth curve of the cultures used for the Hfq CLASH experiments, with OD_{600} at which cells were cross-linked indicated by circles, and each growth stage is indicated above the plot. The results show the mean and standard deviations of two biological replicates. Source data are provided as a Source Data file. (**C**) Cultures at the same OD_{600} cross-linked and harvested by filtration were analysed by Hfq CLASH, RNA-seq and Western blotting to detect Hfq. All the experiments were done in duplicate.

Figure 2. Hfq CLASH detects RNA-RNA interactions in *E. coli*.

(**A**) Intermolecular transcript combinations found in chimeras captured by Hfq CLASH. Combination count of all uniquely annotated hybrids on genomic features. *tRNA-tRNA and rRNA-rRNA chimeras originating from different genomic regions were removed because tRNA and rRNA gene copies are very similar and therefore we could not unambiguously determine if these represented intermolecular or intramolecular interactions. (**B**) Venn diagram comparing the sRNA-mRNA interactions found in RIL-seq S-chimera data and Hfq CLASH data. (**C**) Venn diagram showing the intersection between interactions from statistically filtered CLASH data from two biological replicates, recovered at three main growth stages: exponential (OD_{600} 0.4 and 0.8), transition (OD_{600} 1.2, 1.8, 2.4) and early stationary (OD_{600} 3.0 and 4.0). (**D**) Same as in (**C**) but for sRNA-mRNA interactions. (**E**) Distribution of mRNA fragments in sRNA-mRNA chimeras over all *E. coli* protein-coding genes. Each gene was divided in 100 bins and the number of mRNA fragments that mapped to each bin (hit density; y-axis) was calculated. (**F**) Distribution of the mRNA fragments of sRNA-mRNA chimeras around the translational start codon (AUG). The pink line indicates the position of the start codon (**G-H**) Enriched motifs in mRNA fragments of chimeras that uniquely overlap 5'UTRs and 3'UTRs; the logos were drawn using the top 20 K-mers.

Figure 3. *In silico* folding of sRNA-mRNA chimeras shows Hfq CLASH sRNA-mRNA interactions are significantly more structured than randomly matched pairs.

(**A**) Cumulative distribution of the predicted folding energy (ΔG) values between sRNA and matching mRNA found in all statistically filtered sRNA-mRNA interactions. Chimera folding energies were calculated using RNADuplex (Lorenz et al., 2011) and their distribution was compared to the control distributions of chimeric reads in which the fragments were randomly shuffled over the same gene, or over genes belonging to the same class of genes (e.g sRNAs or mRNAs), respectively. Significance was tested with Kolmgorov-Smirnov test. (**B)** As in (A) but now for the chimeras unique to the CLASH data. (**C**) As in (A) but now for chimeras that are supported by less than 4 reads. (**D**) as in (A) but now for chimeras unique to the CLASH data and supported by less than 4 reads.

Figure 4. Total number of interactions for sRNAs and in how many cases enriched sequence motifs were found.

(**A** and **B**) The heatmaps show the number of different mRNA interactions identified with independently transcribed sRNAs (**A**) or (putative) 3'UTR-derived sRNAs (**B**). Only sRNA for which we recovered at least 5 different interactions with mRNAs (highlighted in black) were further analysed for enriched motifs in the putative mRNA targets. The black-and-white heatmaps indicate if enriched motifs were identified in predicted mRNA targets of sRNAs (black is Yes and white is No). Motif analysis was performed using the MEME suite (Bailey et al., 2009). The number of target sequences that contained the common motif and the E-value of MEME is also shown. The identified motifs in the mRNA targets also show sequence complementarity to the sRNA sequence. The Motif Alignment Search Tool (MAST) was used to determine the degree of complementarity between the identified motifs in putative mRNA targets and the putative sRNA. An sRNA was considered to have an enriched motif if motif identified by MEME had an E-value <= 0.1 and/or the MAST p-value of the motif, which indicates the overall match between the identified motifs and the sRNA sequence (Bailey et al., 2009), was <= 0.001. (**C**-**D**) Motif analyses of mRNA sequences found in RyjB sRNA-mRNA and *ahpF*-3'UTR-mRNA interactions. All of the RyjB and *ahpF-3'UTR* interactions with mRNAs we found were uniquely detected in our CLASH data.

Figure 5. A subset of putative mRNA targets identified by CLASH show gene expression changes upon over-expression of the sRNA.

The Venn diagrams show how many of the predicted mRNA targets were also found to be differentially expressed in sRNA over-expression RNA-seq data (Faigenbaum-Romm et al., 2020). The GcvB and MicA CLASH mRNA targets are highly enriched for genes that are differentially expressed in the over-expression RNA-seq data (p-value < 0.001). The statistical significance was calculated using a hypergeometric test. Interactions that are generally presented by a relatively low number of reads ('CLASH unique' and 'less four

reads' categories) are not significantly enriched for differentially expressed genes. (**B**) The mRNA targets found in GcvB and MicA interactions found in both RIL-seq and CLASH show significantly higher fold-changes in the over-expression data compared to the interactions uniquely found in the CLASH data. The violin plots show the distribution of fold-changes in mRNA target expression (y-axis) in the over-expression RNA-seq data for chimeras supported by more than three reads and those supported by less than four reads (x-axis). Statistical significance between the two groups was calculated using a Mann-Whitney U test.

Figure 6. sRNA-RNA interactions identified by CLASH

(**A**) Hfq CLASH uncovers sRNA-sRNA interaction networks: comparison between statistically filtered sRNA-sRNA interactions in the Hfq CLASH data, RIL-seq S-chimeras (Melamed et al., 2016) (log and stationary) and RNase E CLASH (Waters et al., 2017). Only core genome sRNAs were considered. (**B**-**C**) Heatmaps showing the read density (log_2(chimera count+1)) of chimeric fragments mapping to ArcZ (**B**) and CyaR (**C**). The location of the known sRNA seed sequences as well as the predicted new CyaR seed is indicated above the heatmap.

Figure 7. ArcZ can influence CyaR levels.

(**A**) Base-pairing interactions predicted from the ArcZ-CyaR chimeras using RNACofold. The nucleotide substitutions for experimental validation of direct base-pairing are shown as red or green residues. (**B**) Northern blot analysis of ArcZ and CyaR. The cells containing both the empty pZA and pJV300 plasmids (lanes 1, 5, 9) do not express ArcZ and CyaR at detectable levels. (**C**) Validation of ArcZ-CyaR interaction by over-expression analyses. ArcZ, CyaR were overexpressed and the levels of their targets were monitored by RT-qPCR. The *tpx* and *sdaC* mRNAs are ArcZ mRNA targets. The *nadE* and *yqaE* mRNAs are CyaR targets. The dashed horizontal line indicates the level in the control plasmid (pJV300) that expresses a ~50 nt randomly generated RNA sequence. I ArcZ and CyaR directly interact. Panel III: The sRNAs and mutants as in were ectopically co-expressed in *E. coli* and CyaR and CyaR 38-39 levels were quantified by RT-qPCR. Experiments were performed in biological and technical triplicates; Error bars indicate the standard error of the mean (SEM) of the three biological replicates. (**D**) ArcZ and CyaR were overexpressed from a plasmid-borne IPTG inducible promoter (pZE-ArcZ and pZE-CyaR) and the data were compared to data from cells carrying plasmid pJV300. The co-expressed candidate target sRNAs (expressed from pZA-derived backbone) were induced with anhydrotetracycline hydrochloride (panels I and II). The bars indicate the mean fold-change in expression relative to the level of 5S rRNA (*rrfD*) in cells with the indicated vector. In panel III endogenous ArcZ levels were measured upon over-expression of CyaR. Error bars indicate

the standard error of the mean from three biological replicates and three technical replicates per experiment. Source data are provided as a Source Data file.

Figure 8. Hfq CLASH uncovers novel 3'UTR-derived sRNAs

(**A**) Genes of which the 3'UTRs were found fused to mRNAs, were selected from the statistically filtered CLASH data and RIL-seq S-chimera data. The RIL-seq RNA-RNA interaction set (Melamed et al., 2016) S-chimeras for Log and Stationary phases of growth was filtered for the 3'UTR/EST3UTR annotations on either orientation of the mRNA-mRNA pairs. Both were intersected with the set of mRNAs that were predicted by TIER-seq studies (Chao et al., 2017) to harbour sRNAs that get released from 3'UTRs by RNase E processing. Known (CpxQ, SdhX, MicL, GadF, *glnA*-3'UTR and SroC) and novel 3'UTR derived sRNAs (MalH, *flgL* 3'UTR, *ahpF*-3'UTR and YgaN) are indicated. See Supplementary File 5 for the detailed comparison. (**B**) MalH is transiently expressed during the transition from exponential to stationary phase. RybB was probed as a sRNA positive control and 5S rRNA as the loading control. See Figure 8 - figure supplement 4 for full-size blots. (**C**) Genome-browser snapshots of several regions containing candidate sRNAs for optical densities at which the RNA steady-state was maximal for each candidate; the candidate names and OD_{600} are indicated at the left side of the y-axes; the y-axis shows the normalized reads (RPM: reads per million); red: RPM of RNA steady-states from an RNA-seq experiment, blue: Hfq cross-linking from a CLASH experiment; black: unique chimeric reads found in this region.

Source data legends

Figure 1 - source data 1. Source data for Figure 1B

Figure 7 - source data 1. Source data for Figure 7B

Figure 7 - source data 2. Source data for Figure 7C

Figure 7 - source data 3. Source data for Figure 7D

Supplementary Figure legends

Figure 1 - figure supplement 1. Hfq expression and Hfq binding to RNAs at different cell densities in UV-irradiated *E. coli*.

(**A**) Western blot analyses of Hfq levels during various growth stages. Hfq-HTF was detected using an anti-TAP primary antibody, and a fluorescent secondary antibody. GroEL was used as a loading control.
(**B**) Quantification of Hfq levels from the Western blot result. The fluorescent signal for Hfq-HTF and GroEL was measured with the LI-COR from biological replicate experiments. The levels of Hfq were normalized to GroEL and expressed as fold-change relative to OD_{600} 0.4.
(**C**) Hfq crosslinking to RNA is similar at each optical density. Autoradiogram showing the purified radioactively labelled Hfq-RNA complexes for each OD_{600} after elution from the nickel beads. Source data for (**A**-**B**) are provided as a Source Data file.

Figure 1 - figure supplement 2. RNA-seq and Hfq CLASH replicate datasets are highly correlated.
(**A, B**) Scatter plots showing the distribution of log_2 Transcripts Per Million (TPM) normalized read counts for Hfq CLASH (**A**) and RNA-seq (**B**) biological replicates. Pearson R coefficients describing the correlation between the two independent experiments at each OD_{600} are included.

Figure 1 - figure supplement 3. Transcriptome-wide maps of Hfq binding to mRNA genes.
(**A**) Heatmaps showing the distribution of Hfq binding sites across all mRNA genes at OD_{600} 0.8 and 4.0. The genes are sorted by their sequence length (x-axis); the darker a nucleotide is, the more Hfq is crosslinked to it. To generate the heatmap, Hfq binding clusters were generated. A 5' and 3'UTR length of 200 nt was used. (**B**) Hfq binds to poly-U tracks. Significant k-mers (4-8 nt in length) were identified using the pyMotif tool of the pyCRAC package (Webb et al., 2014) and the motif logo was generated using all k-mers with a Z-score > 3, with kpLogo(Wu and Bartel, 2017). (**C**) A more stringent selection of the genes used to generate the distribution of Hfq binding to the transcriptome: all genes with overlapping 5' or 3'UTRs were removed from the analysis to avoid 'duplicate' counting. For all remaining cDNAs, FDR intervals of minimum 20 nt were considered for distribution plotting. The interval length (with UTR flanks as in the GTF annotation file) for each gene was normalized over 100 bins (x-axis), and the fraction of hits in each bin was calculated (y-axis).

Figure 2 - figure supplement 1. Analysis of experimentally verified sRNA-and mRNA-containing chimeras in the Hfq CLASH data.
(**A**) The sRNAs with experimentally verified interactions are frequently paired with mRNA fragments in Hfq CLASH chimeras. The pie chart shows how frequently sRNAs with

experimentally verified interactions were found fused to other genomic features in the data. For this analysis, all statistically filtered chimeras containing the sRNAs RprA, RybB, MgrR, GcvB, DsrA, MicA, Spot42, MicL, RyhB, ChiX, SdhX and CpxQ were considered. (**B**) As in (**A**) but now for the mRNAs with experimentally verified seed sequences. (**C**) Known sRNA seed sequences of experimentally validated sRNA-mRNA interactions are frequently recovered in chimera fragments. The heatmap shows the distribution of sRNA chimera fragments around known seed sequences, which were normalized to an 8-nucleotide length (indicated by the vertical dashed line). The results show that for all of the experimentally verified sRNA-mRNA interactions found in our data, the known sRNA seed sequence is almost always recovered. For the interaction indicated in red no overlap was found with the known seed. (**D**) as in (**C**) but now for mRNAs with experimentally verified seed sequences (normalized to an 8-nucleotide length). The results show that for all of the experimentally verified interactions found in our data, the known mRNA seed sequence is always recovered.

Figure 2 - figure supplement 2. sRNAs are most frequently found paired with mRNAs, and *vice versa,* in CLASH chimeras and are enriched in seed sequences. (**A**) The pie chart shows the count for the chimeras that contained sRNA fragments fused to other genomic features. (**B**) As in (**A**), but now for all the mRNA chimeras. (**C**) Known sRNA seed sequences derived from all experimentally validated sRNA-mRNA interactions are recovered in sRNA-mRNA chimera fragments. The heatmap shows the distribution of sRNA chimera fragments around known sRNA seed sequences (normalized to an 8-nucleotide length, indicated by the vertical dashed line).

Figure 2 - figure supplement 3. Interactions shared between RIL-seq and CLASH are supported by a large number of chimeras.

The violin plot shows the distribution of chimera counts for interactions shared between CLASH and RIL-seq, those uniquely found in the CLASH data (CLASH unique) and those supported by less than four reads. Statistical significance between the two distributions was calculated using a Mann-Whitney U test.

Figure 2 - figure supplement 4. sRNAs are most frequently found paired with mRNAs, and *vice versa,* in CLASH chimeras and are enriched in seed sequences.

(**A**-**C**) Same as in Figure 2 - figure supplement 2, but now for the chimeras that represent interactions uniquely found in the CLASH data

Figure 2 - figure supplement 5. sRNAs are most frequently found paired with mRNAs, and *vice versa,* in CLASH chimeras and are enriched in seed sequences.

(**A**-**C**) Same as in Figure 2 - figure supplement 3, but now for the chimeras that represent interactions uniquely found in the CLASH data and with read counts of less than 4.

Figure 4 - figure supplement 1. Identification of complementary sequence motifs in predicted ChiX mRNA targets.

(**A**) Motif analyses of mRNA sequences found in ChiX sRNA-mRNA interactions. Because almost all of the ChiX fragments found in chimeras mapped to the same region, a cluster analysis was not necessary. Motif analyses was performed using the MEME suite (Bailey et al., 2009). The Venn diagram shows the overlap between the interactions found in all the ChiX sRNA-mRNA interactions, those interactions uniquely found in the CLASH data (CLASH unique) and those supported by less than four reads (chimeras < 4 reads).The number of target sequences that contained the common motif and the E-value of MEME is also shown. (**B**) Identified motifs show sequence complementarity to known seed sequences. The green coloured nucleotide sequence indicates experimentally verified seed sequences. The Motif Alignment Search Tool (MAST) was used to determine the degree of complementarity between the identified motifs in putative mRNA targets and the sRNA. The MAST p-values indicate the overall match between the identified motifs and the sRNA sequence (Bailey et al., 2009).

Figure 4 - figure supplement 2. Identification of complementary sequence motifs in predicted SdsR mRNA targets.

(**A**-**B**) Motif analyses of mRNA sequences found in SdsR sRNA-mRNA interactions. Most of the SdsR interactions with mRNAs we found were uniquely detected in our CLASH data, as illustrated by the Venn diagram. Motif analyses was performed using MEME suite (Bailey et al., 2009). The number of target sequences that contained the common motif and the E-value of MEME is also shown. The identified motifs in the mRNA targets also show sequence complementarity to the sRNA sequence. The Motif Alignment Search Tool (MAST) was used to determine the degree of complementarity between the identified motifs in putative mRNA targets and the putative sRNA. The MAST p-values indicate the overall match between the identified motifs and the sRNA sequence (Bailey et al., 2009).

Figure 4 - figure supplement 3. Identification of complementary sequence motifs in predicted GadY mRNA targets.

(**A**) K-means cluster analyses of sRNA sequences found in GadY sRNA-mRNA chimeras. (**B**) Motif analyses of mRNA sequences found in sRNA-mRNA interactions from each

cluster. Motif analyses was performed using MEME suite (Bailey et al., 2009). The number of target sequences that contained the common motif and the E-value of MEME is also shown. The Venn diagram shows the overlap between the interactions found in all the GadY sRNA-mRNA interactions, those interactions uniquely found in the CLASH data (CLASH unique) and those supported by less than four reads (chimeras < 4 reads). (**C**) Identified motifs show sequence complementarity to known seed sequences. The Motif Alignment Search Tool (MAST) was used to determine the degree of complementarity between the identified motifs in putative mRNA targets and the sRNA. The MAST p-values indicate the overall match between the identified motifs and the sRNA sequence (Bailey et al., 2009).

Figure 4 - figure supplement 4. Identification of complementary sequence motifs in predicted ArcZ mRNA targets.

(**A**) K-means cluster analyses of sRNA sequences found in ArcZ sRNA-mRNA chimeras. The Venn diagram shows the overlap between the interactions found in all the ArcZ sRNA-mRNA interactions, those interactions uniquely found in the CLASH data (CLASH unique) and those supported by less than four reads (chimeras < 4 reads). (**B**) Motif analyses of mRNA sequences found in sRNA-mRNA interactions from each cluster. Motif analyses was performed using MEME suite (Bailey et al., 2009). The number of target sequences that contained the common motif and the E-value of MEME is also shown. (**C**) Identified motifs show sequence complementarity to known seed sequences. The green coloured nucleotide sequence indicates experimentally verified seed sequences. The Motif Alignment Search Tool (MAST) was used to determine the degree of complementarity between the identified motifs in putative mRNA targets and the sRNA. The MAST p-values indicate the overall match between the identified motifs and the sRNA sequence (Bailey et al., 2009).

Figure 4 - figure supplement 5. Identification of complementary sequence motifs in predicted GadY mRNA targets.

Same as in Figure 4 - figure supplement 4, but now for CyaR.

Figure 4 - figure supplement 6. Identification of complementary sequence motifs in predicted GcvB mRNA targets.

Same as in Figure 4 - figure supplement 3, but now for GcvB.

Figure 4 - figure supplement 7. Identification of complementary sequence motifs in predicted MgrR mRNA targets.

Same as in Figure 4 - figure supplement 1, but now for MgrR. The Venn diagram shows the overlap between the interactions found in all the MgrR sRNA-mRNA interactions, those

interactions uniquely found in the CLASH data (CLASH unique) and those supported by less than four reads (chimeras < 4 reads). Although the motif identified in the RIL-seq data was not significantly enriched, we identified as second complementary sequence motif that is significantly enriched in the CLASH unique data.

Figure 4 - figure supplement 8. Identification of complementary sequence motifs in predicted MicA mRNA targets.

Same as in Figure 4 - figure supplement 7, but now for MicA.

Figure 4 - figure supplement 9. Identification of complementary sequence motifs in predicted RybB mRNA targets.

Same as in Figure 4 - figure supplement 7, but now for RybB.

Figure 4 - figure supplement 10. Identification of complementary sequence motifs in predicted OmrB mRNA targets.

Same as in Figure 4 - figure supplement 7, but now for OmrB.

Figure 4 - figure supplement 11. Identification of complementary sequence motifs in predicted RyhB mRNA targets.

Same as in Figure 4 - figure supplement 7, but now for RyhB.

Figure 4 - figure supplement 12. Identification of complementary sequence motifs in predicted RprA mRNA targets.

Same as in Figure 4 - figure supplement 7, but now for RprA.

Figure 4 - figure supplement 13. CLASH targets are highly enriched in MAPS data

(**A**) Predicted CyaR mRNA targets are highly enriched in MAPS data (Lalaouna et al., 2018). The cumulative distribution plots show the cumulative frequencies of the log2-fold enrichment of transcripts in the MAPS data relative to the control sample. Values of the interacting mRNA partners found in the CLASH chimeras are shown in red, blue or yellow and all the other genes are in black. (**B**) Predicted GcvB mRNA targets are highly enriched in MAPS data (Lalaouna et al., 2019). The cumulative distribution plots show the cumulative frequencies of the log2-fold enrichment of transcripts in the MAPS data relative to the control sample. Values of the interacting mRNA partners found in the CLASH data are shown in red, blue or yellow and all the other genes are in black. The statistical significance of the

difference between the two distributions is represented as a p-value using Kolmogorov-Smirnov test.

Figure 5 - figure supplement 1. Impact of the identified interactions on gene expression levels of GcvB mRNA targets predicted by CLASH.

Plotted on the y-axis is the average expression profiles of the data from the wild-type strain. The x-axis shows the log2-fold change in expression of the targets upon GcvB over-expression in *Salmonella typhimurium* (Sharma et al., 2011). We assumed that over-expression of sRNAs in *S. typhimurium* would have a similar effect as in *E. coli.* We analysed all the mRNA fragments found in chimeras with GcvB (red), interactions only found in the CLASH data (CLASH unique; yellow) and those supported by less than four reads (less four chimeras; blue). The cumulative distribution plots show the cumulative frequencies of the t-statistics values of the interacting partners in red, blue or yellow and all other genes in black. The statistical significance of the difference between these two distributions is represented as a p-value using Kolmogorov-Smirnov test. T-statistic values were calculated using the eBayes function of the limma package (Ritchie et al., 2015).

Figure 5 - figure supplement 2. Impact of the identified interactions on gene expression levels of CyaR mRNA targets predicted by CLASH.

(**A**) Plotted on the y-axis is the average expression profiles of the data from the wild-type strain. The x-axis shows the log2-fold change in expression of the targets upon CyaR over-expression in *Escherichia coli* (De Lay and Gottesman, 2009). We analysed all the mRNA fragments found in chimeras with CyaR (red), interactions only found in the CLASH data (CLASH unique; yellow) and those supported by less than four reads (less four chimeras; blue). The cumulative distribution plots show the cumulative frequencies of the t-statistics values of the interacting partners in red, blue or yellow and all other genes in black. The statistical significance of the difference between these two distributions is represented as a p-value using Kolmogorov-Smirnov test.

Figure 5 - figure supplement 3. Impact of the identified interactions on gene expression levels of Spot42 mRNA targets predicted by CLASH.

Plotted on the y-axis is the average expression profiles of the data from the wild-type strain. The x-axis shows the log2-fold change in expression of the targets upon Spot42 over-expression in *Escherichia coli* (Beisel and Storz, 2011). We analysed all the mRNA fragments found in chimeras with Spot42, the predicted interactions only found in the CLASH data (CLASH unique) and those supported by less than four reads (less four chimeras). The cumulative distribution plots show the cumulative frequencies of the t-

statistics values of the interacting partners in red, blue or yellow and all other genes in black. The statistical significance of the difference between these two distributions is represented as a p-value using Kolmogorov-Smirnov test. T-statistic values were calculated using the eBayes function of the limma package (Ritchie et al., 2015).

Figure 5 - figure supplement 4. Impact of the identified interactions on gene expression levels of ArcZ mRNA targets predicted by CLASH.
Plotted on the y-axis is the average expression profiles of the data from the wild-type strain. The x-axis shows the log2-fold change in expression of the targets upon ArcZ over-expression in *Salmonella typhimurium* (Papenfort et al., 2009). We assumed that over-expression of sRNAs in *S. typhimurium* would have a similar effect as in *E. coli.* We analysed all the mRNA fragments found in chimeras with ArcZ, the predicted interactions only found in the CLASH data (CLASH unique) and those supported by less than four reads (less four chimeras). The cumulative distribution plots show the cumulative frequencies of the t-statistics values of the interacting partners in red, blue or yellow and all other genes in black. The statistical significance of the difference between these two distributions is represented as a p-value using Kolmogorov-Smirnov test. T-statistic values were calculated using the eBayes function of the limma package (Ritchie et al., 2015).

Figure 6 - figure supplement 1. sRNA-RNA interactions identified by CLASH are growth-stage specific. sRNA-sRNA network generated from the statistically significant CLASH interactions from two biological replicates, recovered at three main growth stages: exponential (OD_{600} 0.4 and 0.8), transition (OD_{600} 1.2, 1.8, 2.4) and early stationary (OD_{600} 3.0 and 4.0). The thickness of the edges is proportional to the $\log_2$(unique chimera count for each interaction). Only sRNAs transcribed from independent promoters were included in the analysis.

Figure 6 - figure supplement 2. Interactions between ArcZ, CyaR and GcvB are conserved. Alignments of ArcZ, CyaR and GcvB were compiled as previously described(van Nues et al., 2016). Names of the enteric bacteria from which the sequence was retrieved are given on the left. Indicated are possible stem-loops (brackets), seed regions (boxed in dashed lines) and their interactions with various sections of ArcZ, CyaR or GcvB (blue and purple bars) or with other sRNAs and mRNAs (black bars). The CyaR sequence indicated with a blue bar is predicted to interact with two regions in GcvB (see blue bars in GcvB alignment), including the second seed sequence. A second interaction (pink bars) involves the seed sequence regions of CyaR and GcvB.

Figure 8 - figure supplement 1. Identification of complementary sequence motifs in predicted glnA-3'UTR mRNA targets.

(**A**) Motif analyses of mRNA sequences found in *glnA*-3'UTR-mRNA interactions. All of the *glnA-3'UTR* interactions with mRNAs we found were only detected in our CLASH data. Motif analyses was performed using MEME suite (Bailey et al., 2009). The number of target sequences that contained the common motif and the E-value of MEME is also shown. (**B**) Identified motifs show sequence complementarity to the 3'UTR of *glnA*. Note that a very similar motif was identified in the RIL-seq data for *glnA*-3'UTR mRNA targets (Melamed et al., 2016). The Motif Alignment Search Tool (MAST) was used to determine the degree of complementarity between the identified motifs in putative mRNA targets and the putative sRNA. The MAST p-values indicate the overall match between the identified motifs and the sRNA sequence (Bailey et al., 2009).

Figure 8 - figure supplement 2. Identification of complementary sequence motifs in predicted CpxQ mRNA targets.

(**A**) Motif analyses of mRNA sequences found in *cpxP*-3'UTR/CpxQ interactions. The Venn diagram shows the overlap between the interactions found in all the CpxQ sRNA-mRNA interactions, those interactions uniquely found in the CLASH data (CLASH unique) and those supported by less than four reads (chimeras < 4 reads). Motif analyses was performed using MEME suite (Bailey et al., 2009). The number of target sequences that contained the common motif and the E-value of MEME is also shown. (**B**) Identified motifs show sequence complementarity to the 3'UTR of *cpxP*. These data are in good agreement with CpxQ mRNA target motifs identified in the RIL-seq data (Melamed et al., 2016). The Motif Alignment Search Tool (MAST) was used to determine the degree of complementarity between the identified motifs in putative mRNA targets and the putative sRNA. The MAST p-values indicate the overall match between the identified motifs and the sRNA sequence (Bailey et al., 2009). The green coloured nucleotide sequence indicates experimentally verified seed sequences (Chao and Vogel, 2016).

Figure 8 - figure supplement 3. Identification of complementary sequence motifs in predicted GadF mRNA targets

As in Figure 8 – supplement 2 but now for the GadF sRNA that originates from the 3' end of the *gadE* mRNA (this work and (Melamed et al., 2016))

Figure 8 - figure supplement 4. *YgaM*, *gadE* and *malG* contain sRNAs in their 3'UTRs.

Validation of *malG* 3'UTR (MalH), *ygaM* 3'UTR (YgaN) and *gadE* 3'UTR (GadF) sRNAs by Northern blot. Total RNA extracted from cells at the indicated optical densities (OD_{600}) was resolved on 8% PAA-UREA gels and subjected to Northern blotting using oligos that hybridize with the 3'UTR of the respective transcripts. The asterisk indicates cross-reactivity of the probe with the 5S rRNA. The locations of the 3'UTR-derived fragments are indicated. MalH and YgaN are ~110nt, whereas the GadF fragment is ~ 90nt.

Figure 8 - figure supplement 5. Hfq CLASH identifies known interactions between 3'-UTR derived sRNAs and mRNA targets.

(**A-C**) Heatmaps illustrating the number of chimeric fragments containing MicL (**A**) and SdhX (**C**) and where in the sRNA they map with respect to the known seed sequences(s). The boxes above indicate the known, experimentally validated seed sequences for the respective sRNAs. (**B**) The predicted base-pairing between MicL and a known mRNA target (*lpp)*. (**D**) The base-paring between SdhX and known targets (*katG* and *ackA*; 2 and 3 chimeras, respectively) represented by low chimera count are shown. The grey colored nucleotides represent the binding site in the mRNA target. The predicted interactions between the sRNAs and their mRNA targets are fully consistent with the literature (De Mets et al., 2018; Guo et al., 2014; Miyakoshi et al., 2018).

Figure 8 - figure supplement 6. Analysis of Exonuclease (TEX) RNA-seq datasets.

(**A, B**) Analysis of Terminator 5'-Phosphate Dependent Exonuclease (TEX) RNA-seq datasets (Thomason et al., 2015) indicates that YgaN has an independent promoter, while MalH is a degradation product of the *malEFG* operon. Genome browser tracks showing the location and normalized reads of *ygaM* and *malG* fragments in the absence of TEX (–TEX) and in the presence of TEX (+TEX). The *ygaM* and putative YgaN promoters are indicated. Independently transcribed YgaN could be further processed by RNases, at the site marked with a dashed vertical line.

Supplementary File legends

Supplementary File 1. Hyb pipeline output from the merged Hfq CLASH data.
Chromosome indicates the *E. coli* chromosome, sequence start and sequence end are the positions in the chimeric read that correspond to the first and second fragment.
Chromosome start and chromosome end are the positions in the *E. coli* K12 reference genome.

Supplementary File 2. Statistically filtered data. Chimeric reads were subsequently analyzed using a statistical pipeline described by (Waters et al., 2017). Only chimeric reads that had a Benjami-Hochberg adjusted p-value (bh_adj_p_value) of 0.05 or less were considered
The last three columns indicate in which growth phases the interactions were identified.
Min. MFE indicates the minimal folding energies of the chimera, which was calculated using RNADuplex from the ViennaRNA package (Lorenz et al., 2011).The two pairs in the intermolecular base-pairs and structure columns are separated by "&".

Supplementary File 3. Overview of sRNA-mRNA interactions found in the Hfq CLASH data and compared to the RIL-seq data. Shown are the statisitcally filtered sRNA-mRNA interactions identified in the Hfq CLASH data. Genomic sequences of the sRNA and mRNA fragments found in the chimeras are also provided. Total_hybrids indicates the total number of interactions involving these sequences that were found. Min. MFE indicates the minimal folding enrgies of the chimera, which was calculated using RNADuplex from the ViennaRNA package (Lorenz et al., 2011). The last column indicates which of the sRNA-mRNA interactions were also found in the RIL-seq S-chimera data (Melamed et al., 2016).

Supplementary File 4. Overview of sRNA-sRNA interactions found in the Hfq CLASH data and compared to the RIL-seq data. Shown are the statistically filtered sRNA-sRNA interactions identified in the Hfq CLASH data. Genomic sequences of the sRNA fragments found in the chimeras are also provided. Total_hybrids indicates the total number of interactions involving these sequences that were found. Min. MFE indicates the minimal folding enrgies of the chimera, which was calculated using RNADuplex from the ViennaRNA package (Lorenz et al., 2011). The last column indicates which of the sRNA-mRNA interactions were also found in the RIL-seq S-chimera data (Melamed et al., 2016).

Supplementary File 5. Overview of putative 3'UTR derived sRNAs. 3'UTR-mRNA and mRNA-3'UTR interactions were isolated from the statistically filtered data and compared against the RILseq data (Melamed et al., 2016), Salmonella TIERseq data (Chao et al., 2012) and RNA-seq data that was used transcription start sites in *E. coli* (Thomason et al.,

2015). TEX insensitive are RNA fragments in 3'UTRs that are not sensitive to Terminator 5'-Phosphate Dependent Exonuclease treatment and therefore may be generated by an independent promoter. TEX sensitive are RNA fragments that likely have 5' monophosphates as, according to the TEX data, they were degraded by TEX.

Supplementary File 6. Overview of 3'UTR-mRNA interactions found in the Hfq CLASH data and compared to the RIL-seq data. Shown are the statistically filtered 3'UTR-mRNA interactions identified in the Hfq CLASH data. Genomic sequences of the 3'UTR and mRNA fragments found in the chimeras are also provided. Total_hybrids indicates the total number of interactions involving these sequences that were found. Min. MFE indicates the minimal folding enrgies of the chimera, which was calculated using RNADuplex from the ViennaRNA package (Lorenz et al., 2011). The last column indicates which of the sRNA-mRNA interactions were also found in the RIL-seq S-chimera data (Melamed et al., 2016). The mRNA fragment location column indicates where in the mRNA target the putative 3'UTR-derived sRNA was base-paired.

Supplementary File 7. Experimentally validated interactions in the statistically filtered Hfq CLASH data. Chimeric reads were analyzed using a statistical pipeline described by (Waters et al., 2017). Only chimeric reads that had a Benjami-Hochberg adjusted p-value (bh_adj_p_value) of 0.05 or less were considered. Shown are the sRNA-mRNA interactions that were experimentally validated, retrieved from sRNATarbase 3.0 (Wang et al., 2016) and recent literature (Bianco et al., 2019; Chao and Vogel, 2016; De Mets et al., 2018; Guo et al., 2014; Lalaouna et al., 2015b; Miyakoshi et al., 2018). Min. MFE indicates the minimal folding energies of the chimera, which was calculated using RNADuplex from the ViennaRNA package (Lorenz et al., 2011). The last three columns indicate in which growth phases the interactions were identified.

Supplementary File 8. Motif analyses of chimeric fragments that mapped to 5' UTRs.
PyMotif from the pyCRAC package was used for these analyses. For the motif search analyses we first clustered overlapping chimeric fragments into a single contig. For the 5'UTR motif analyses we used 356 clusters.

Supplementary File 9. Motif analyses of chimeric fragments that mapped to 3' UTRs.
PyMotif from the pyCRAC package was used for these analyses. For the motif search analyses we first clustered overlapping chimeric fragments into a single contig. For the 3'UTR motif analyses we used 188 clusters.

Supplementary File 10. Oligonucleotides used in this study

Supplementary Source data legends

Figure 1 - figure supplement 1 - source data 1. Source data for Figure 1 - figure supplement 1A and B.

References

Andrade JM, Santos RF, Chelysheva I, Ignatova Z, Arraiano CM. 2018. The RNA-binding protein Hfq is important for ribosome biogenesis and affects translation fidelity. *EMBO J* **37**. doi:10.15252/embj.201797631

Azam MS, Vanderpool CK. 2015. Talk among yourselves: RNA sponges mediate cross talk between functionally related messenger RNAs. *EMBO J* **34**:1436–1438.

Baev M V., Baev D, Jansco Radek A, Campbell JW. 2006a. Growth of Escherichia coli MG1655 on LB medium: Monitoring utilization of amino acids, peptides, and nucleotides with transcriptional microarrays. *Appl Microbiol Biotechnol* **71**:317–322. doi:10.1007/s00253-005-0310-5

Baev M V., Baev D, Radek AJ, Campbell JW. 2006b. Growth of Escherichia coli MG1655 on LB medium: Determining metabolic strategy with transcriptional microarrays. *Appl Microbiol Biotechnol* **71**:323–328. doi:10.1007/s00253-006-0392-8

Bailey TL, Boden M, Buske FA, Frith M, Grant CE, Clementi L, Ren J, Li WW, Noble WS. 2009. MEME Suite: Tools for motif discovery and searching. *Nucleic Acids Res*. doi:10.1093/nar/gkp335

Balleza E, López-Bojorquez LN, Martínez-Antonio A, Resendis-Antonio O, Lozada-Chávez I, Balderas-Martínez YI, Encarnación S, Collado-Vides J. 2009. Regulation by transcription factors in bacteria: Beyond description. *FEMS Microbiol Rev* **33**:133–151. doi:10.1111/j.1574-6976.2008.00145.x

Bandyra KJ, Said N, Pfeiffer V, Górna MW, Vogel J, Luisi BF. 2012. The Seed Region of a Small RNA Drives the Controlled Destruction of the Target mRNA by the Endoribonuclease RNase E. *Mol Cell* **47**:943–953. doi:10.1016/j.molcel.2012.07.015

Beisel CL, Storz G. 2011. The Base-Pairing RNA Spot 42 Participates in a Multioutput Feedforward Loop to Help Enact Catabolite Repression in Escherichia coli. *Mol Cell* **41**:286–297. doi:10.1016/j.molcel.2010.12.027

Bianco CM, Fröhlich KSA, Vanderpoola CK. 2019. Bacterial cyclopropane fatty acid synthase mRNA is targeted by activating and repressing small RNAs. *J Bacteriol*.

doi:10.1128/JB.00461-19
Blattner FR, Plunkett G, Bloch CA, Perna NT, Burland V, Riley M, Collado-Vides J, Glasner JD, Rode CK, Mayhew GF, Gregor J, Davis NW, Kirkpatrick HA, Goeden MA, Rose DJ, Mau B, Shao Y. 1997. The complete genome sequence of Escherichia coli K-12. *Science (80-)*. doi:10.1126/science.277.5331.1453
Bouvier M, Sharma CM, Mika F, Nierhaus KH, Vogel J. 2008. Small RNA binding to 5' mRNA coding region inhibits translational initiation. *Mol Cell* **32**:827–837.
Bruce HA, Du D, Matak-Vinkovic D, Bandyra KJ, Broadhurst RW, Martin E, Sobott F, Shkumatov A V., Luisi BF. 2018. Analysis of the natively unstructured RNA/protein-recognition core in the Escherichia coli RNA degradosome and its interactions with regulatory RNA/Hfq complexes. *Nucleic Acids Res*. doi:10.1093/nar/gkx1083
Chao Y, Li L, Girodat D, Forstner KU, Said N, Corcoran C, Smiga M, Papenfort K, Reinhardt R, Wieden HJ, Luisi BF, Vogel J. 2017. *in vivo* cleavage map illuminates the central cole of RNase E in coding and non-coding RNA pathways. *Mol Cell* **65**:39–51. doi:10.1016/j.molcel.2016.11.002
Chao Y, Papenfort K, Reinhardt R, Sharma CM, Vogel J. 2012. An atlas of Hfq-bound transcripts reveals 3' UTRs as a genomic reservoir of regulatory small RNAs. *EMBO J* **31**:4005–4019.
Chao Y, Vogel J. 2016. A 3' UTR-Derived Small RNA Provides the Regulatory Noncoding Arm of the Inner Membrane Stress Response. *Mol Cell* **61**:352–363. doi:10.1016/j.molcel.2015.12.023
De Lay N, Gottesman S. 2009. The crp-activated small noncoding regulatory RNA CyaR (RyeE) links nutritional status to group behavior. *J Bacteriol* **191**:461–476. doi:10.1128/JB.01157-08
De Mets F, Van Melderen L, Gottesman S. 2018. Regulation of acetate metabolism and coordination with the TCA cycle via a processed small RNA. *Proc Natl Acad Sci*. doi:10.1073/pnas.1815288116
Faigenbaum-Romm R, Reich A, Gatt YE, Barsheshet M, Argaman L, Margalit H. 2020. Hierarchy in Hfq Chaperon Occupancy of Small RNA Targets Plays a Major Role in Their Regulation. *Cell Rep* **30**:3127-3138.e6. doi:10.1016/j.celrep.2020.02.016
Feng L, Rutherford ST, Papenfort K, Bagert JD, Van Kessel JC, Tirrell DA, Wingreen NS, Bassler BL. 2015. A Qrr noncoding RNA deploys four different regulatory mechanisms to optimize quorum-sensing dynamics. *Cell* **160**:228–240. doi:10.1016/j.cell.2014.11.051
Figueroa-Bossi N, Bossi L. 2018. Sponges and Predators in the Small RNA WorldRegulating with RNA in Bacteria and Archaea. American Society of Microbiology. pp. 441–451. doi:10.1128/microbiolspec.rwr-0021-2018

Granneman S, Kudla G, Petfalski E, Tollervey D. 2009. Identification of protein binding sites on U3 snoRNA and pre-rRNA by UV cross-linking and high-throughput analysis of cDNAs. *Proc Natl Acad Sci U S A* **106**:9613–9618. doi:10.1073/pnas.0901997106

Gulliver EL, Wright A, Lucas DD, Mégroz M, Kleifeld O, Schittenhelm RB, Powell DR, Seemann T, Bulitta JB, Harper M, Boyce JD. 2018. Determination of the small RNA GcvB regulon in the Gram-negative bacterial pathogen Pasteurella multocida and identification of the GcvB seed binding region. *RNA*. doi:10.1261/rna.063248.117

Guo MS, Updegrove TB, Gogol EB, Shabalina SA, Gross CA, Storz G. 2014. MicL, a new σE-dependent sRNA, combats envelope stress by repressing synthesis of Lpp, the major outer membrane lipoprotein. *Genes Dev* **28**:1620–1634. doi:10.1101/gad.243485.114

Han K, Tjaden B, Lory S. 2016. GRIL-seq provides a method for identifying direct targets of bacterial small regulatory RNA by in vivo proximity ligation. *Nat Microbiol* **2**:16239.

Helwak A, Kudla G, Dudnakova T, Tollervey D. 2013. Mapping the human miRNA interactome by CLASH reveals frequent noncanonical binding. *Cell* **153**:654–665.

Holmqvist E, Vogel J. 2018. RNA-binding proteins in bacteria. *Nat Rev Microbiol*. doi:10.1038/s41579-018-0049-5

Holmqvist E, Wagner EGH. 2017. Impact of bacterial sRNAs in stress responses. *Biochem Soc Trans*. doi:10.1042/BST20160363

Holmqvist E, Wright PR, Li L, Bischler T, Barquist L, Reinhardt R, Backofen R, Vogel J. 2016. Global RNA recognition patterns of post-transcriptional regulators Hfq and CsrA revealed by UV crosslinking in~vivo. *EMBO J* **35**:e201593360--1011.

Hör J, Gorski SA, Vogel J. 2018. Bacterial RNA Biology on a Genome Scale. *Mol Cell* 785–799. doi:10.1016/j.molcel.2017.12.023

Hör J, Vogel J. 2017. Global snapshots of bacterial RNA networks. *EMBO J* **36**:245–247. doi:10.15252/embj.201696072

Jost D, Nowojewski A, Levine E. 2013. Regulating the many to benefit the few: Role of weak small RNA targets. *Biophys J*. doi:10.1016/j.bpj.2013.02.020

Kavita K, de Mets F, Gottesman S. 2018. New aspects of RNA-based regulation by Hfq and its partner sRNAs. *Curr Opin Microbiol* **42**:53–61. doi:10.1016/j.mib.2017.10.014

Kortmann J, Narberhaus F. 2012. Bacterial RNA thermometers: molecular zippers and switches. *Nat Rev Microbiol* **10**:255–265.

Kudla G, Granneman S, Hahn D, Beggs JD, Tollervey D. 2011. Cross-linking, ligation, and sequencing of hybrids reveals RNA-RNA interactions in yeast. *Proc Natl Acad Sci U S A* **108**:10010–10015. doi:10.1073/pnas.1017386108

Lalaouna D, Carrier M-C, Semsey S, Brouard J-S, Wang J, Wade JT, Massé E. 2015a. A 3' External Transcribed Spacer in a tRNA Transcript Acts as a Sponge for Small RNAs to

Prevent Transcriptional Noise. *Mol Cell* **58**:393–405.
Lalaouna D, Eyraud A, Devinck A, Prévost K, Massé E. 2019. GcvB small RNA uses two distinct seed regions to regulate an extensive targetome. *Mol Microbiol*. doi:10.1111/mmi.14168
Lalaouna D, Morissette A, Carrier MC, Massé E. 2015b. DsrA regulatory RNA represses both hns and rbsD mRNAs through distinct mechanisms in Escherichia coli. *Mol Microbiol* **98**:357–369. doi:10.1111/mmi.13129
Lalaouna D, Prévost K, Laliberté G, Houé V, Massé E. 2018. Contrasting silencing mechanisms of the same target mRNA by two regulatory RNAs in Escherichia coli. *Nucleic Acids Res*. doi:10.1093/nar/gkx1287
Lorenz R, Bernhart SH, Höner Zu Siederdissen C, Tafer H, Flamm C, Stadler PF, Hofacker IL. 2011. ViennaRNA Package 2.0. *Algorithms Mol Biol* **6**:26. doi:10.1186/1748-7188-6-26
Mäder U, Nicolas P, Depke M, Pané-Farré J, Debarbouille M, van der Kooi-Pol MM, Guérin C, Dérozier S, Hiron A, Jarmer H, Leduc A, Michalik S, Reilman E, Schaffer M, Schmidt F, Bessières P, Noirot P, Hecker M, Msadek T, Völker U, van Dijl JM. 2016. Staphylococcus aureus Transcriptome Architecture: From Laboratory to Infection-Mimicking Conditions. *PLOS Genet* **12**:e1005962. doi:10.1371/journal.pgen.1005962
Magoč T, Salzberg SL. 2011. FLASH: Fast length adjustment of short reads to improve genome assemblies. *Bioinformatics*. doi:10.1093/bioinformatics/btr507
Martínez-Antonio A, Janga SC, Thieffry D. 2008. Functional organisation of Escherichia coli transcriptional regulatory network. *J Mol Biol* **381**:238–247. doi:10.1016/j.jmb.2008.05.054
Melamed S, Adams PP, Zhang A, Zhang H, Storz G. 2020. RNA-RNA Interactomes of ProQ and Hfq Reveal Overlapping and Competing Roles. *Mol Cell* **77**:411-425.e7. doi:10.1016/j.molcel.2019.10.022
Melamed S, Faigenbaum-Romm R, Peer A, Reiss N, Shechter O, Bar A, Altuvia Y, Argaman L, Margalit H. 2018. Mapping the small RNA interactome in bacteria using RIL-seq. *Nat Protoc* **13**:1–33.
Melamed S, Peer A, Faigenbaum-Romm R, Gatt YE, Reiss N, Bar A, Altuvia Y, Argaman L, Margalit H. 2016. Global Mapping of Small RNA-Target Interactions in Resource Global Mapping of Small RNA-Target Interactions in Bacteria. *Mol Cell* **63**:884–897. doi:10.1016/j.molcel.2016.07.026
Miyakoshi M, Chao Y, Vogel J. 2015a. Regulatory small RNAs from the 3’ regions of bacterial mRNAs. *Curr Opin Microbiol*. doi:10.1016/j.mib.2015.01.013
Miyakoshi M, Chao Y, Vogel J. 2015b. Cross talk between ABC transporter mRNAs via a target mRNA-derived sponge of the GcvB small RNA. *EMBO J* **34**:e201490546--1492.

doi:10.15252/embj.201490546
Miyakoshi M, Matera G, Maki K, Sone Y, Vogel J. 2018. Functional expansion of a TCA cycle operon mRNA by a 3′ end-derived small RNA. *Nucleic Acids Res*. doi:10.1093/nar/gky1243
Mohammad F, Green R, Buskirk AR. 2019. A systematically-revised ribosome profiling method for bacteria reveals pauses at single-codon resolution. *Elife* **8**. doi:10.7554/eLife.42591
Monteiro C, Papenfort K, Hentrich K, Ahmad I, Le Guyon S, Reimann R, Grantcharova N, Römling U. 2012. Hfq and Hfq-dependent small RNAs are major contributors to multicellular development in Salmonella enterica serovar typhimurium. *RNA Biol*. doi:10.4161/rna.19682
Moon K, Gottesman S. 2011. Competition among Hfq-binding small RNAs in Escherichia coli. *Mol Microbiol* **82**:1545–1562. doi:10.1111/j.1365-2958.2011.07907.x
Morita T, Maki K, Aiba H. 2005. RNase E-based ribonucleoprotein complexes: Mechanical basis of mRNA destabilization mediated by bacterial noncoding RNAs. *Genes Dev*. doi:10.1101/gad.1330405
Mouali Y El, Gaviria-Cantin T, Sá Nchez-Romero MA, Gibert M, Westermann AJ, Rg Vogel J, Balsalobre C. 2018. CRP-cAMP mediates silencing of Salmonella virulence at the post-transcriptional level 1–26. doi:10.1371/journal.pgen.1007401
Navarro Llorens JM, Tormo A, Martínez-García E. 2010. Stationary phase in gram-negative bacteria. *FEMS Microbiol Rev* **34**:476–495. doi:10.1111/j.1574-6976.2010.00213.x
Nitzan M, Rehani R, Margalit H. 2017. Integration of Bacterial Small RNAs in Regulatory Networks. *Annu Rev Biophys* **46**:131–148. doi:10.1146/annurev-biophys-070816-034058
Papenfort K, Pfeiffer V, Lucchini S, Sonawane A, Hinton JCD, Vogel J. 2008. Systematic deletion of Salmonella small RNA genes identifies CyaR, a conserved CRP-dependent riboregulator of OmpX synthesis. *Mol Microbiol*. doi:10.1111/j.1365-2958.2008.06189.x
Papenfort K, Said N, Welsink T, Lucchini S, Hinton JCDD, Vogel J. 2009. Specific and pleiotropic patterns of mRNA regulation by ArcZ, a conserved, Hfq-dependent small RNA. *Mol Microbiol* **74**:139–158. doi:10.1111/j.1365-2958.2009.06857.x
Pei XY, Dendooven T, Sonnleitner E, Chen S, Bläsi U, Luisi BF. 2019. Architectural principles for Hfq/Crc-mediated regulation of gene expression. *Elife* **8**. doi:10.7554/eLife.43158
Pletnev P, Osterman I, Sergiev P, Bogdanov A, Dontsova O. 2015. Survival guide: Escherichia coli in the stationary phase. *Acta Naturae* **7**:22–33.
Quinlan AR, Hall IM. 2010. BEDTools: a flexible suite of utilities for comparing genomic features. *Bioinformatics* **26**:841–842.

Ritchie ME, Phipson B, Wu D, Hu Y, Law CW, Shi W, Smyth GK. 2015. Limma powers differential expression analyses for RNA-sequencing and microarray studies. *Nucleic Acids Res*. doi:10.1093/nar/gkv007

Salvail H, Caron M-P, Bélanger J, Massé E. 2013. Antagonistic functions between the RNA chaperone Hfq and an sRNA regulate sensitivity to the antibiotic colicin. *EMBO J* **32**:2764–2778. doi:10.1038/emboj.2013.205

Santiago-Frangos A, Woodson SA. 2018. Hfq chaperone brings speed dating to bacterial sRNA. *Wiley Interdiscip Rev RNA* **9**:e1475. doi:10.1002/wrna.1475

Sedlyarova N, Shamovsky I, Bharati BK, Epshtein V, Chen J, Gottesman S, Schroeder R, Nudler E. 2016. sRNA-Mediated Control of Transcription Termination in E.~coli. *Cell* **167**:111--121.e13.

Sezonov G, Joseleau-Petit D, D'Ari R. 2007. Escherichia coli physiology in Luria-Bertani broth. *J Bacteriol* **189**:8746–8749. doi:10.1128/JB.01368-07

Sharma CM, Papenfort K, Pernitzsch SR, Mollenkopf H-J, Hinton JCD, Vogel J. 2011. Pervasive post-transcriptional control of genes involved in amino acid metabolism by the Hfq-dependent GcvB small RNA. *Mol Microbiol* **81**:1144–1165.

Sharma E, Sterne-Weiler T, O'Hanlon D, Blencowe BJ. 2016. Global Mapping of Human RNA-RNA Interactions. *Mol Cell* **62**:618–626. doi:10.1016/j.molcel.2016.04.030

Shimoni Y, Friedlander G, Hetzroni G, Niv G, Altuvia S, Biham O, Margalit H. 2007. Regulation of gene expression by small non-coding RNAs: a quantitative view. *Mol Syst Biol* **3**:138.

Sittka A, Pfeiffer V, Tedin K, Vogel J. 2007. The RNA chaperone Hfq is essential for the virulence of Salmonella typhimurium. *Mol Microbiol*. doi:10.1111/j.1365-2958.2006.05489.x

Smirnov A, Förstner KU, Holmqvist E, Otto A, Günster R, Becher D, Reinhardt R, Vogel J. 2016. Grad-seq guides the discovery of ProQ as a major small RNA-binding protein. *Proc Natl Acad Sci* **113**:11591–11596. doi:10.1073/pnas.1609981113

Smirnov A, Wang C, Drewry LL, Vogel J. 2017. Molecular mechanism of mRNA repression in *trans* by a ProQ-dependent small RNA. *EMBO J* **36**:1029–1045. doi:10.15252/embj.201696127

Sonnleitner E, Bläsi U. 2014. Regulation of Hfq by the RNA CrcZ in Pseudomonas aeruginosa Carbon Catabolite Repression. *PLoS Genet* **10**:e1004440. doi:10.1371/journal.pgen.1004440

Storz G, Vogel J, Wassarman KM. 2011. Regulation by Small RNAs in Bacteria: Expanding Frontiers. *Mol Cell* **43**:880–891. doi:10.1016/j.molcel.2011.08.022

Thomason MK, Bischler T, Eisenbart SK, Förstner KU, Zhang A, Herbig A, Nieselt K, Sharma CM, Storza G. 2015. Global transcriptional start site mapping using differential

1748 RNA sequencing reveals novel antisense RNAs in Escherichia coli. *J Bacteriol*.
1749 doi:10.1128/JB.02096-14
1750 Tjaden B. 2015. De novo assembly of bacterial transcriptomes from RNA-seq data. *Genome*
1751 *Biol* **16**:1–10. doi:10.1186/s13059-014-0572-2
1752 Travis AJ, Moody J, Helwak A, Tollervey D, Kudla G. 2013. Hyb: A bioinformatics pipeline
1753 for the analysis of CLASH (crosslinking, ligation and sequencing of hybrids) data.
1754 *Methods*.
1755 Tree JJ, Granneman S, McAteer SP, Tollervey D, Gally DL. 2014. Identification of
1756 bacteriophage-encoded anti-sRNAs in pathogenic Escherichia coli. *Mol Cell* **55**:199–
1757 213. doi:10.1016/j.molcel.2014.05.006
1758 Updegrove TB, Zhang A, Storz G. 2016. Hfq: The flexible RNA matchmaker. *Curr Opin*
1759 *Microbiol* **30**:133–138. doi:10.1016/j.mib.2016.02.003
1760 van Nues R, Schweikert G, de Leau E, Selega A, Langford A, Franklin R, Iosub I,
1761 Wadsworth P, Sanguinetti G, Granneman S. 2017. Kinetic CRAC uncovers a role for
1762 Nab3 in determining gene expression profiles during stress. *Nat Commun* **8**:12.
1763 doi:10.1038/s41467-017-00025-5
1764 van Nues RW, Castro-Roa D, Yuzenkova Y, Zenkin N. 2016. Ribonucleoprotein particles of
1765 bacterial small non-coding RNA IsrA (IS61 or McaS) and its interaction with RNA
1766 polymerase core may link transcription to mRNA fate. *Nucleic Acids Res* **44**:2577–
1767 2592.
1768 Vogel J, Luisi BF. 2011. Hfq and its constellation of RNA. *Nat Rev Microbiol* **9**:578–589.
1769 Wang J, Liu T, Zhao B, Lu Q, Wang Z, Cao Y, Li W. 2016. sRNATarBase 3.0: An updated
1770 database for sRNA-target interactions in bacteria. *Nucleic Acids Res* **44**:D248–D253.
1771 doi:10.1093/nar/gkv1127
1772 Wang J, Rennie W, Liu C, Carmack CS, Prévost K, Caron MP, Massé E, Ding Y, Wade JT.
1773 2015. Identification of bacterial sRNA regulatory targets using ribosome profiling.
1774 *Nucleic Acids Res*. doi:10.1093/nar/gkv1158
1775 Waters LS, Storz G. 2009. Regulatory RNAs in Bacteria. *Cell* **136**:615–628.
1776 doi:10.1016/j.cell.2009.01.043
1777 Waters SA, McAteer SP, Kudla G, Pang I, Deshpande NP, Amos TG, Leong KW, Wilkins
1778 MR, Strugnell R, Gally DL, Tollervey D, Tree JJ. 2017. Small RNA interactome of
1779 pathogenic *E. coli* revealed through crosslinking of RNase E. *EMBO J* **36**:374–387.
1780 doi:10.15252/embj.201694639
1781 Webb S, Hector RD, Kudla G, Granneman S. 2014. PAR-CLIP data indicate that Nrd1-
1782 Nab3-dependent transcription termination regulates expression of hundreds of protein
1783 coding genes in yeast. *Genome Biol* **15**:R8. doi:10.1186/gb-2014-15-1-r8
1784 Wilson KS, Hippel PH Von. 1995. Transcription termination at intrinsic terminators: The role

of the RNA hairpin (Escherichia coli/RNA polymerase/rho-independent termination). *Biochemistry* **92**:8793–8797. doi:10.1073/pnas.92.19.8793

Wu X, Bartel DP. 2017. KpLogo: Positional k -mer analysis reveals hidden specificity in biological sequences. *Nucleic Acids Res*. doi:10.1093/nar/gkx323

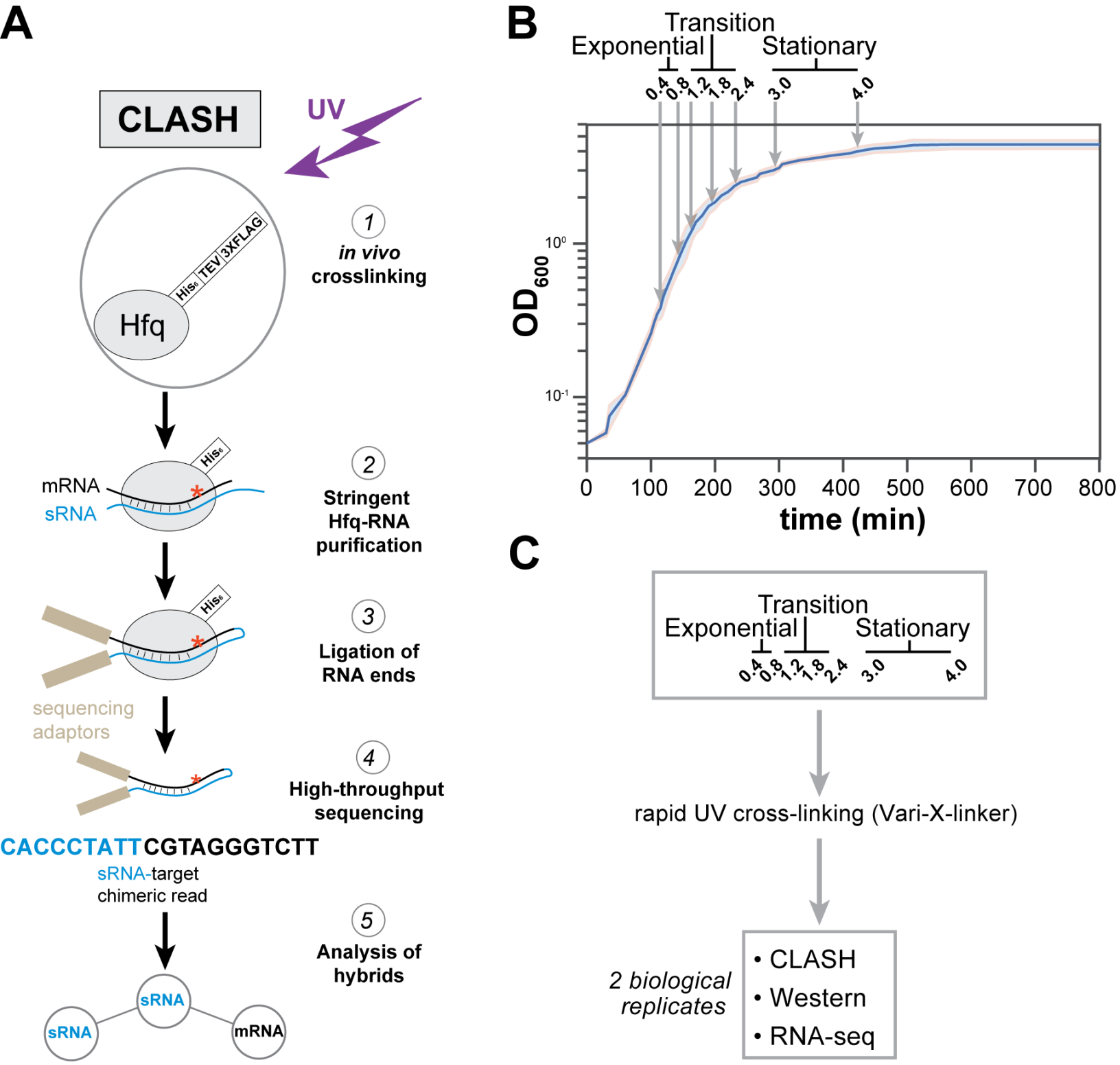
A
CLASH
UV
Hfq
His6 TEV 3XFLAG
1
in vivo
crosslinking
mRNA
sRNA
His6
2
Stringent
Hfq-RNA
purification
His6
3
Ligation of
RNA ends
sequencing
adaptors
4
High-throughput
sequencing
CACCCTATTCGTAGGGTCTT
sRNA-target
chimeric read
5
Analysis of
hybrids
sRNA
sRNA
mRNA
B
Transition
Exponential
Stationary
0.4
0.8
1.2
1.8
2.4
3.0
4.0
OD600
10^0
10^-1
0
100
200
300
400
500
600
700
800
time (min)
C
Transition
Exponential
Stationary
0.4
0.8
1.2
1.8
2.4
3.0
4.0
rapid UV cross-linking (Vari-X-linker)
2 biological
replicates
• CLASH
• Western
• RNA-seq

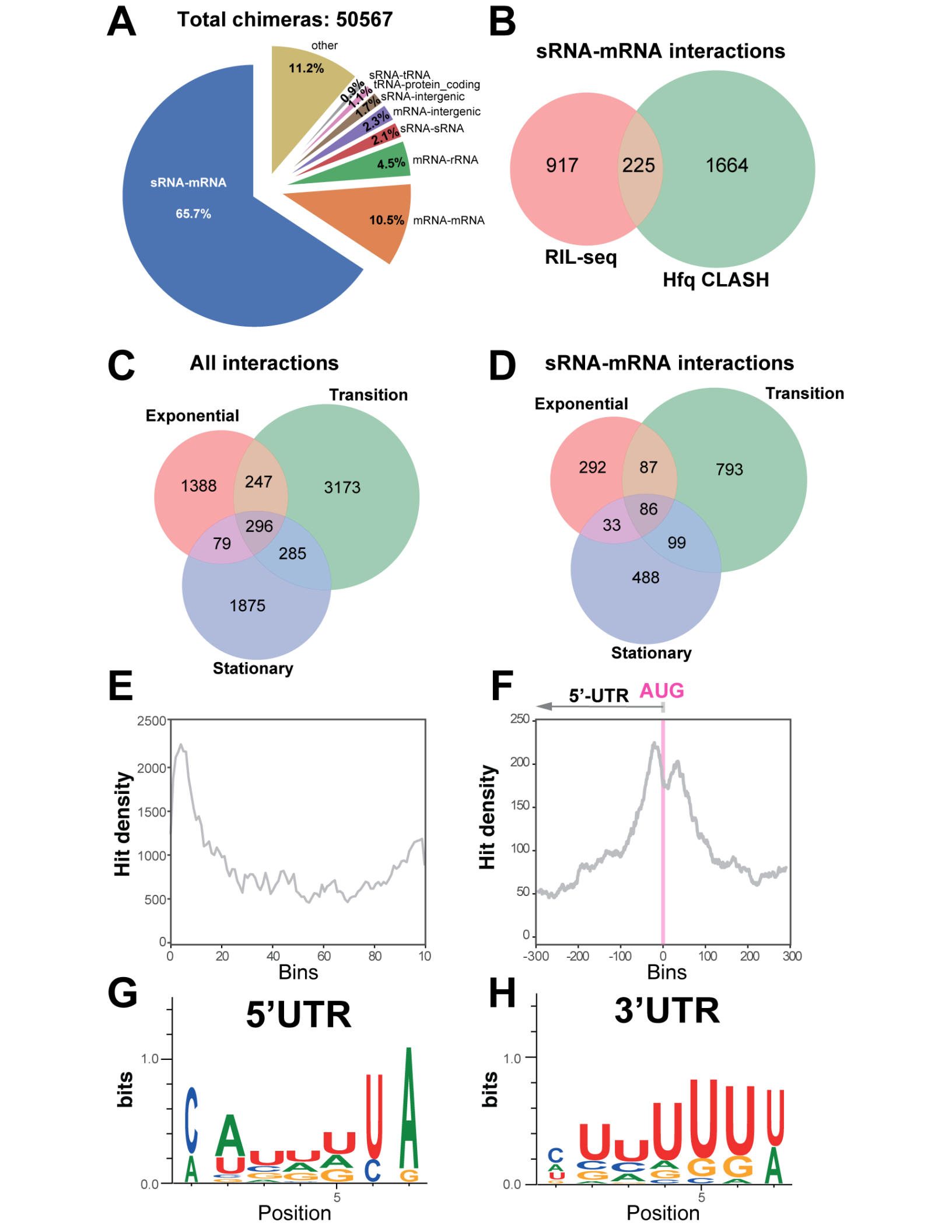
A
Total chimeras: 50567
other
11.2%
sRNA-tRNA
0.9%
tRNA-protein_coding
1.1%
sRNA-intergenic
1.7%
mRNA-intergenic
2.3%
sRNA-sRNA
2.1%
mRNA-rRNA
4.5%
mRNA-mRNA
10.5%
sRNA-mRNA
65.7%
B
sRNA-mRNA interactions
917
225
1664
RIL-seq
Hfq CLASH
C
All interactions
Exponential
Transition
Stationary
1388
247
3173
296
79
285
1875
D
sRNA-mRNA interactions
Exponential
Transition
Stationary
292
87
793
86
33
99
488
E
Hit density
Bins
F
5'-UTR
AUG
Hit density
Bins
G
5'UTR
bits
Position
H
3'UTR
bits
Position

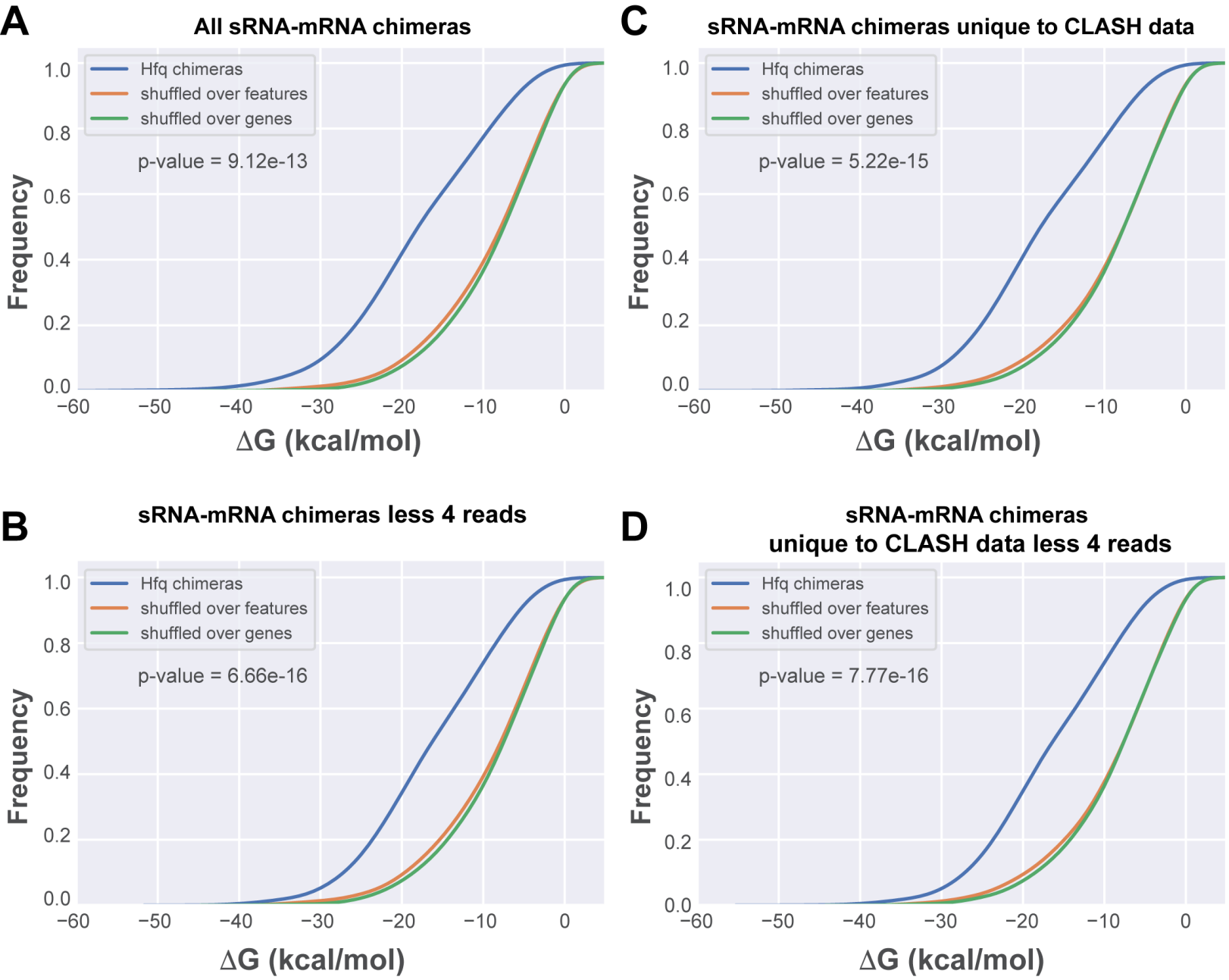
A
All sRNA-mRNA chimeras
Hfq chimeras
shuffled over features
shuffled over genes
p-value = 9.12e-13
Frequency
ΔG (kcal/mol)
C
sRNA-mRNA chimeras unique to CLASH data
Hfq chimeras
shuffled over features
shuffled over genes
p-value = 5.22e-15
Frequency
ΔG (kcal/mol)
B
sRNA-mRNA chimeras less 4 reads
Hfq chimeras
shuffled over features
shuffled over genes
p-value = 6.66e-16
Frequency
ΔG (kcal/mol)
D
sRNA-mRNA chimeras
unique to CLASH data less 4 reads
Hfq chimeras
shuffled over features
shuffled over genes
p-value = 7.77e-16
Frequency
ΔG (kcal/mol)

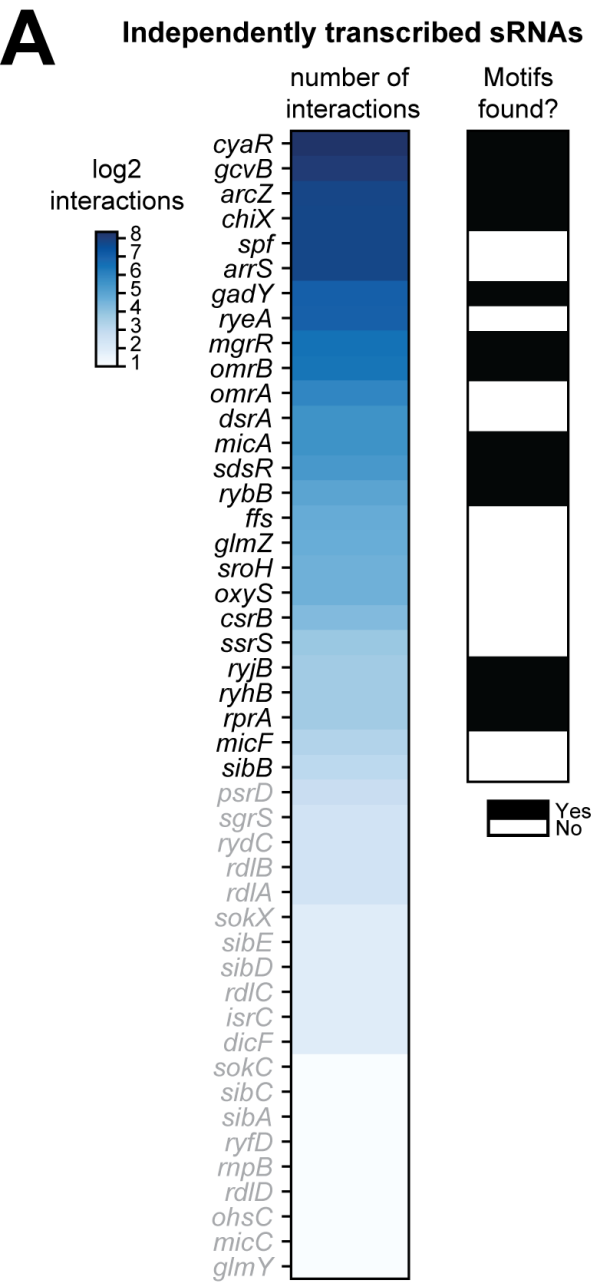
A
Independently transcribed sRNAs
number of interactions
Motifs found?
log2 interactions
8
7
6
5
4
3
2
1
cyaR
gcvB
arcZ
chiX
spf
arrS
gadY
ryeA
mgrR
omrB
omrA
dsrA
micA
sdsR
rybB
ffs
glmZ
sroH
oxyS
csrB
ssrS
ryjB
ryhB
rprA
micF
sibB
psrD
sgrS
rydC
rdlB
rdlA
sokX
sibE
sibD
rdlC
isrC
dicF
sokC
sibC
sibA
ryfD
rnpB
rdlD
ohsC
micC
glmY
Yes
No

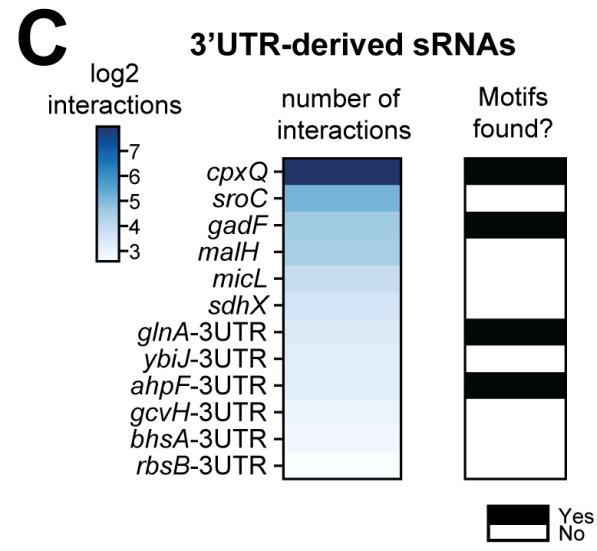
C
3'UTR-derived sRNAs
log2 interactions
number of interactions
Motifs found?
7
6
5
4
3
cpxQ
sroC
gadF
malH
micL
sdhX
glnA-3UTR
ybiJ-3UTR
ahpF-3UTR
gcvH-3UTR
bhsA-3UTR
rbsB-3UTR
Yes
No

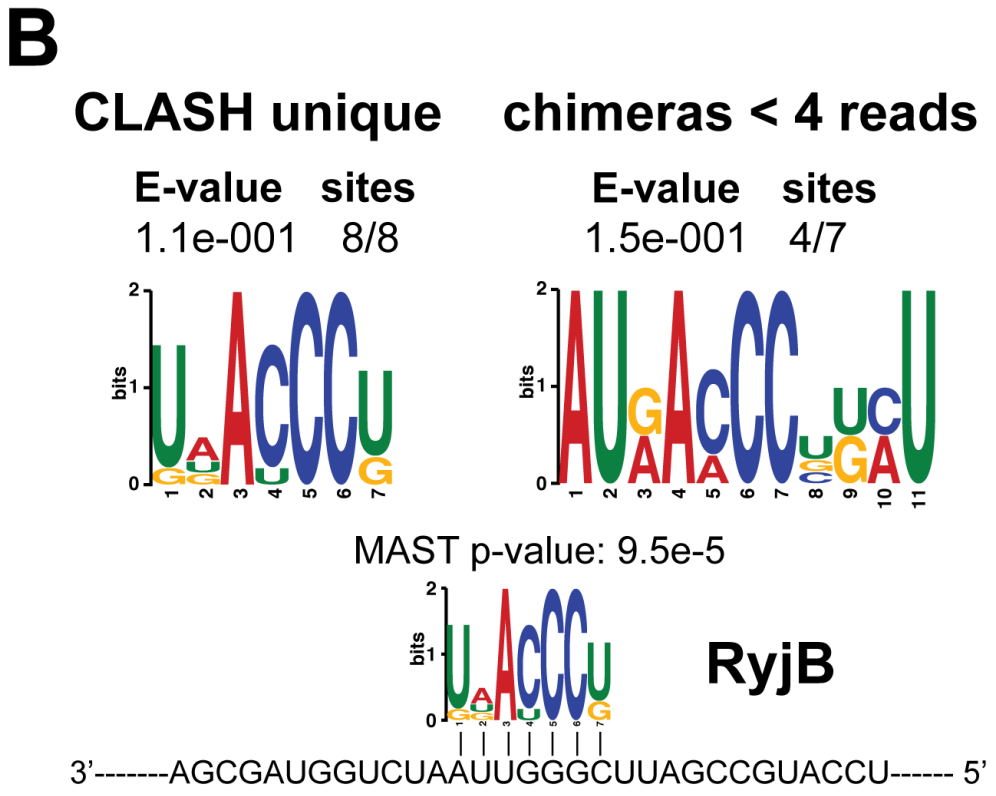
B
CLASH unique
chimeras < 4 reads
E-value
sites
1.1e-001
8/8
E-value
sites
1.5e-001
4/7
bits
MAST p-value: 9.5e-5
RyjB
3'-------AGCGAUGGUCUAAUUGGGCUUAGCCGUACCU------ 5'

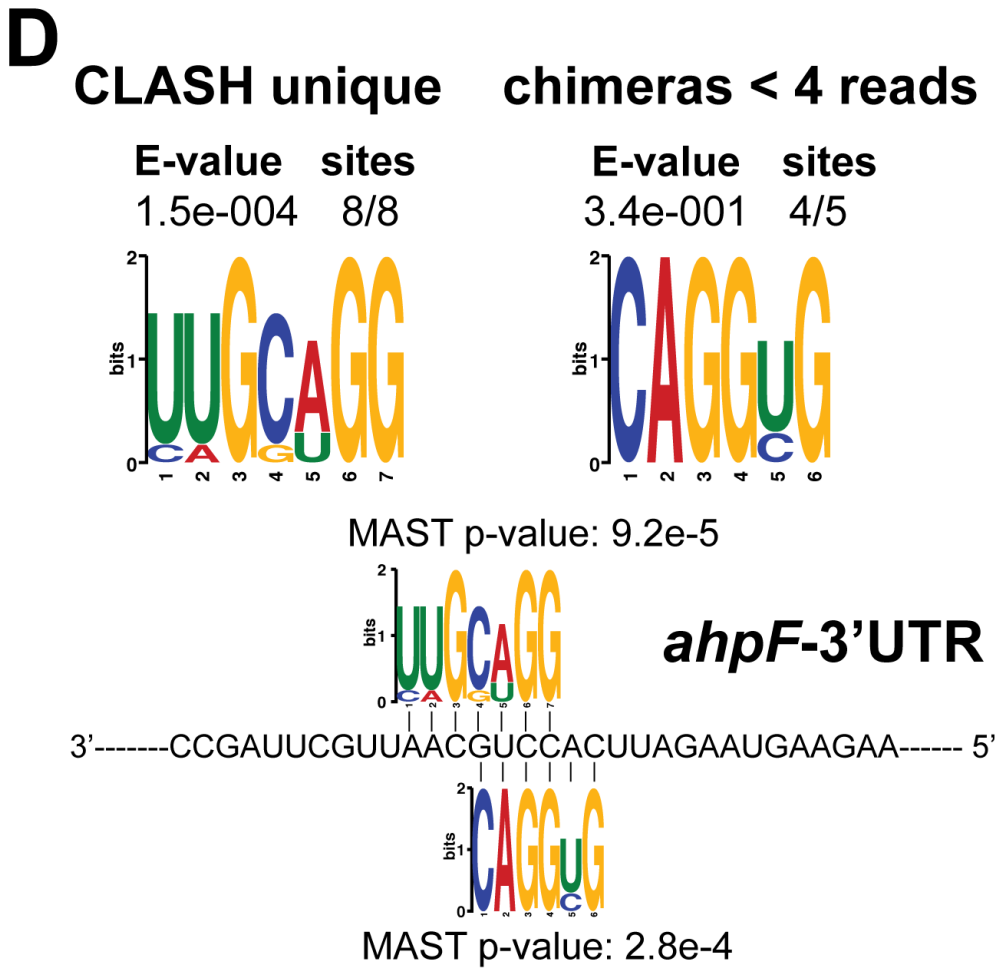
D
CLASH unique
chimeras < 4 reads
E-value
sites
1.5e-004
8/8
E-value
sites
3.4e-001
4/5
bits
MAST p-value: 9.2e-5
ahpF-3'UTR
3'-------CCGAUUCGUUAACGUCCACUUAGAAUGAAGAA------ 5'
MAST p-value: 2.8e-4

A

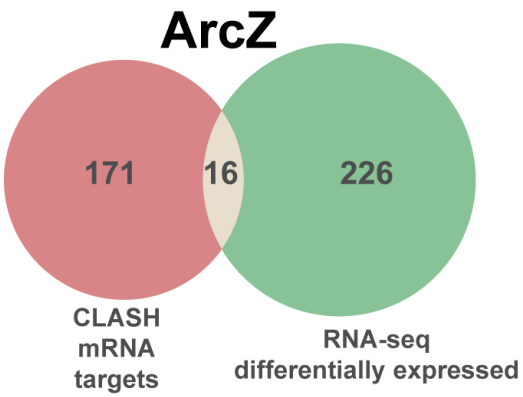

sRNA-mRNA interactions	p-value
All	0.06997
Unique to CLASH	0.10931
less four reads	0.13185

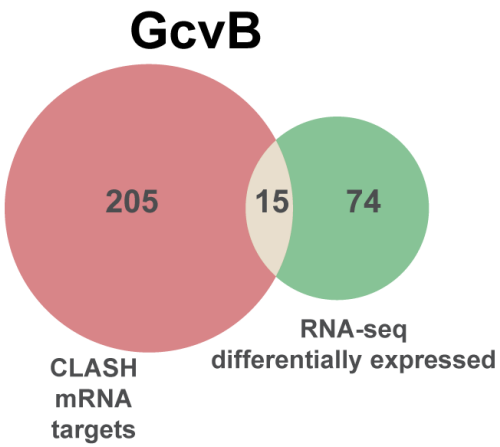

sRNA-mRNA interactions	p-value
All	0.00000457
Unique to CLASH	0.52782
less four reads	0.02742

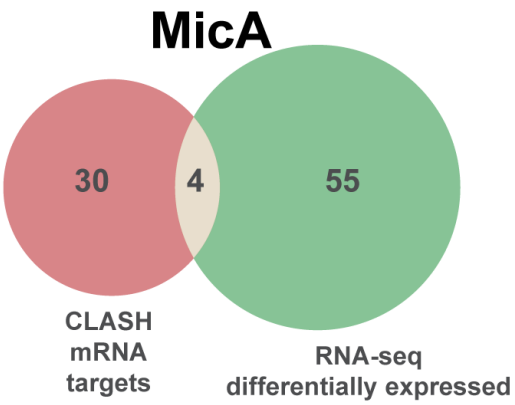

sRNA-mRNA interactions	p-value
All	0.00089
Unique to CLASH	0.71542
less four reads	0.26036

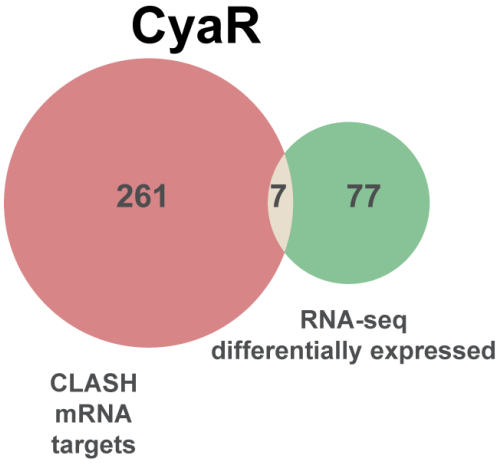

sRNA-mRNA interactions	p-value
All	0.10790
Unique to CLASH	0.15334
less four reads	0.12742

B

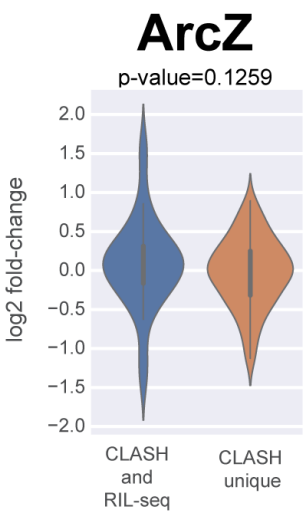

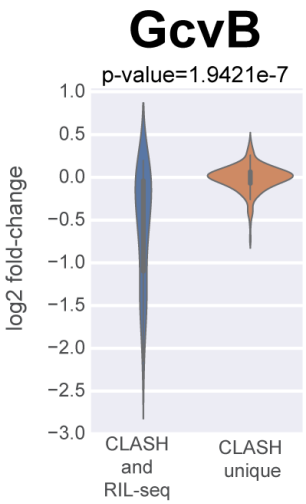

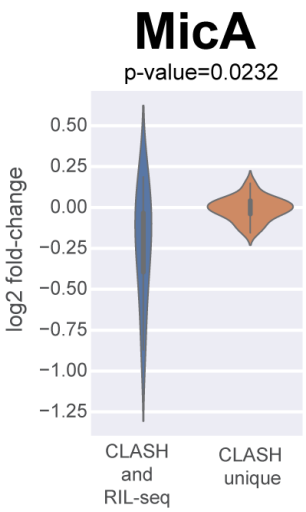

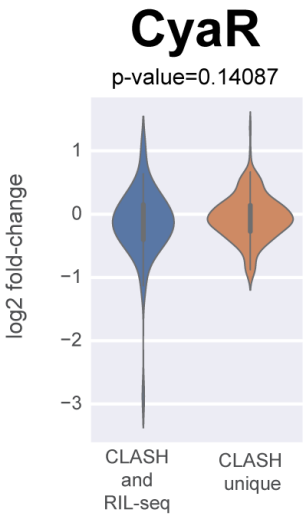

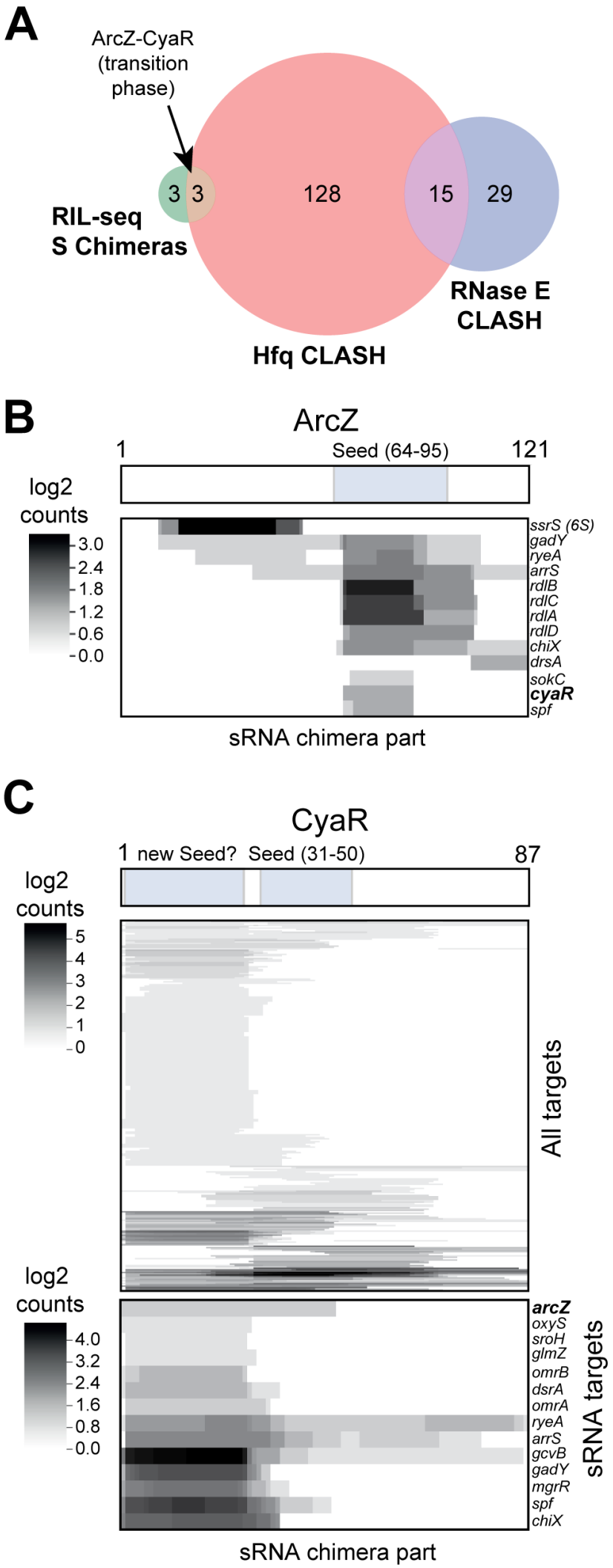
A
ArcZ-CyaR
(transition
phase)
3
3
128
15
29
RIL-seq
S Chimeras
RNase E
CLASH
Hfq CLASH
B
ArcZ
1
Seed (64-95)
121
log2
counts
3.0
2.4
1.8
1.2
0.6
0.0
ssrS (6S)
gadY
ryeA
arrS
rdlB
rdlC
rdlA
rdlD
chiX
drsA
sokC
cyaR
spf
sRNA chimera part
C
CyaR
1
new Seed?
Seed (31-50)
87
log2
counts
5
4
3
2
1
0
All targets
log2
counts
4.0
3.2
2.4
1.6
0.8
0.0
arcZ
oxyS
sroH
glmZ
omrB
dsrA
omrA
ryeA
arrS
gcvB
gadY
mgrR
spf
chiX
sRNA targets
sRNA chimera part

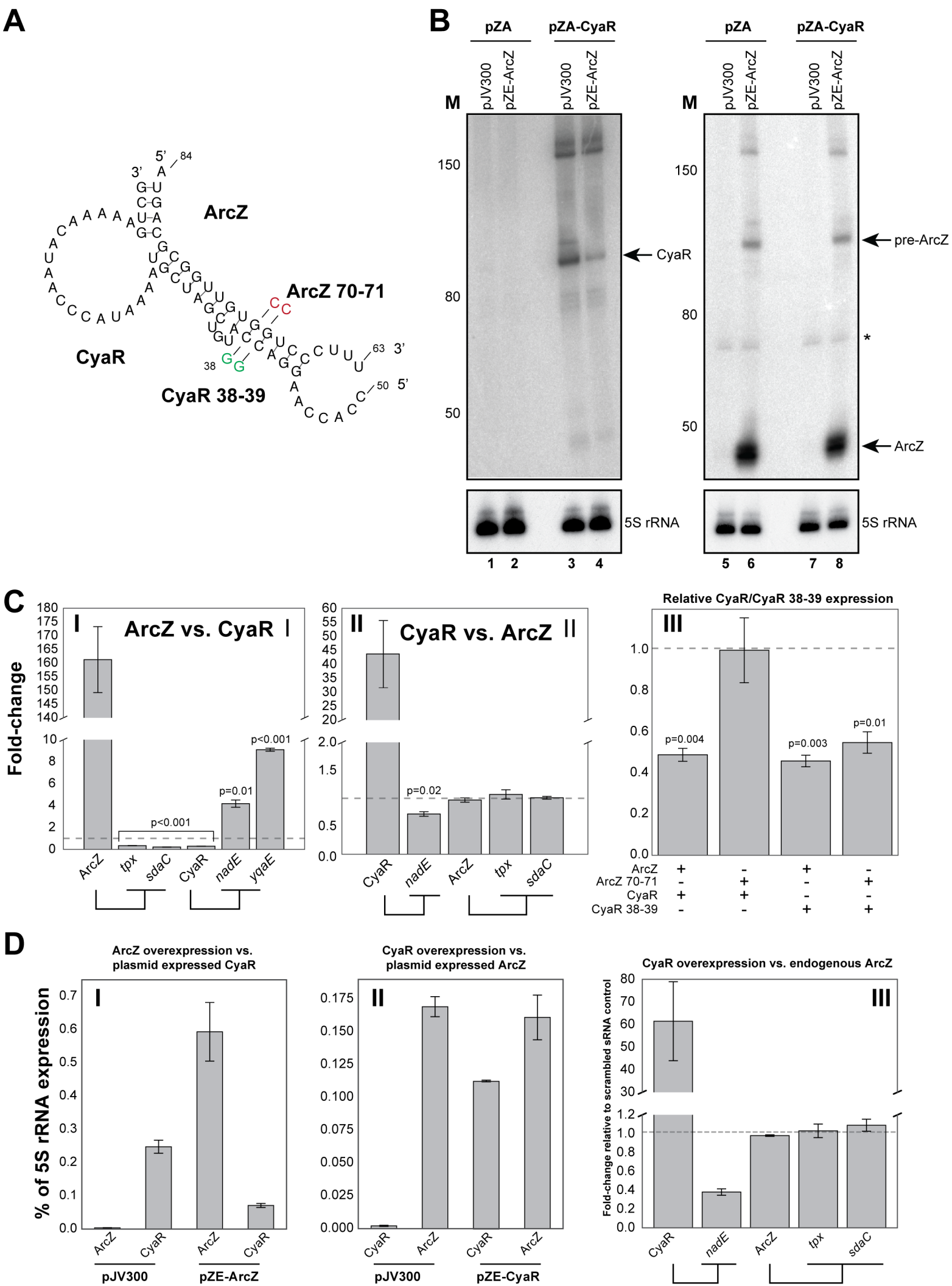
A
ArcZ
ArcZ 70-71
CyaR
CyaR 38-39
5'
3'
84
63
38
50
B
pZA
pZA-CyaR
pJV300
pZE-ArcZ
M
150
80
50
CyaR
pre-ArcZ
*
ArcZ
5S rRNA
1 2 3 4
5 6 7 8
C
Fold-change
I ArcZ vs. CyaR I
II CyaR vs. ArcZ II
III
Relative CyaR/CyaR 38-39 expression
p<0.001
p=0.01
p<0.001
p=0.02
p=0.004
p=0.003
p=0.01
ArcZ
tpx
sdaC
CyaR
nadE
yqaE
ArcZ 70-71
CyaR 38-39
D
% of 5S rRNA expression
ArcZ overexpression vs. plasmid expressed CyaR
CyaR overexpression vs. plasmid expressed ArcZ
CyaR overexpression vs. endogenous ArcZ
Fold-change relative to scrambled sRNA control
pJV300
pZE-ArcZ
pZE-CyaR

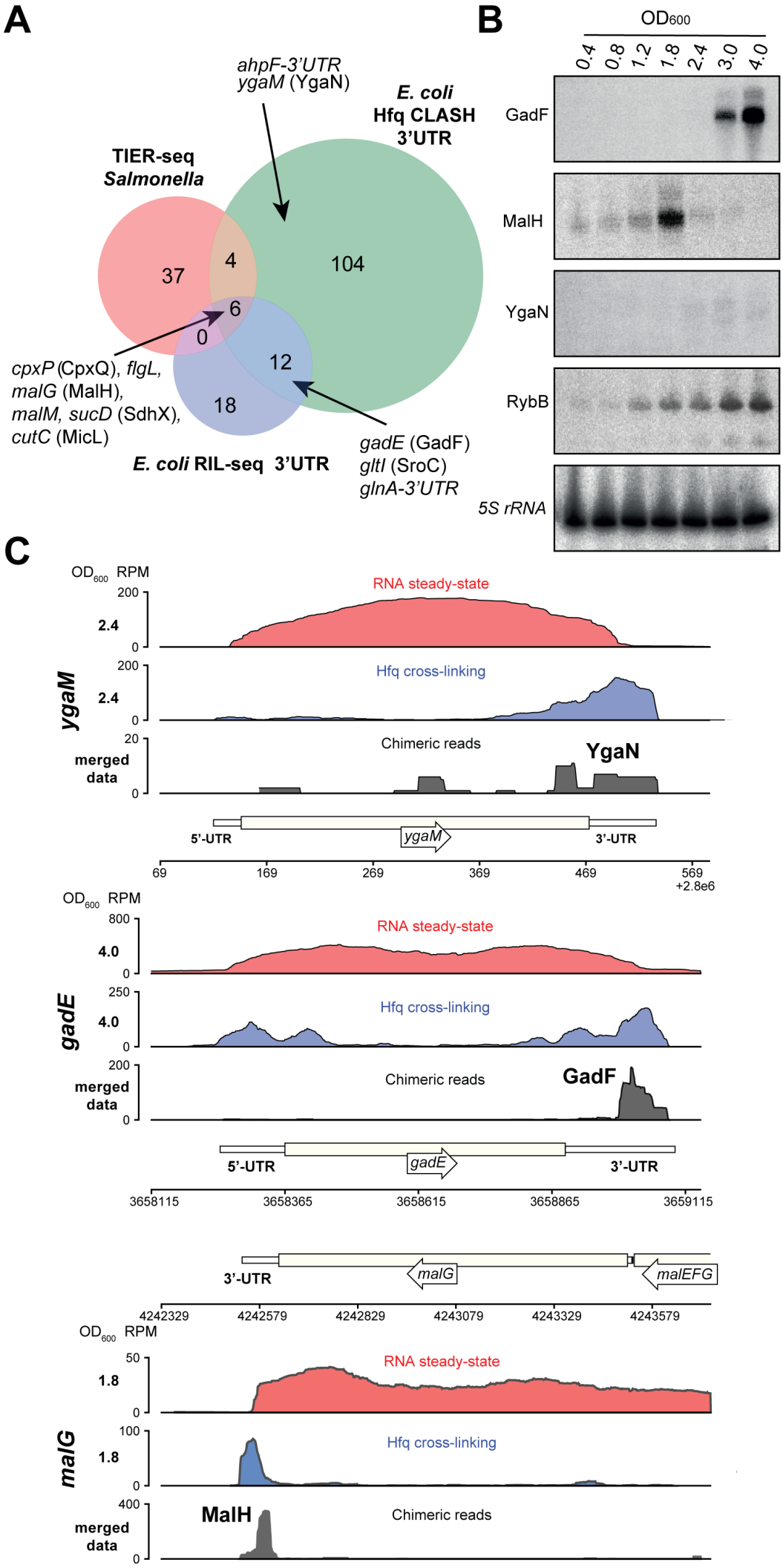
A
ahpF-3'UTR
ygaM (YgaN)
E. coli
Hfq CLASH
3'UTR
TIER-seq
Salmonella
37
4
104
6
0
12
18
cpxP (CpxQ), flgL,
malG (MalH),
malM, sucD (SdhX),
cutC (MicL)
E. coli RIL-seq 3'UTR
gadE (GadF)
gltI (SroC)
glnA-3'UTR
B
OD600
0.4
0.8
1.2
1.8
2.4
3.0
4.0
GadF
MalH
YgaN
RybB
5S rRNA
C
OD600 RPM
RNA steady-state
Hfq cross-linking
Chimeric reads
YgaN
merged data
ygaM
5'-UTR
3'-UTR
69
169
269
369
469
569
+2.8e6
GadF
gadE
3658115
3658365
3658615
3658865
3659115
malG
malEFG
4242329
4242579
4242829
4243079
4243329
4243579
MalH

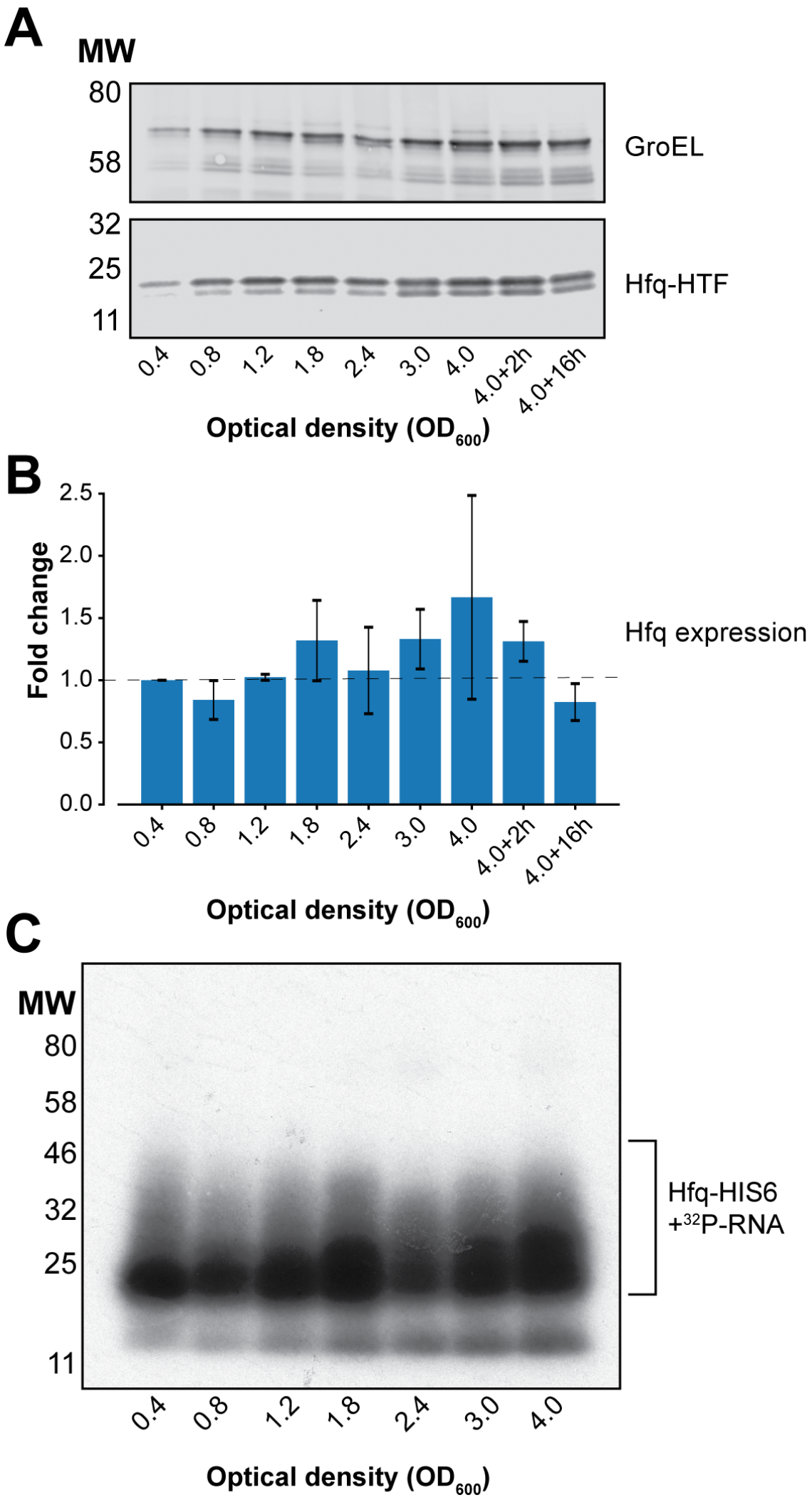
A
MW
80
58
32
25
11
GroEL
Hfq-HTF
0.4
0.8
1.2
1.8
2.4
3.0
4.0
4.0+2h
4.0+16h
Optical density (OD600)
B
Fold change
2.5
2.0
1.5
1.0
0.5
0.0
Hfq expression
Optical density (OD600)
C
MW
80
58
46
32
25
11
Hfq-HIS6
+32P-RNA
Optical density (OD600)

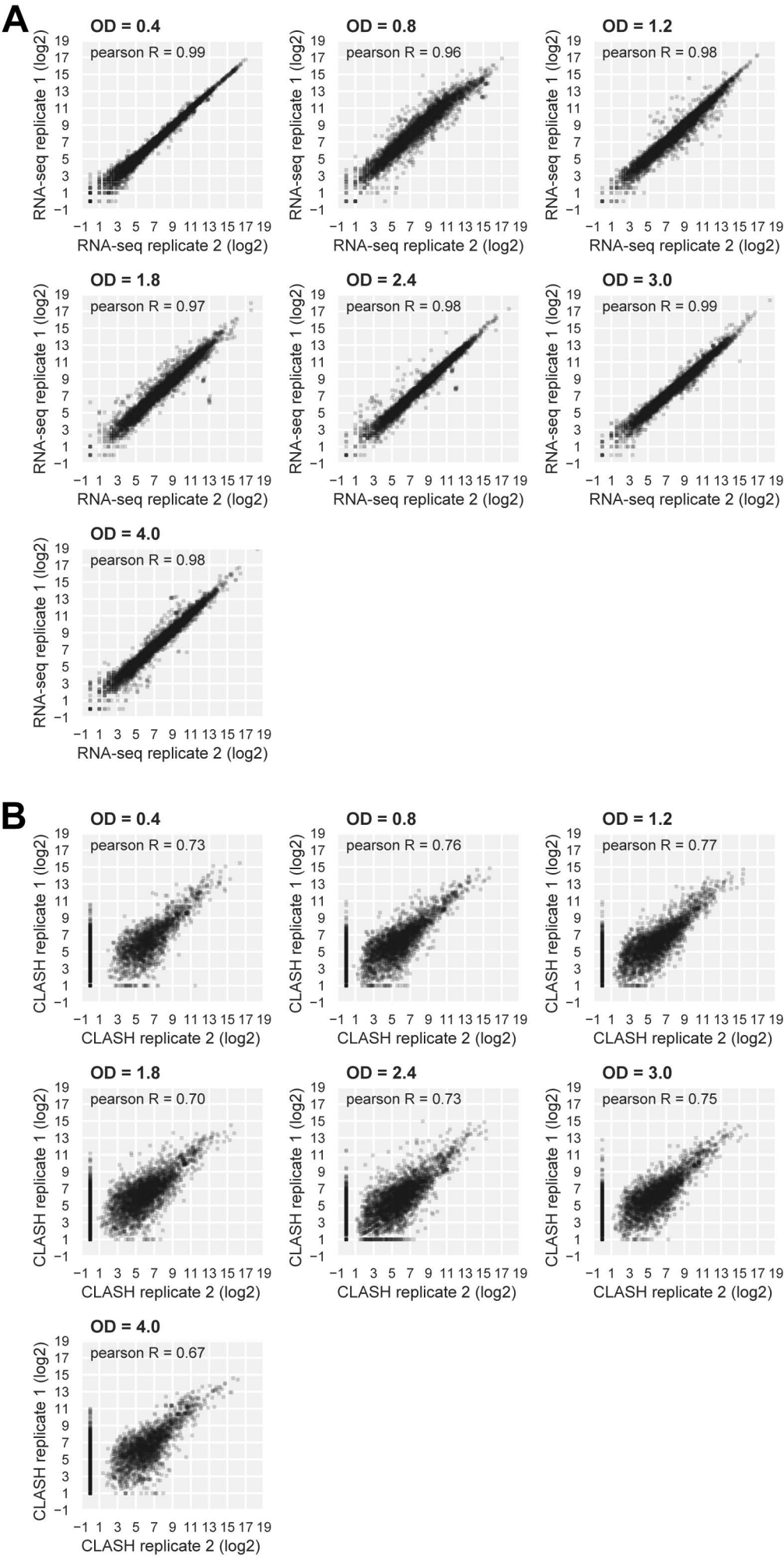
A
OD = 0.4
pearson R = 0.99
OD = 0.8
pearson R = 0.96
OD = 1.2
pearson R = 0.98
OD = 1.8
pearson R = 0.97
OD = 2.4
pearson R = 0.98
OD = 3.0
pearson R = 0.99
OD = 4.0
pearson R = 0.98
RNA-seq replicate 1 (log2)
RNA-seq replicate 2 (log2)
B
OD = 0.4
pearson R = 0.73
OD = 0.8
pearson R = 0.76
OD = 1.2
pearson R = 0.77
OD = 1.8
pearson R = 0.70
OD = 2.4
pearson R = 0.73
OD = 3.0
pearson R = 0.75
OD = 4.0
pearson R = 0.67
CLASH replicate 1 (log2)
CLASH replicate 2 (log2)

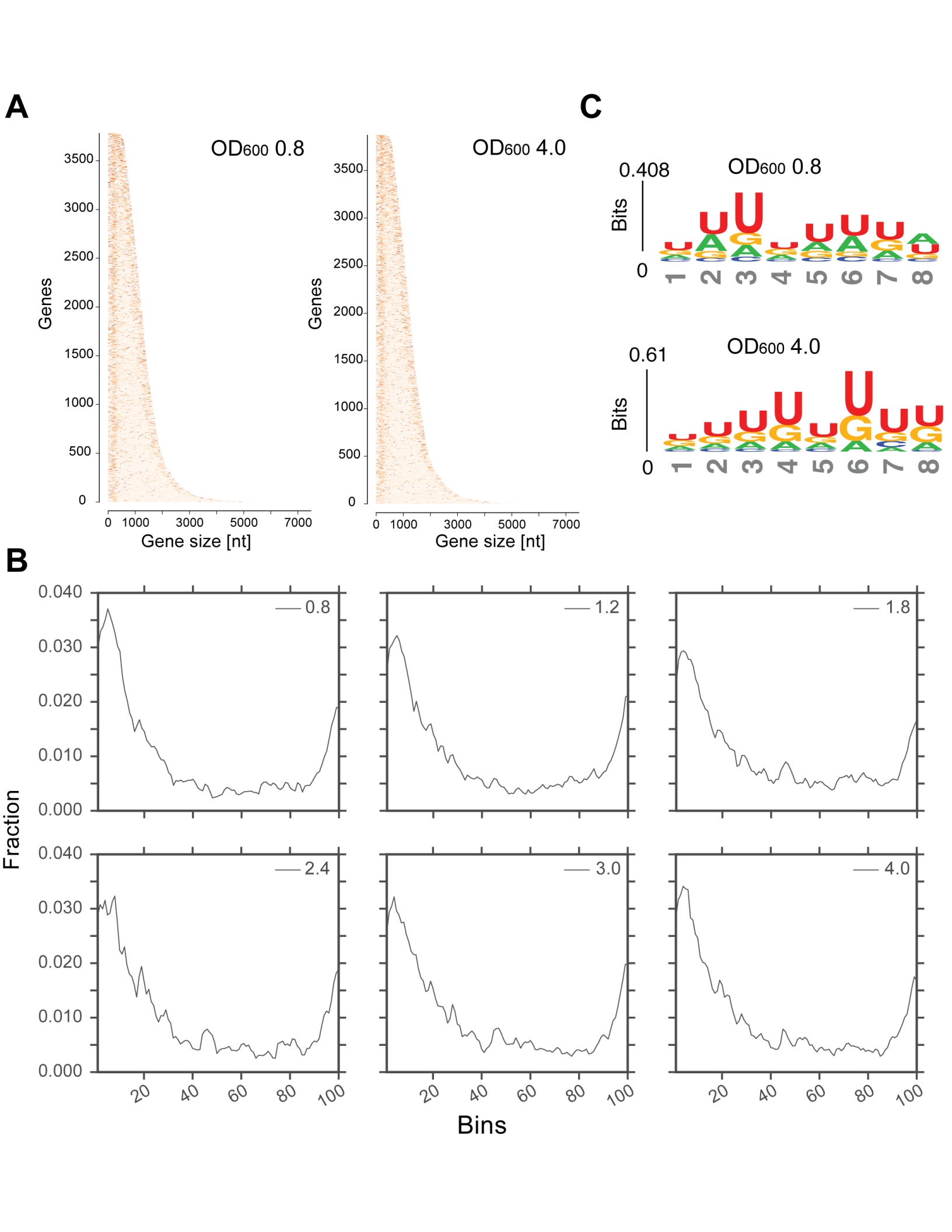
A
OD600 0.8
OD600 4.0
Genes
Gene size [nt]
0
500
1000
1500
2000
2500
3000
3500
0
1000
3000
5000
7000
C
0.408
Bits
0
1
2
3
4
5
6
7
8
0.61
B
0.8
1.2
1.8
2.4
3.0
4.0
Fraction
0.040
0.030
0.020
0.010
0.000
20
40
60
80
100
Bins

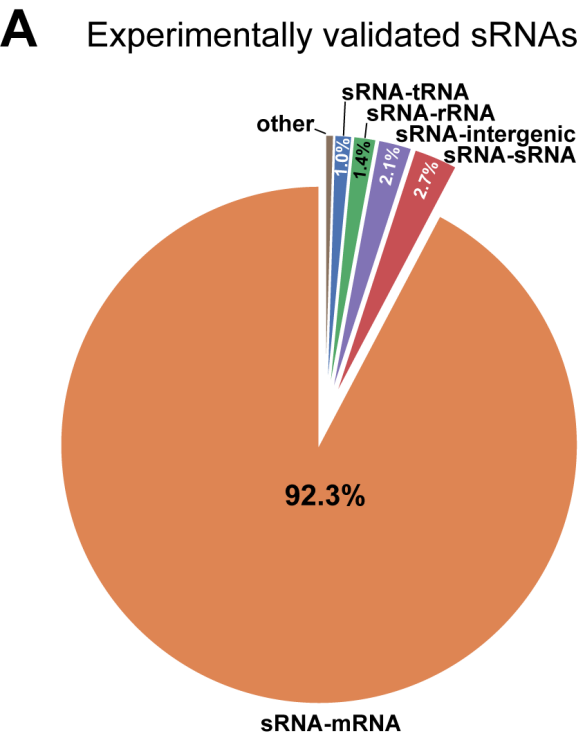
A
Experimentally validated sRNAs
sRNA-tRNA
other
sRNA-rRNA
sRNA-intergenic
sRNA-sRNA
1.0%
1.4%
2.1%
2.7%
92.3%
sRNA-mRNA

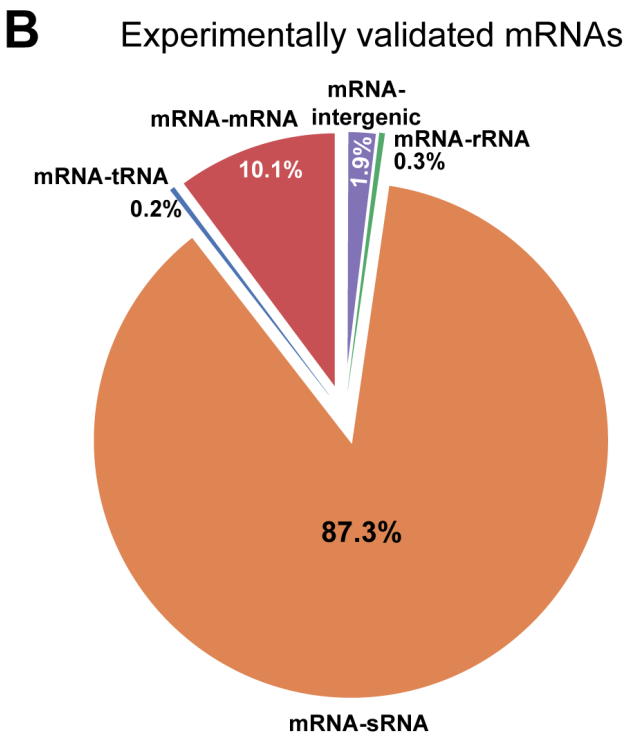
B
Experimentally validated mRNAs
mRNA-
intergenic
mRNA-mRNA
mRNA-rRNA
0.3%
mRNA-tRNA
0.2%
10.1%
1.9%
87.3%
mRNA-sRNA

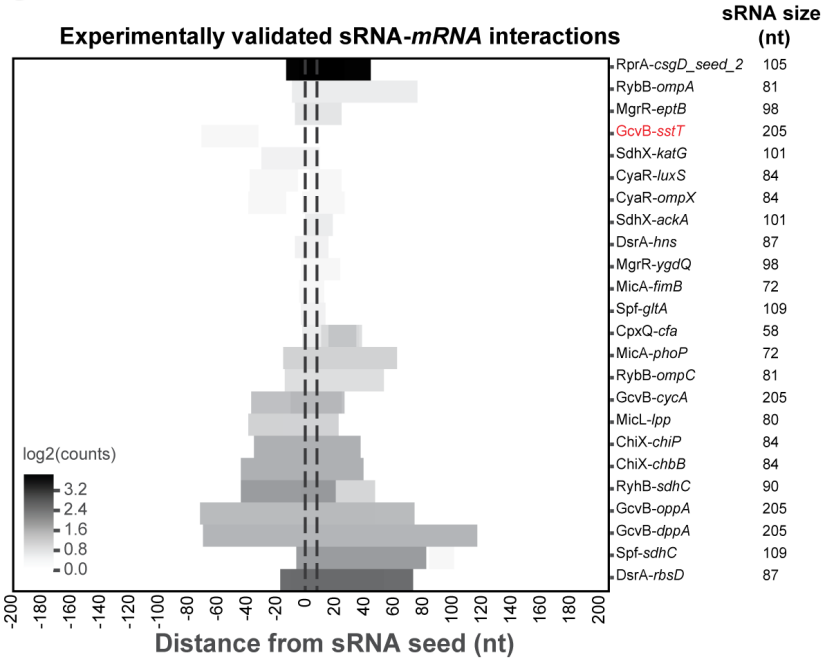
C
Experimentally validated sRNA-mRNA interactions
sRNA size (nt)
RprA-csgD_seed_2 105
RybB-ompA 81
MgrR-eptB 98
GcvB-sstT 205
SdhX-katG 101
CyaR-luxS 84
CyaR-ompX 84
SdhX-ackA 101
DsrA-hns 87
MgrR-ygdQ 98
MicA-fimB 72
Spf-gltA 109
CpxQ-cfa 58
MicA-phoP 72
RybB-ompC 81
GcvB-cycA 205
MicL-lpp 80
ChiX-chiP 84
ChiX-chbB 84
RyhB-sdhC 90
GcvB-oppA 205
GcvB-dppA 205
Spf-sdhC 109
DsrA-rbsD 87
log2(counts)
3.2
2.4
1.6
0.8
0.0
-200 -180 -160 -140 -120 -100 -80 -60 -40 -20 0 20 40 60 80 100 120 140 160 180 200
Distance from sRNA seed (nt)

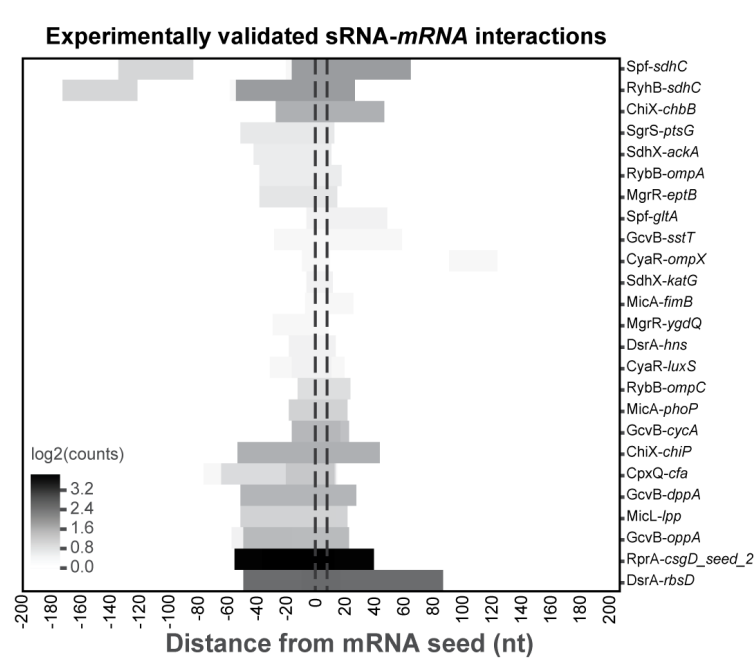
D
Experimentally validated sRNA-mRNA interactions
Spf-sdhC
RyhB-sdhC
ChiX-chbB
SgrS-ptsG
SdhX-ackA
RybB-ompA
MgrR-eptB
Spf-gltA
GcvB-sstT
CyaR-ompX
SdhX-katG
MicA-fimB
MgrR-ygdQ
DsrA-hns
CyaR-luxS
RybB-ompC
MicA-phoP
GcvB-cycA
ChiX-chiP
CpxQ-cfa
GcvB-dppA
MicL-lpp
GcvB-oppA
RprA-csgD_seed_2
DsrA-rbsD
log2(counts)
3.2
2.4
1.6
0.8
0.0
-200 -180 -160 -140 -120 -100 -80 -60 -40 -20 0 20 40 60 80 100 120 140 160 180 200
Distance from mRNA seed (nt)

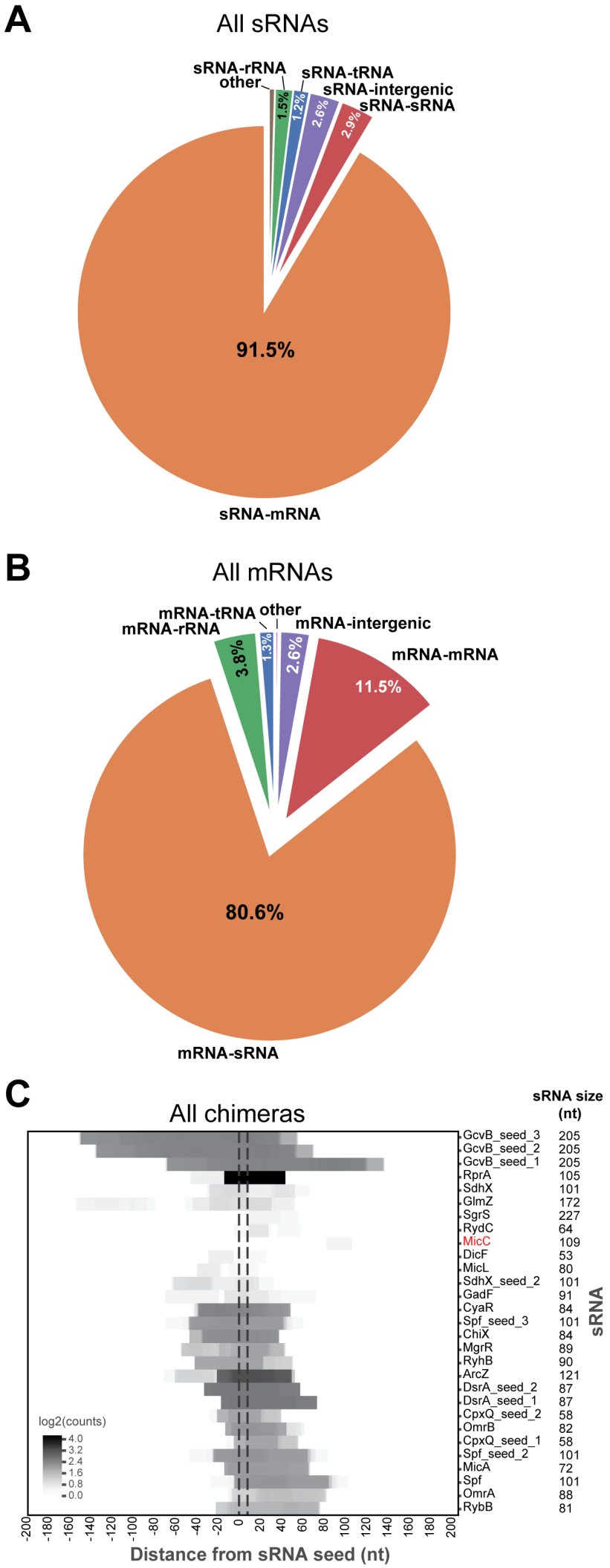
A
All sRNAs
sRNA-rRNA
other
sRNA-tRNA
sRNA-intergenic
sRNA-sRNA
1.5%
1.2%
2.6%
2.9%
91.5%
sRNA-mRNA
B
All mRNAs
mRNA-tRNA
mRNA-rRNA
other
mRNA-intergenic
mRNA-mRNA
3.8%
1.3%
2.6%
11.5%
80.6%
mRNA-sRNA
C
All chimeras
sRNA size (nt)
GcvB_seed_3 205
GcvB_seed_2 205
GcvB_seed_1 205
RprA 105
SdhX 101
GlmZ 172
SgrS 227
RydC 64
MicC 109
DicF 53
MicL 80
SdhX_seed_2 101
GadF 91
CyaR 84
Spf_seed_3 101
ChiX 84
MgrR 89
RyhB 90
ArcZ 121
DsrA_seed_2 87
DsrA_seed_1 87
CpxQ_seed_2 58
OmrB 82
CpxQ_seed_1 58
Spf_seed_2 101
MicA 72
Spf 101
OmrA 88
RybB 81
sRNA
log2(counts)
4.0
3.2
2.4
1.6
0.8
0.0
-200 -180 -160 -140 -120 -100 -80 -60 -40 -20 0 20 40 60 80 100 120 140 160 180 200
Distance from sRNA seed (nt)

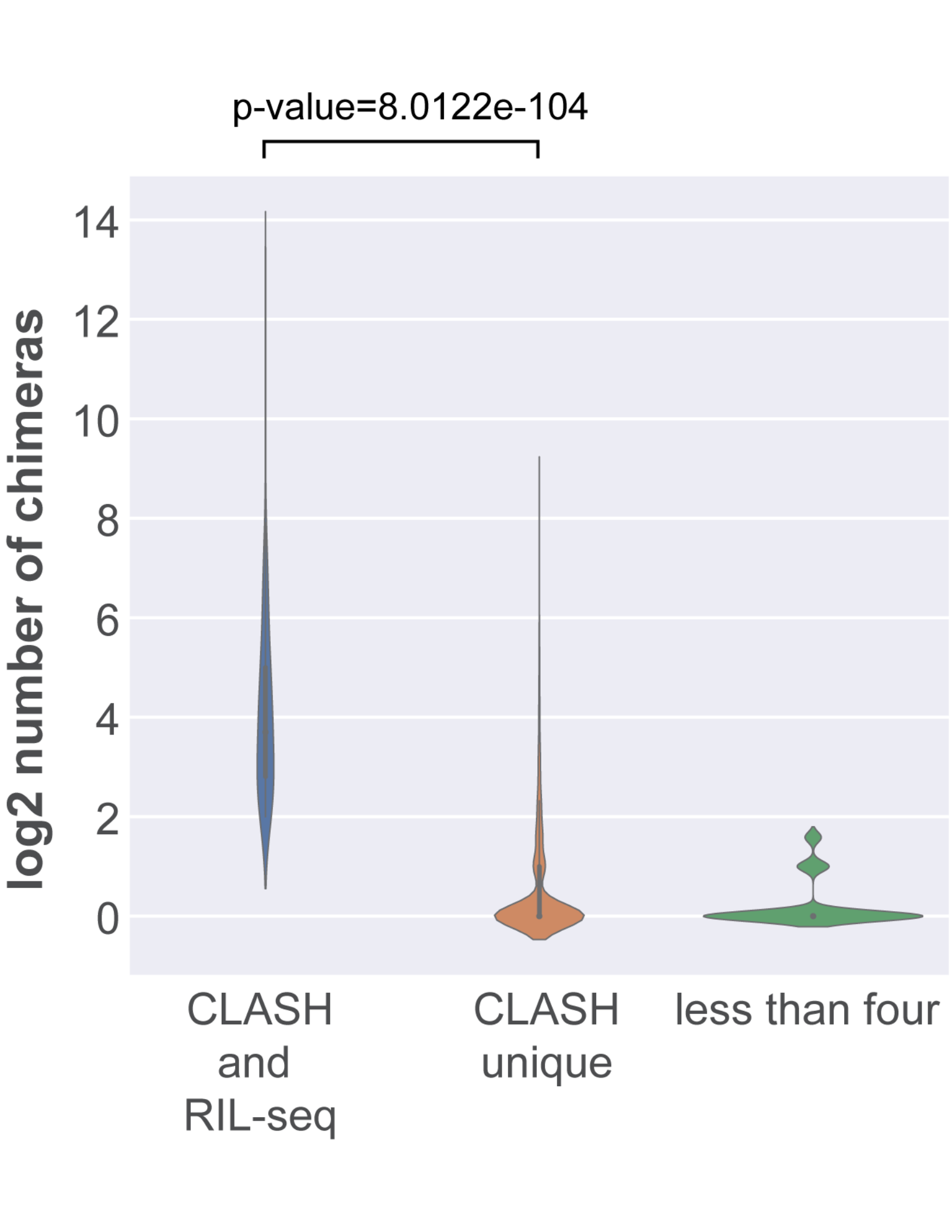
p-value=8.0122e-104
log2 number of chimeras
14
12
10
8
6
4
2
0
CLASH and RIL-seq
CLASH unique
less than four

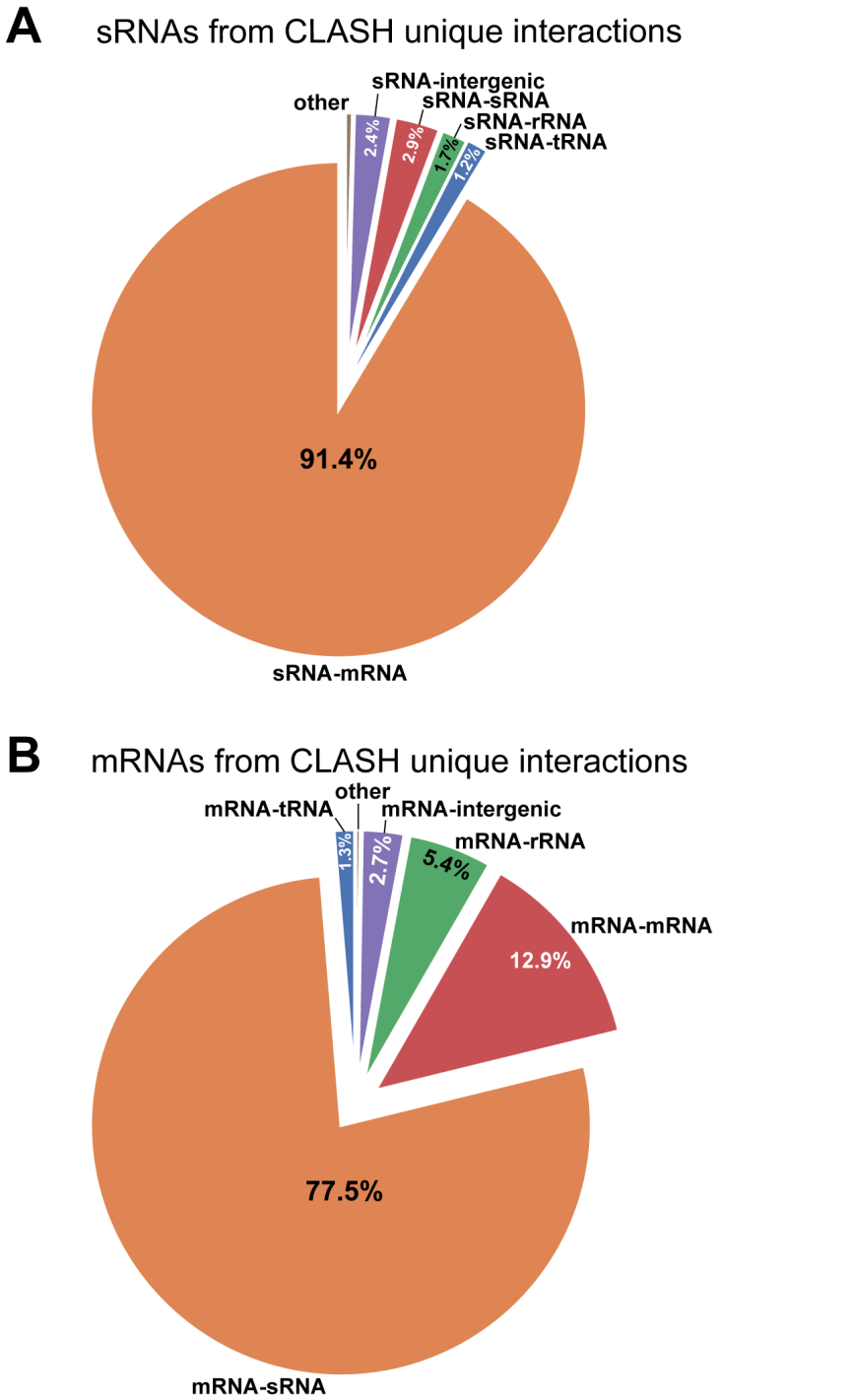
A
sRNAs from CLASH unique interactions
other
sRNA-intergenic
sRNA-sRNA
sRNA-rRNA
sRNA-tRNA
2.4%
2.9%
1.7%
1.2%
91.4%
sRNA-mRNA
B
mRNAs from CLASH unique interactions
mRNA-tRNA
other
mRNA-intergenic
mRNA-rRNA
mRNA-mRNA
1.3%
2.7%
5.4%
12.9%
77.5%
mRNA-sRNA
C
CLASH unique chimeras
sRNA
sRNA size (nt)
GcvB_seed_3 205
GcvB_seed_2 205
GcvB_seed_1 205
SdhX 101
GlmZ 172
SgrS 227
RydC 64
MicC 109
DicF 53
MicL 80
SdhX_seed_2 101
GadF 91
CpxQ_seed_2 58
MicA 72
OmrB 82
CpxQ_seed_1 58
Spf_seed_2 109
Spf_seed_1 109
OmrA 88
RybB 81
DsrA_seed_2 87
ArcZ 121
MgrR 98
ChiX 84
Spf_seed_3 101
CyaR 84
RyhB 90
RprA 105
DsrA 87
log2(counts)
4.0
3.2
2.4
1.6
0.8
0.0
-200 -180 -160 -140 -120 -100 -80 -60 -40 -20 0 20 40 60 80 100 120 140 160 180 200
Distance from sRNA seed (nt)

A sRNAs from CLASH unique interactions < 4 reads

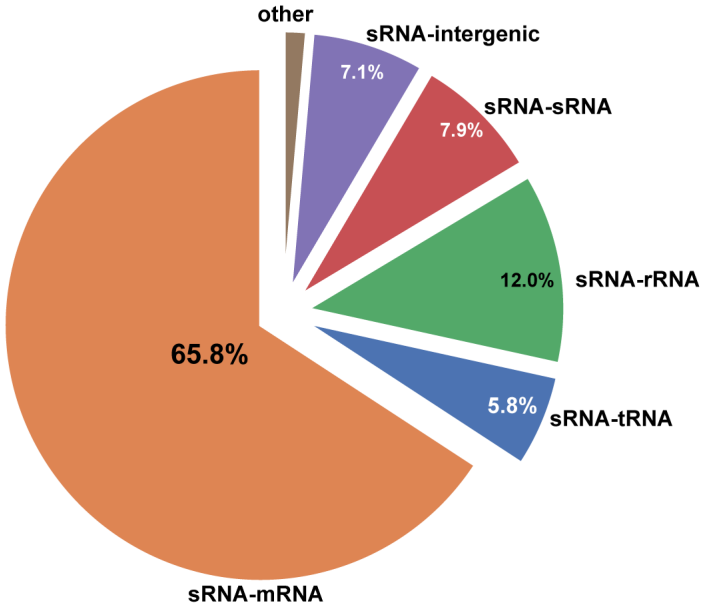

B mRNAs from CLASH unique interactions < 4 reads

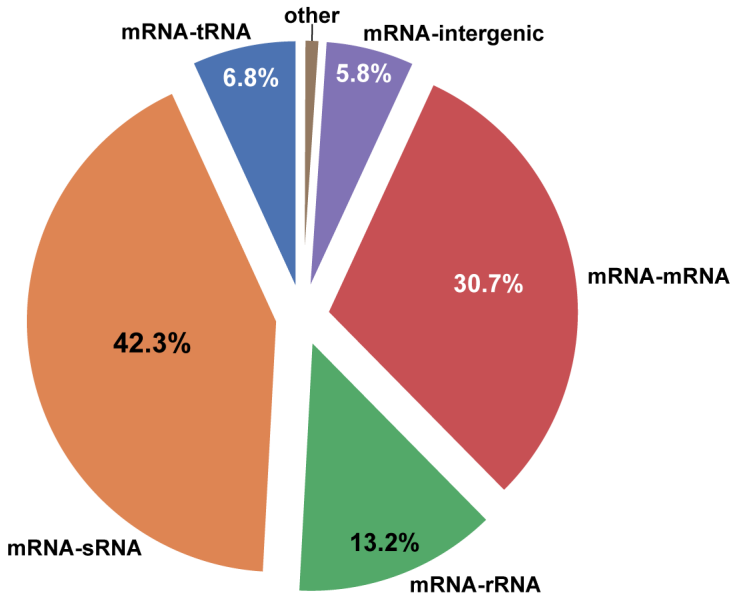

C

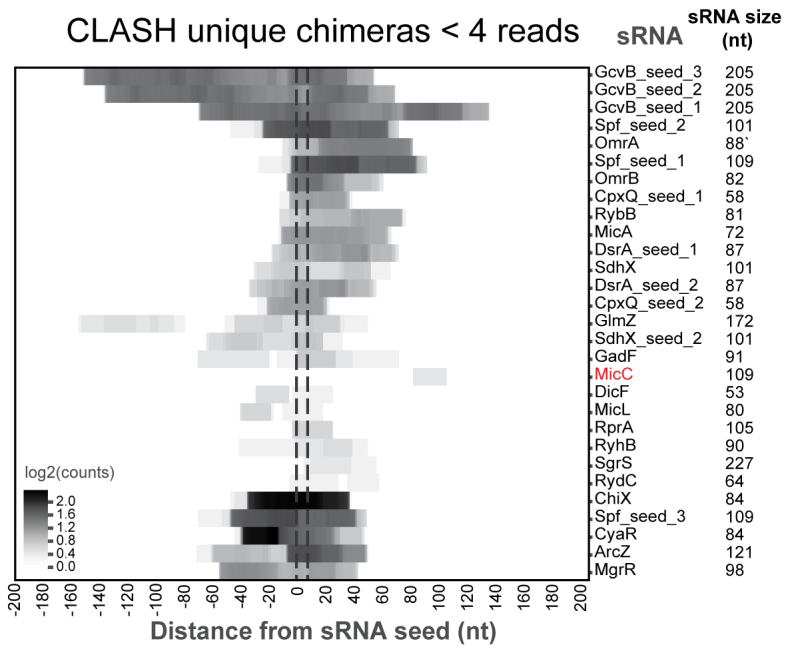

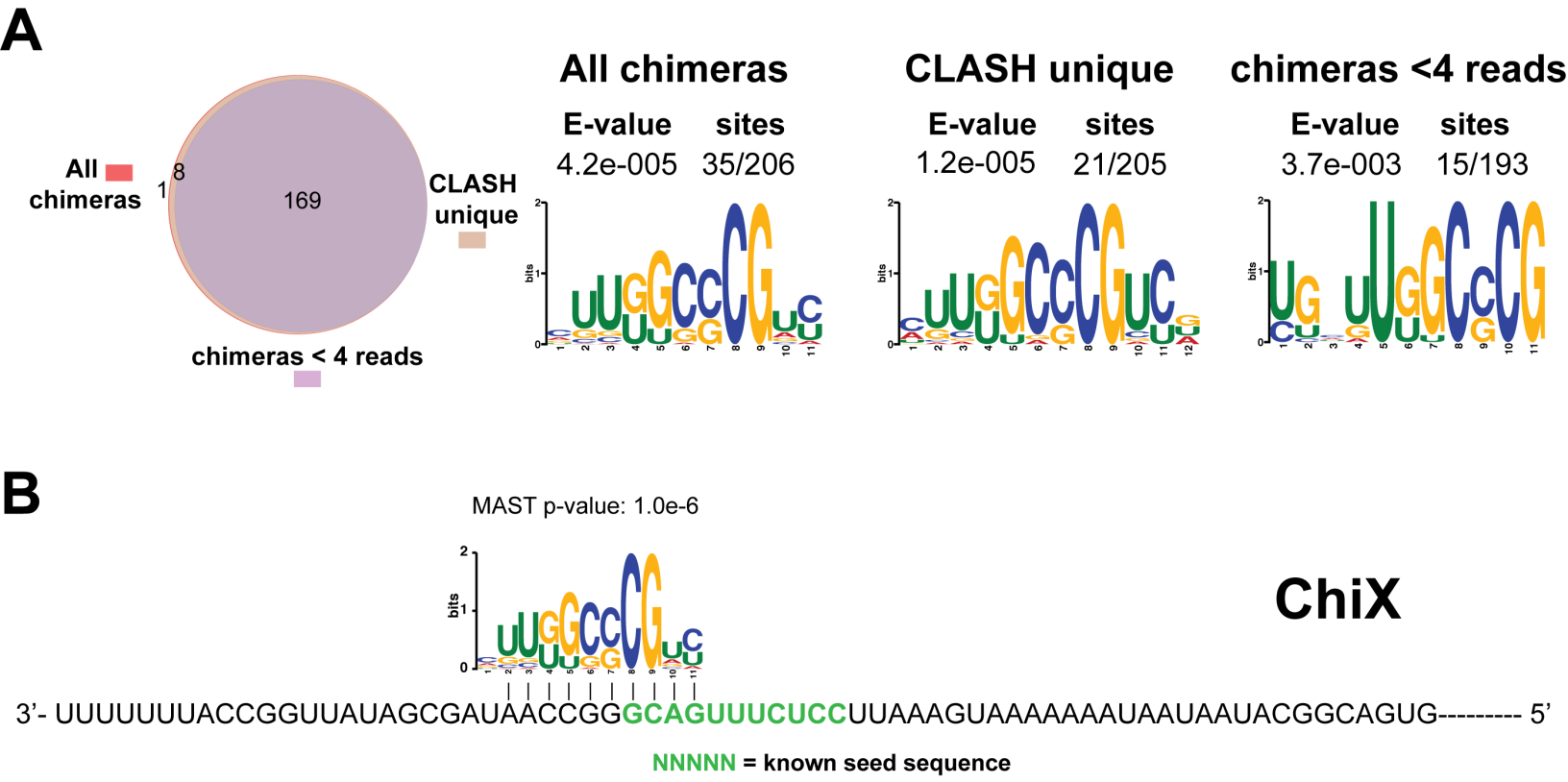
A
All chimeras
CLASH unique
chimeras < 4 reads
1
8
169
All chimeras
E-value
sites
4.2e-005
35/206
CLASH unique
E-value
sites
1.2e-005
21/205
chimeras <4 reads
E-value
sites
3.7e-003
15/193
bits

B
MAST p-value: 1.0e-6
bits
ChiX
3'- UUUUUUUACCGGUUAUAGCGAUAACCGGGCAGUUUCUCCUUAAAGUAAAAAAAAUAAUAAUACGGCAGUG--------- 5'
NNNNN = known seed sequence

A

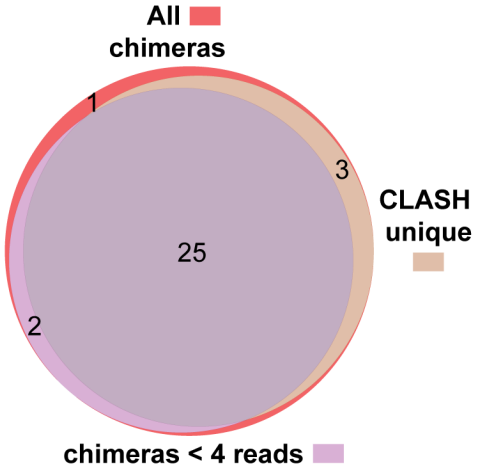

All chimeras

E-value sites
9.8e-007 9/31

CLASH unique

E-value sites
3.7e-004 7/28

chimeras < 4 reads

E-value sites
2.8e-005 9/27

B

MAST p-value: 3.9e-6

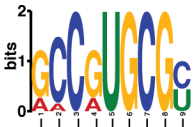

SdsR

3’- --------ACAUAAGCCAGGUCCCUUUACCGAGAACCCUCUCUCGGCAC**GCGAUUUUCAACCGUAAUUACGUCCG**AAUCAACGGAACGG- 5’

NNNNN = known seed sequence

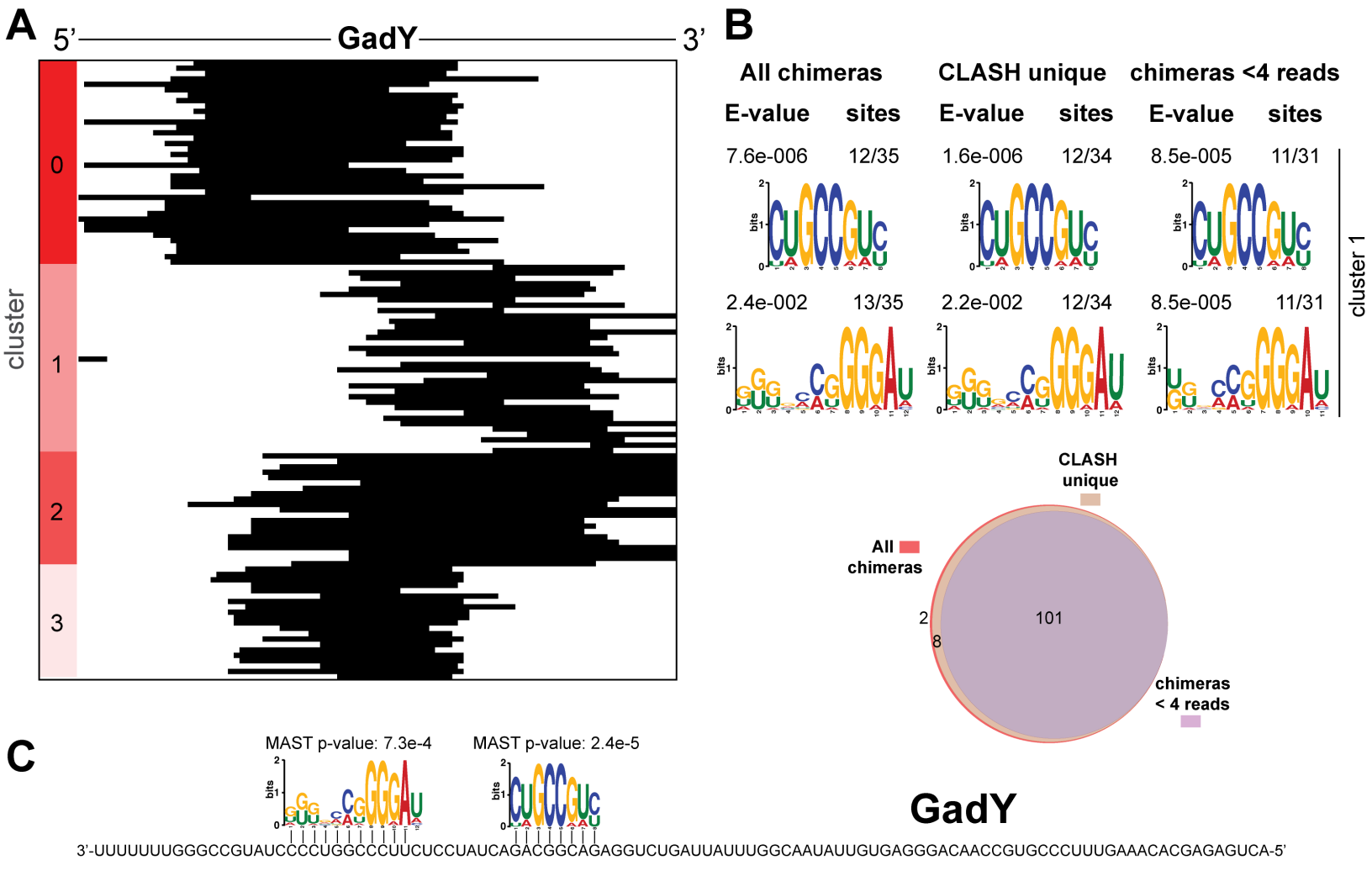
A
5'
GadY
3'
cluster
0
1
2
3
B
All chimeras
CLASH unique
chimeras <4 reads
E-value
sites
7.6e-006
12/35
1.6e-006
12/34
8.5e-005
11/31
2.4e-002
13/35
2.2e-002
12/34
8.5e-005
11/31
cluster 1
CLASH unique
All chimeras
101
2
8
chimeras < 4 reads
C
MAST p-value: 7.3e-4
MAST p-value: 2.4e-5
GadY
3'-UUUUUUUGGGCCGUAUCCCCUGGCCCUUCUCCUAUCAGACGGCAGAGGUCUGAUUAUUUGGCAAUAUUGUGAGGGACAACCGUGCCCUUUGAAACACGAGAGUCA-5'

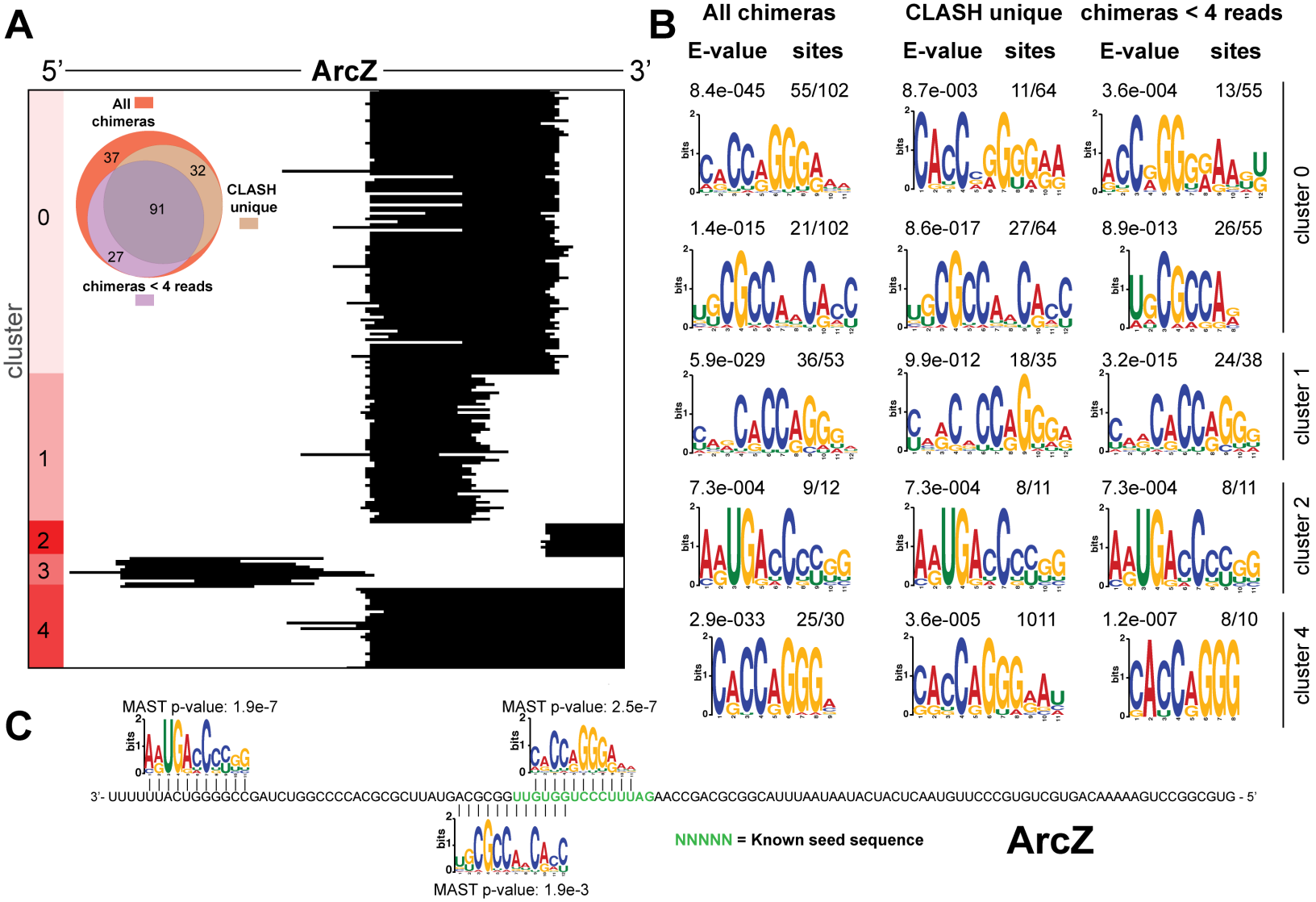
A
5'
ArcZ
3'
All chimeras
37
32
91
27
CLASH unique
chimeras < 4 reads
cluster
0
1
2
3
4
B
All chimeras
CLASH unique
chimeras < 4 reads
E-value
sites
8.4e-045 55/102
8.7e-003 11/64
3.6e-004 13/55
cluster 0
1.4e-015 21/102
8.6e-017 27/64
8.9e-013 26/55
5.9e-029 36/53
9.9e-012 18/35
3.2e-015 24/38
cluster 1
7.3e-004 9/12
7.3e-004 8/11
7.3e-004 8/11
cluster 2
2.9e-033 25/30
3.6e-005 1011
1.2e-007 8/10
cluster 4
C
MAST p-value: 1.9e-7
MAST p-value: 2.5e-7
3'- UUUUUUACUGGGGCCGAUCUGGCCCCACGCGCUUAUGACGCGGUUGUGGUCCCUUUAGAACCGACGCGGCAUUUAAUAAUACUACUCAAUGUUCCCGUGUCGUGACAAAAAGUCCGGCGUG - 5'
MAST p-value: 1.9e-3
NNNNN = Known seed sequence
ArcZ

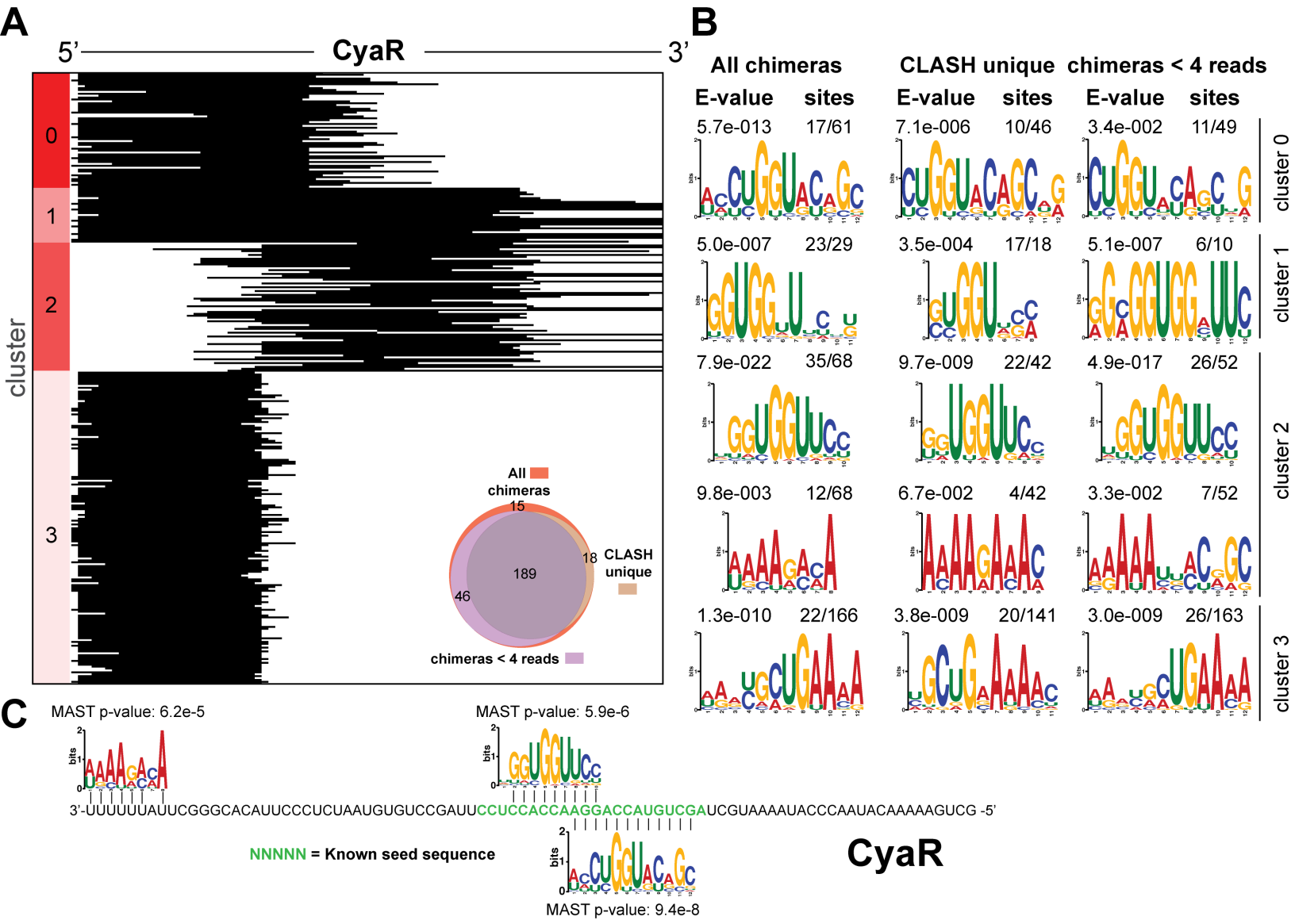
A
5'
CyaR
3'
cluster
0
1
2
3
All chimeras
15
189
18
CLASH unique
46
chimeras < 4 reads
B
All chimeras
CLASH unique
chimeras < 4 reads
E-value
sites
5.7e-013
17/61
7.1e-006
10/46
3.4e-002
11/49
cluster 0
5.0e-007
23/29
3.5e-004
17/18
5.1e-007
6/10
cluster 1
7.9e-022
35/68
9.7e-009
22/42
4.9e-017
26/52
9.8e-003
12/68
6.7e-002
4/42
3.3e-002
7/52
cluster 2
1.3e-010
22/166
3.8e-009
20/141
3.0e-009
26/163
cluster 3
C
MAST p-value: 6.2e-5
MAST p-value: 5.9e-6
3'-UUUUUUAUUCGGGCACAUUCCCUCUAAUGUGUCCGAUUCCUCCACCAAGGACCAUGUCGAUCGUAAAAUACCCAAUACAAAAGUCG -5'
NNNNN = Known seed sequence
MAST p-value: 9.4e-8
CyaR

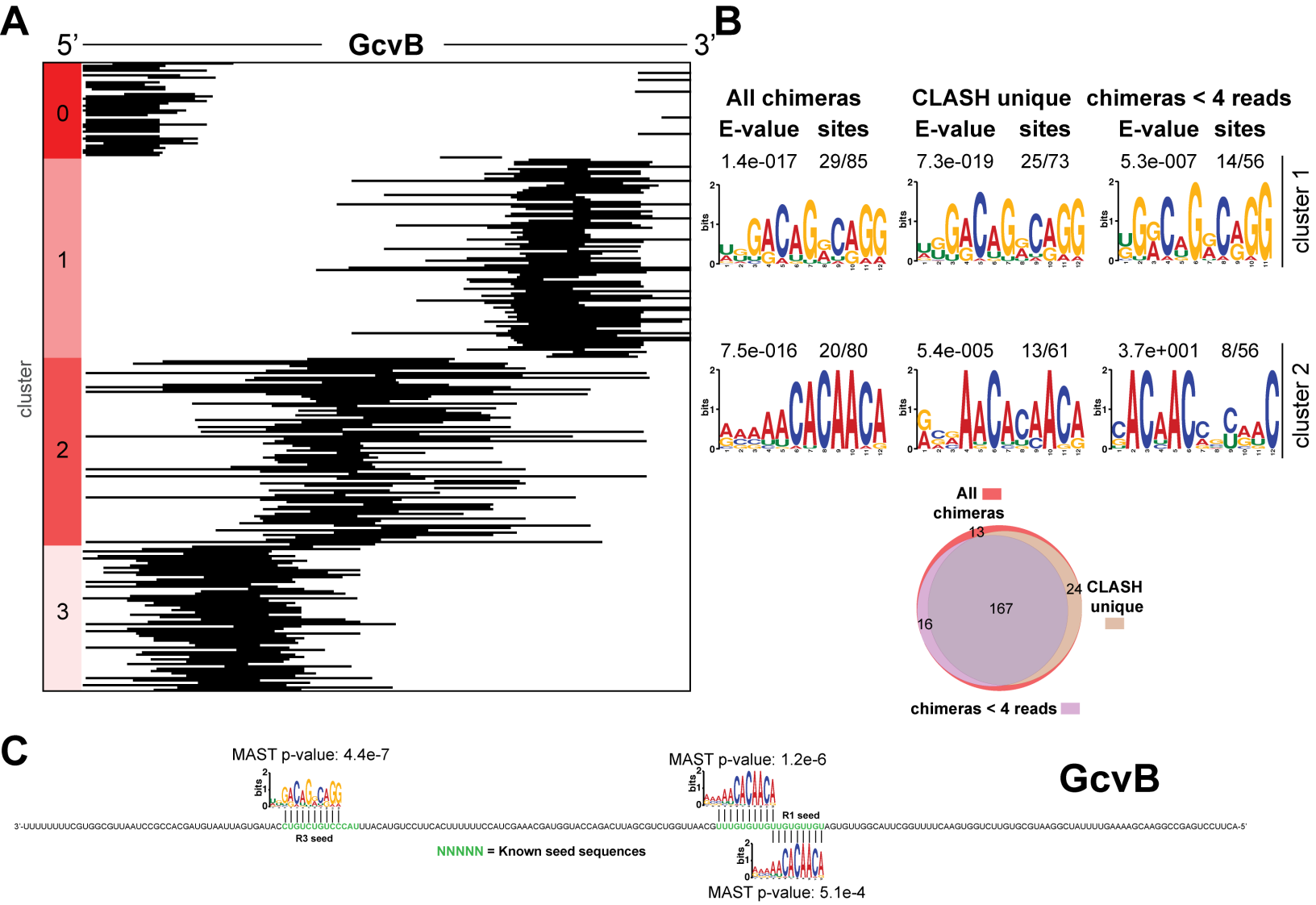
A
5'
GcvB
3'
cluster
0
1
2
3
B
All chimeras
E-value sites
1.4e-017 29/85
CLASH unique
E-value sites
7.3e-019 25/73
chimeras < 4 reads
E-value sites
5.3e-007 14/56
cluster 1
7.5e-016 20/80
5.4e-005 13/61
3.7e+001 8/56
cluster 2
All chimeras
13
24
CLASH unique
167
16
chimeras < 4 reads
C
MAST p-value: 4.4e-7
R3 seed
MAST p-value: 1.2e-6
R1 seed
MAST p-value: 5.1e-4
GcvB
NNNNN = Known seed sequences
3'-UUUUUUUUCGUGGCGUUAAUCCGCCACGAUGUAAUUAGUGAUACCUGUCUGUCCCAUUUACAUGUCCUUCACUUUUUUCCAUCGAAACGAUGGUACCAGACUUAGCGUCUGGUUAACGUUUGUUGUUGUUGUUGUUAGUGUUGGCAUUCGGUUUUCAAGUGGUCUUGUGCGUAAGGCUAUUUUGAAAAGCAAGGCCGAGUCCUUCA-5'

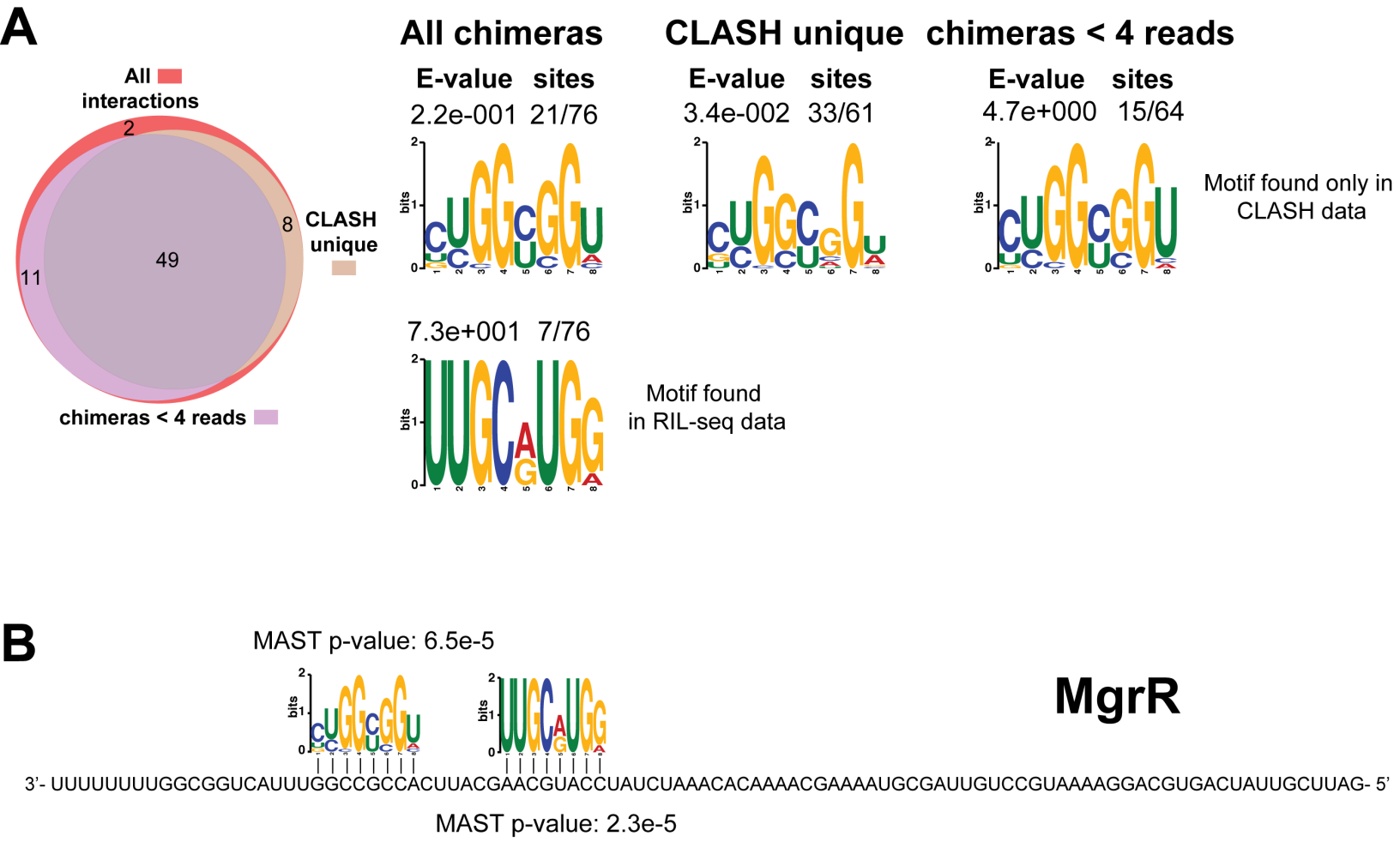
A
All interactions
2
8
CLASH unique
49
11
chimeras < 4 reads
All chimeras
E-value sites
2.2e-001 21/76
7.3e+001 7/76
CLASH unique chimeras < 4 reads
E-value sites
3.4e-002 33/61
E-value sites
4.7e+000 15/64
Motif found only in CLASH data
Motif found in RIL-seq data
B
MAST p-value: 6.5e-5
MgrR
3'- UUUUUUUUGGCGGUCAUUUGGCCGCCACUUACGAACGUACCUAUCUAAACACAAAACGAAAAUGCGAUUGUCCGUAAAAGGACGUGACUAUUGCUUAG- 5'
MAST p-value: 2.3e-5

A

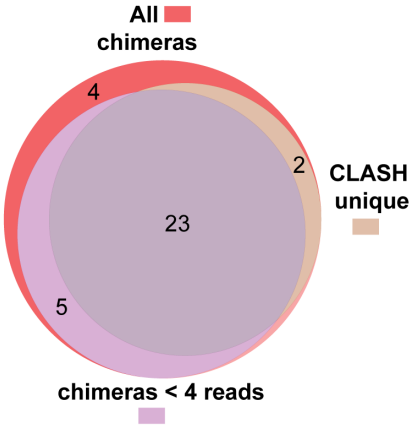

All chimeras

E-value	sites
3.9e-021	14/36

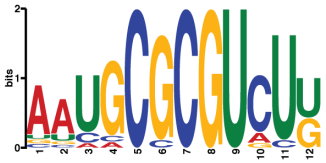

CLASH unique

E-value	sites
2.0e-011	15/25

chimeras < 4 reads

E-value	sites
2.8e-014	11/28

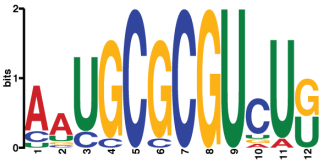

B

MicA

MAST p-value: 6.0e-8

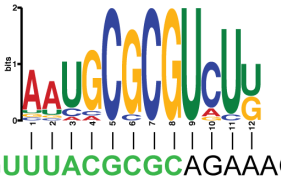

3’- UUUUCUUUUUCCGGUGAGCACUCACCGGUUUUAAAGUAGAGACUUAAGUCCCUACUACUAUUGUUUACGCGCAGAAAG- 5’

NNNNN = known seed sequence

A

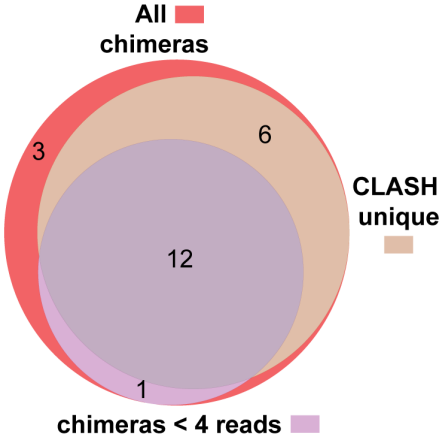

All chimeras

E-value	sites
1.3e-011	12/23

CLASH unique

E-value	sites
8.1e-010	10/19

chimeras < 4 reads

E-value	sites
1.4e+001	7/13

B

RybB

MAST p-value: 7.6e-5

3’- ------GUUGGAACUUGGCUUUACCGCCCCAACUACCCGAGGUGUUUUACCCCUGUAGUUUCUUUUCGUCACCG- 5’

NNNNN = known seed sequence

A

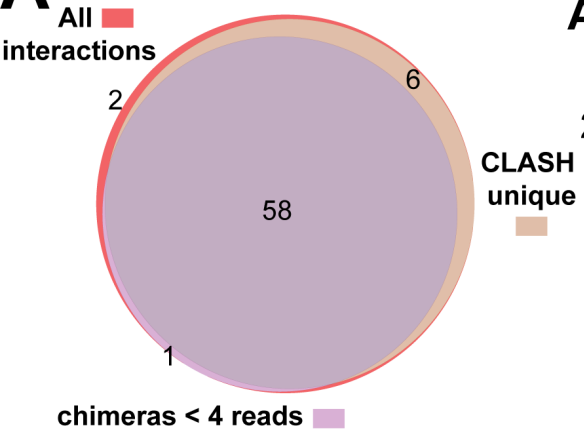

All chimeras		CLASH unique		chimeras < 4 reads	
E-value	sites	E-value	sites	E-value	sites
2.7e-001	22/71	1.1e+000	21/68	2.0e+000	20/63

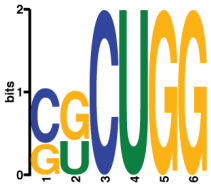

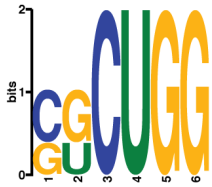

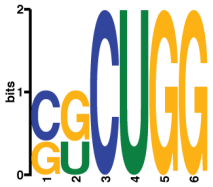

B

OmrB

MAST p-value: 5.0e-4

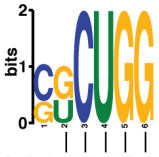

3’- ---GCGUAGACGCGUCCGACCACAUUAAGUACACGAGUUGGGCUUCAACUGAA**GUGGAUAGUUAUGGAGACCC**- 5’

NNNNN = known seed sequence

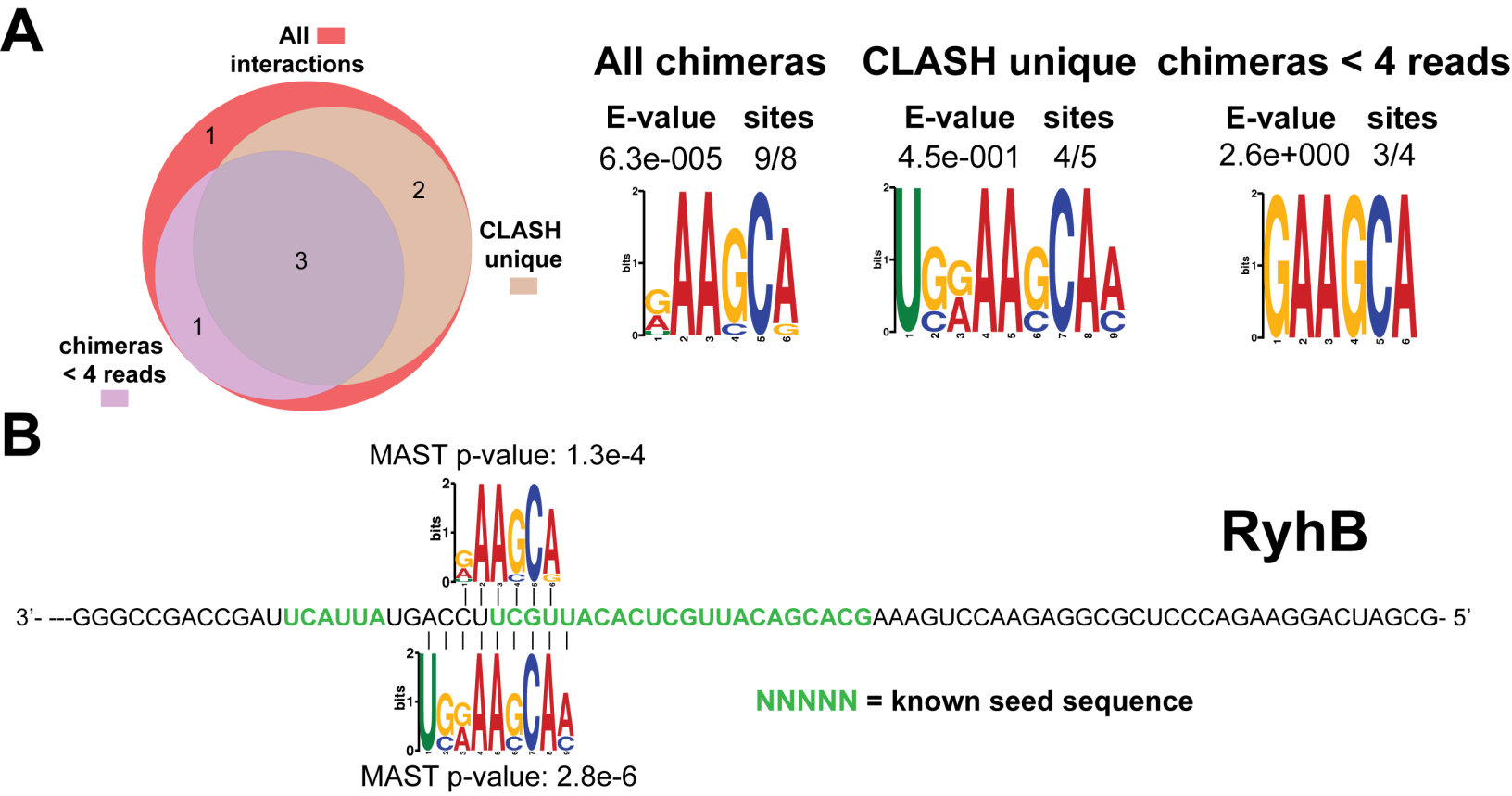
A
All interactions
1
2
3
1
CLASH unique
chimeras < 4 reads
All chimeras
E-value sites
6.3e-005 9/8
CLASH unique
E-value sites
4.5e-001 4/5
chimeras < 4 reads
E-value sites
2.6e+000 3/4
B
MAST p-value: 1.3e-4
RyhB
3'- ---GGGCCGACCGAUUCAUUAUGACCUUCGUUACACUCGUUACAGCACGAAAGUCCAAGAGGCGCUCCCAGAAGGACUAGCG- 5'
NNNNN = known seed sequence
MAST p-value: 2.8e-6

A

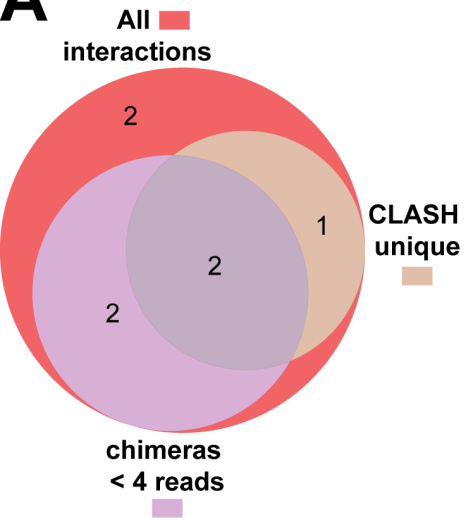

All chimeras

E-value **sites**

1.1e-001 8/8

CLASH unique

E-value **sites**

2.9e+000 2/3

chimeras < 4 reads

E-value **sites**

1.4e+001 3/4

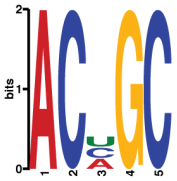

B

MAST p-value: 1.1e-8

RprA

3'- UUUUUUUCGGGUAGCACCCUCUACCCGUUUCUGAUGU**GUGUCGUUAAGC**AACAAA**GUGAGUCCCCUAAAGGUAC**GAAUAUUU----- 5'

NNNNN = known seed sequence

A

GcvB MAPS data

All CLASH targets

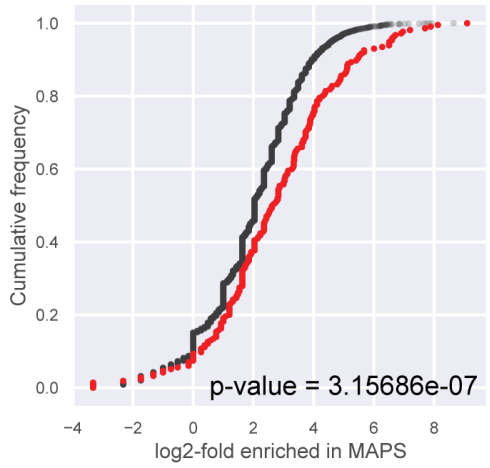

less 4 chimeras

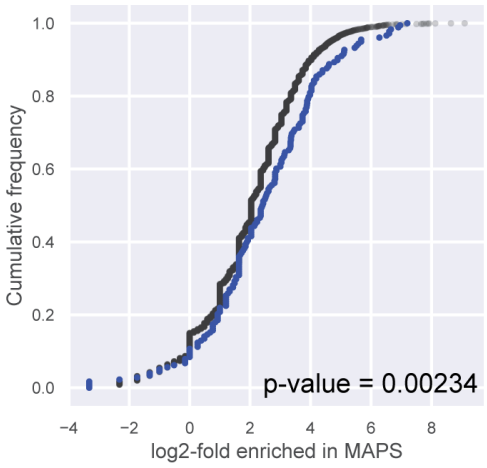

CLASH unique

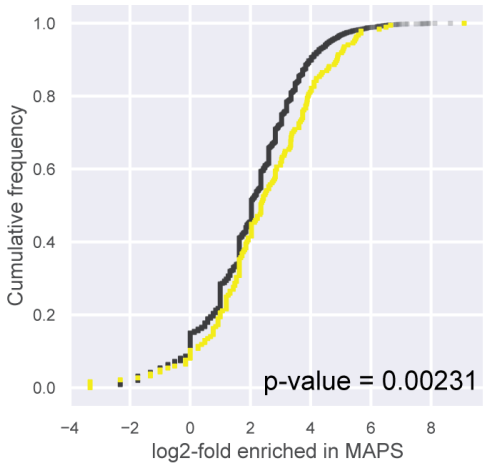

B

CyaR MAPS data

All CLASH targets

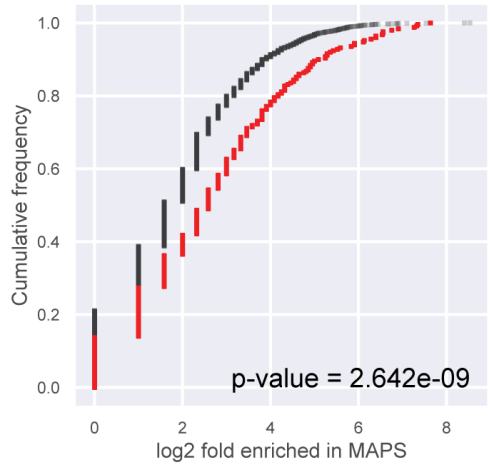

less 4 chimeras

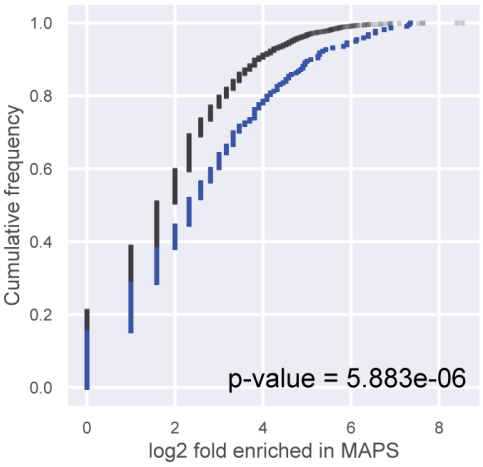

CLASH unique

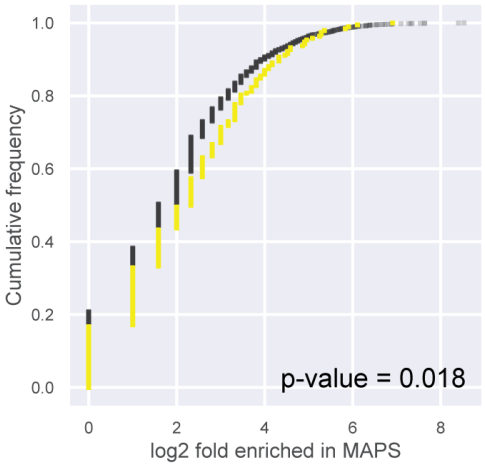

GcvB

All CLASH targets

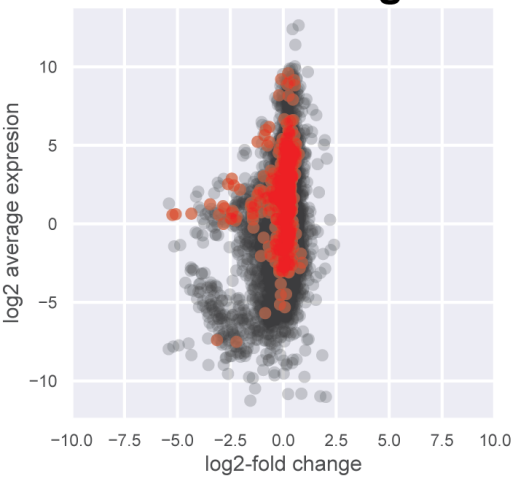

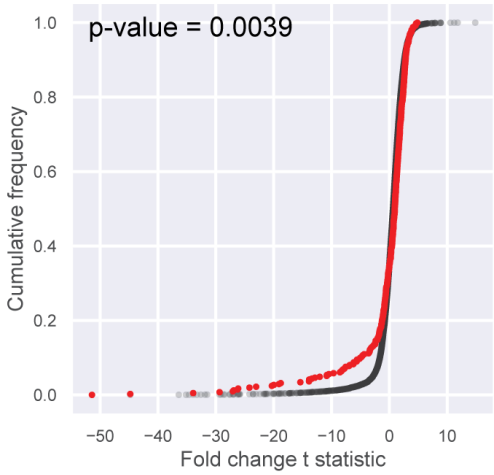

less 4 chimeras

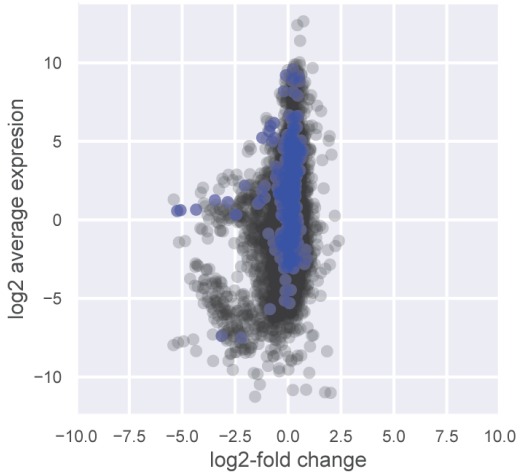

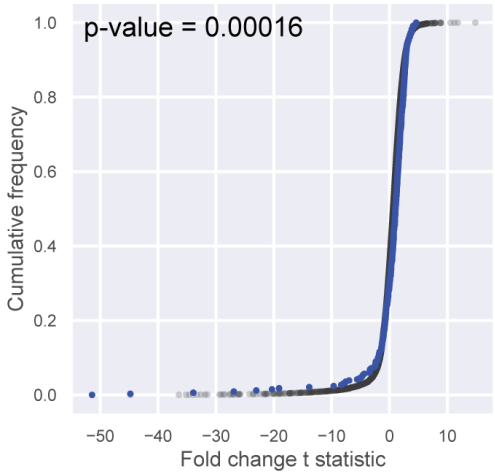

CLASH unique

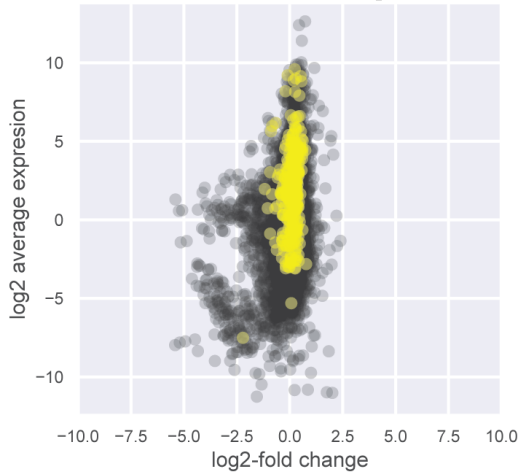

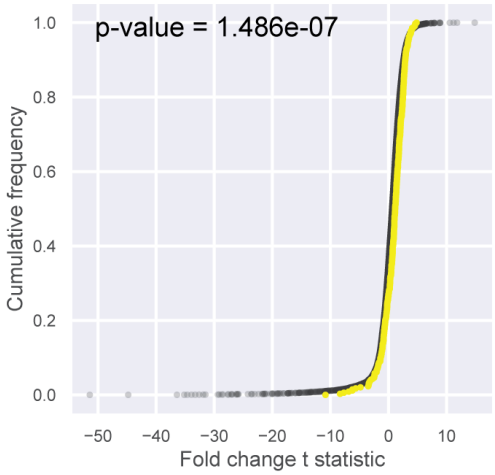

CyaR

All CLASH targets

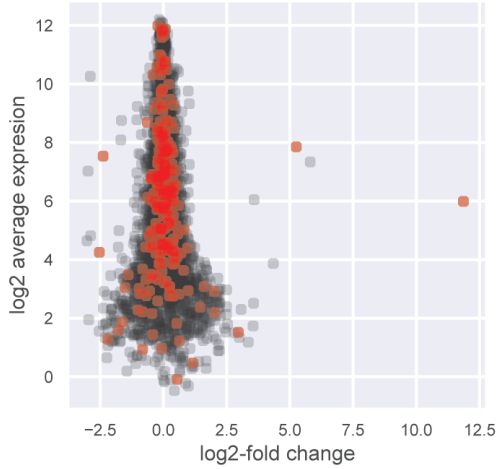

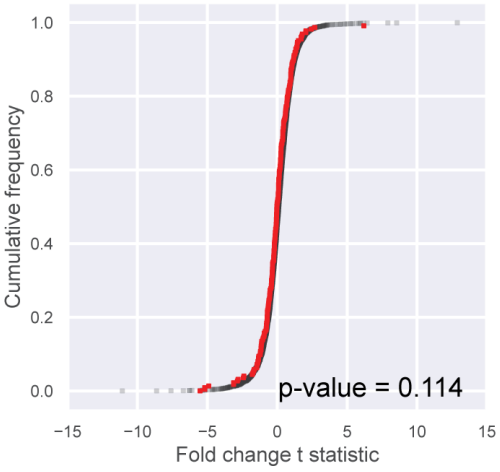

less 4 chimeras

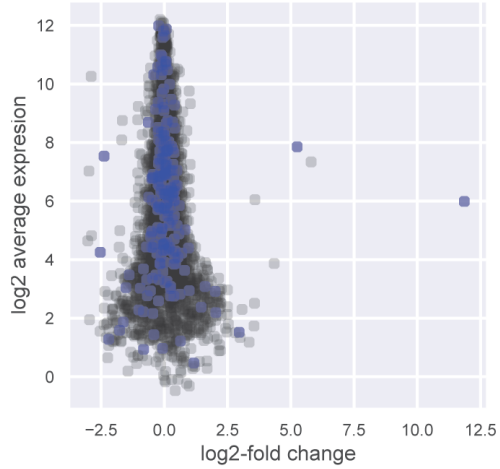

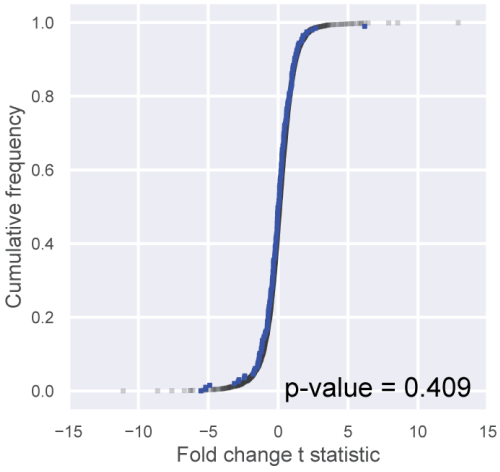

CLASH unique

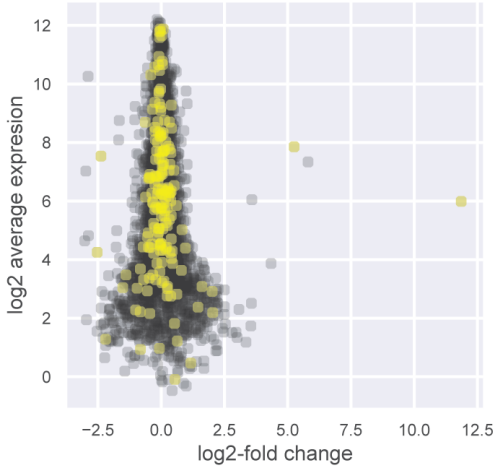

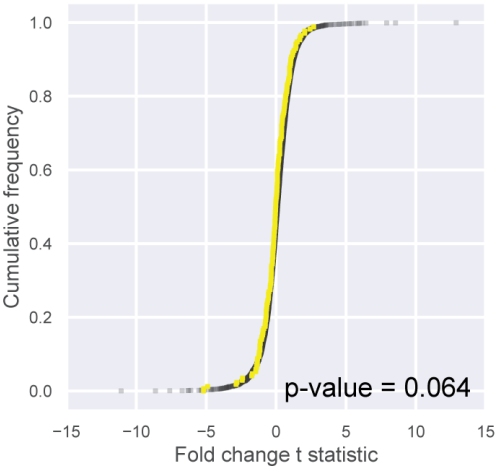

Spot42

All CLASH targets

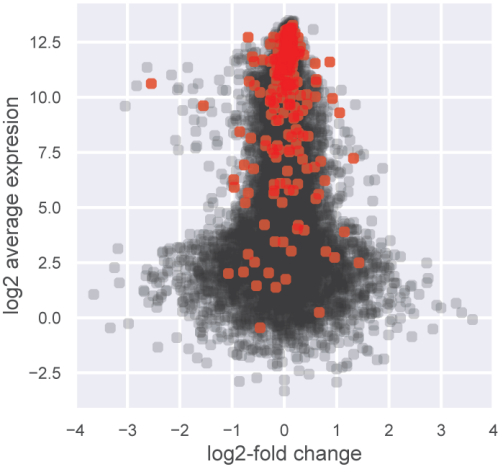

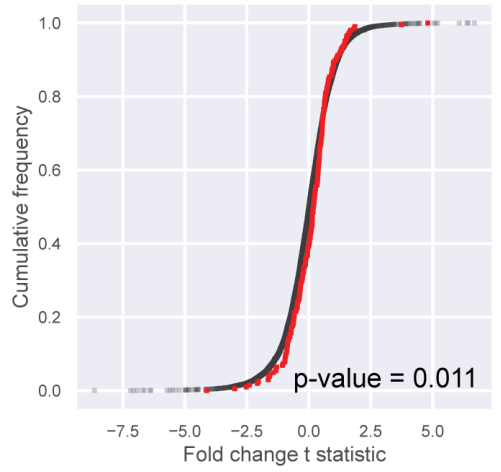

less 4 chimeras

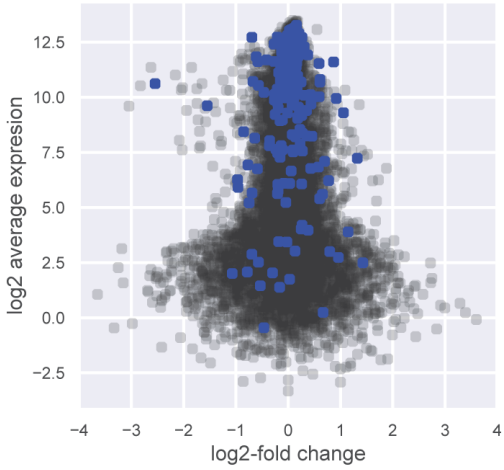

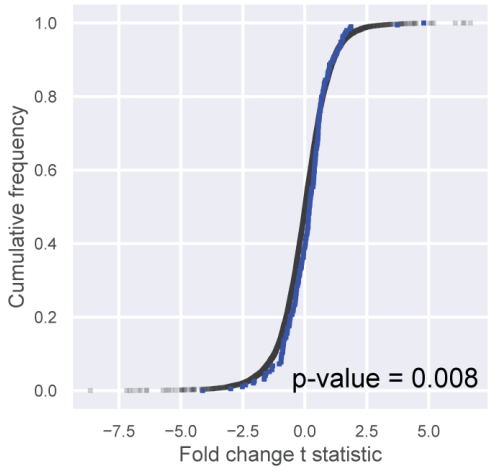

CLASH unique

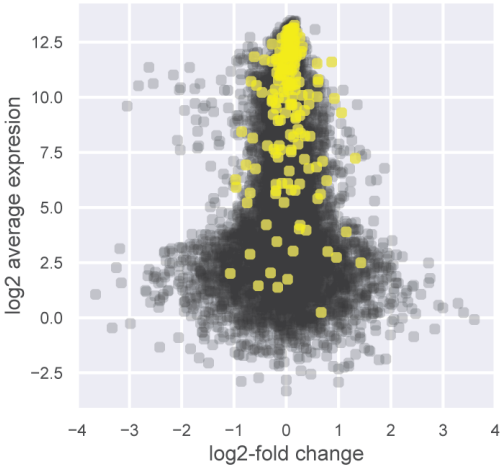

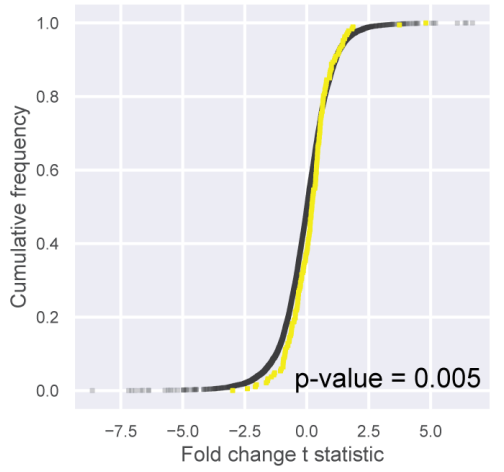

ArcZ

All CLASH targets

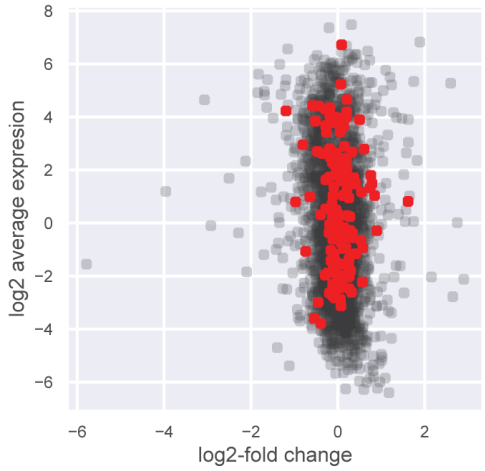

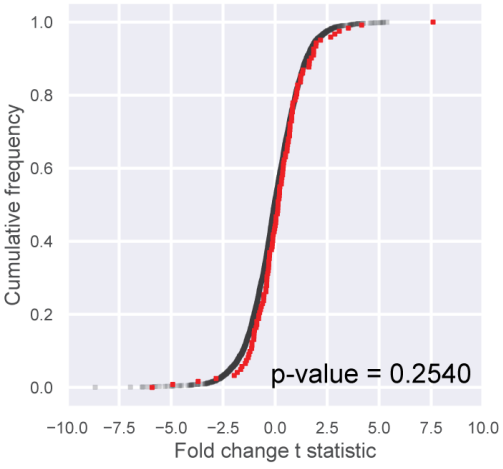

less 4 chimeras

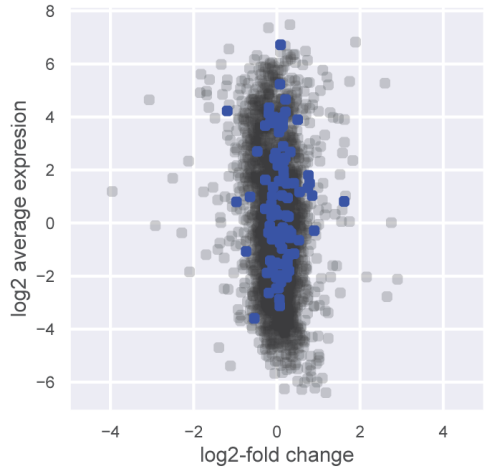

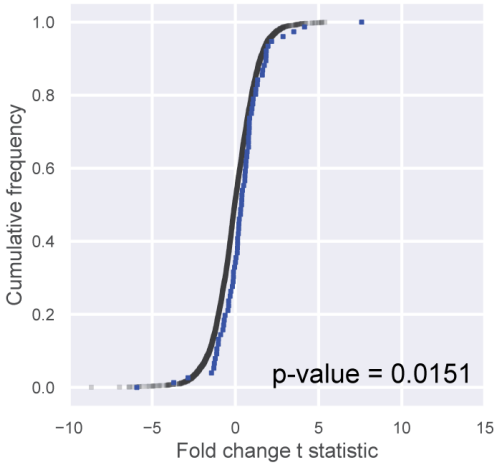

CLASH unique

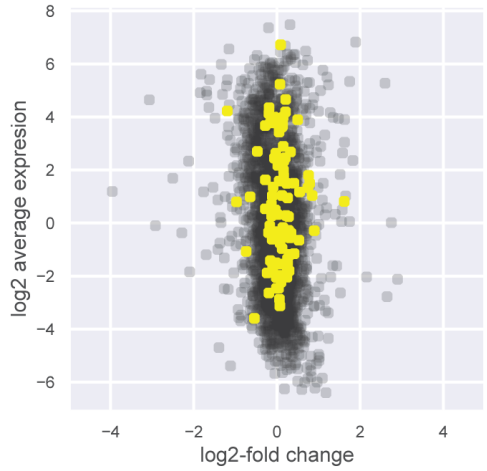

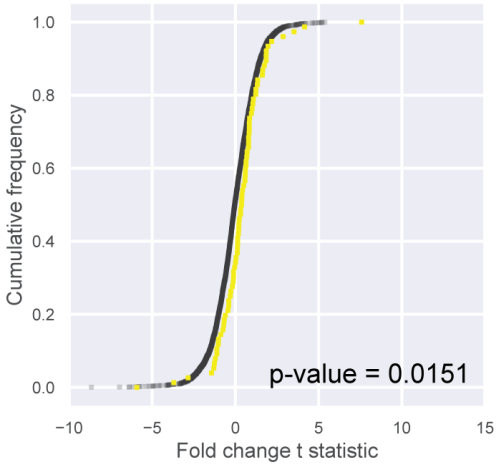

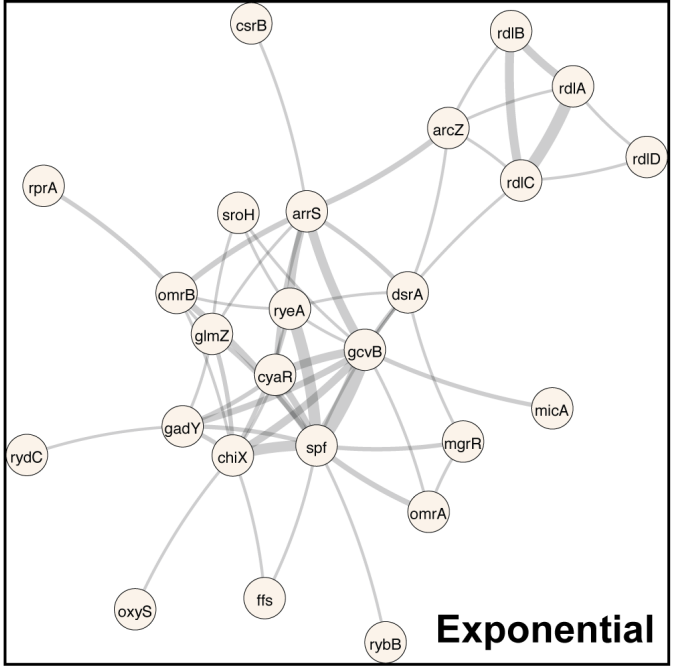

Chimera counts

1
27
86

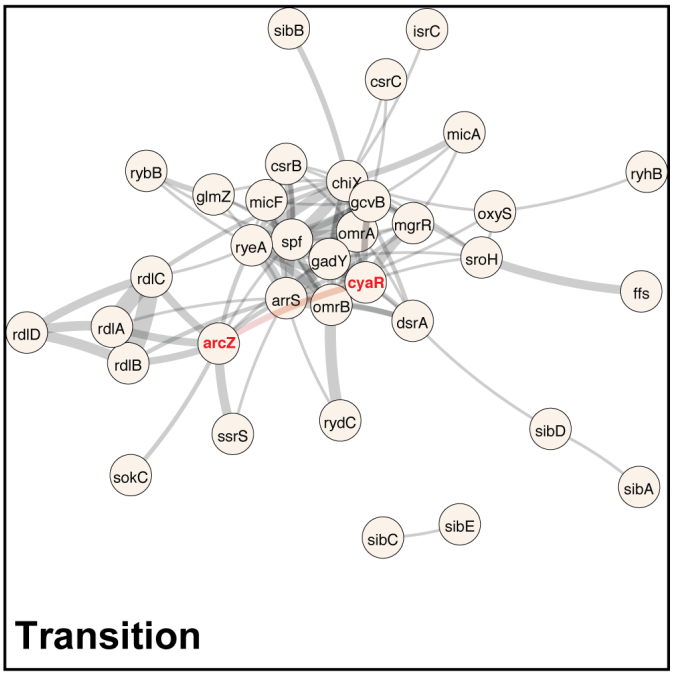

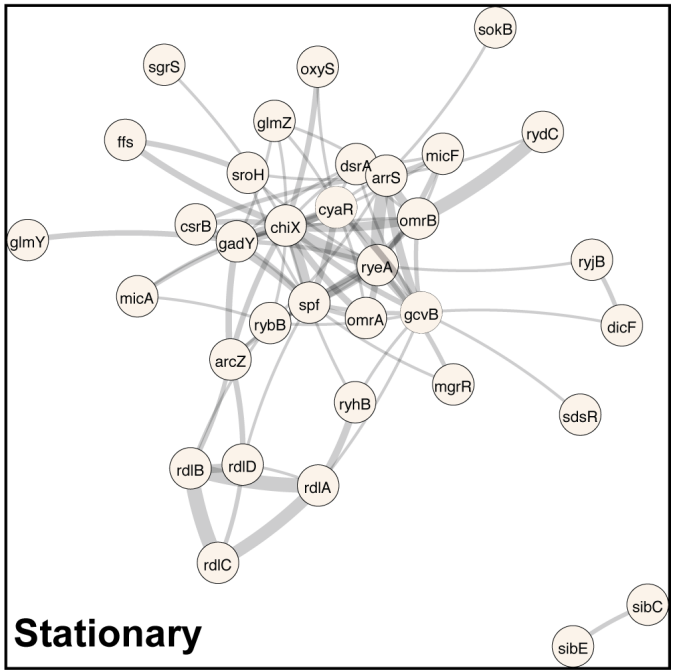

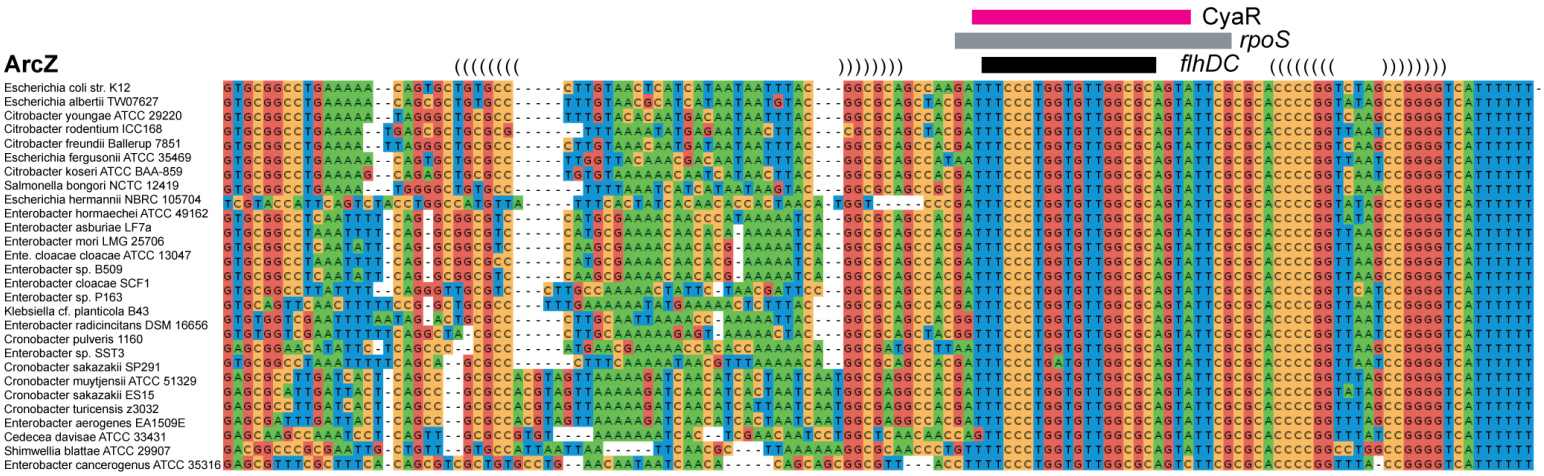
CyaR
rpoS
flhDC
ArcZ
(((((((( ))))))))
(((((((( ))))))))
Escherichia coli str. K12
Escherichia albertii TW07627
Citrobacter youngae ATCC 29220
Citrobacter rodentium ICC168
Citrobacter freundii Ballerup 7851
Escherichia fergusonii ATCC 35469
Citrobacter koseri ATCC BAA-859
Salmonella bongori NCTC 12419
Escherichia hermannii NBRC 105704
Enterobacter hormaechei ATCC 49162
Enterobacter asburiae LF7a
Enterobacter mori LMG 25706
Ente. cloacae cloacae ATCC 13047
Enterobacter sp. B509
Enterobacter cloacae SCF1
Enterobacter sp. P163
Klebsiella cf. planticola B43
Enterobacter radicincitans DSM 16656
Cronobacter pulveris 1160
Enterobacter sp. SST3
Cronobacter sakazakii SP291
Cronobacter muytjensii ATCC 51329
Cronobacter sakazakii ES15
Cronobacter turicensis z3032
Enterobacter aerogenes EA1509E
Cedecea davisae ATCC 33431
Shimwellia blattae ATCC 29907
Enterobacter cancerogenus ATCC 35316

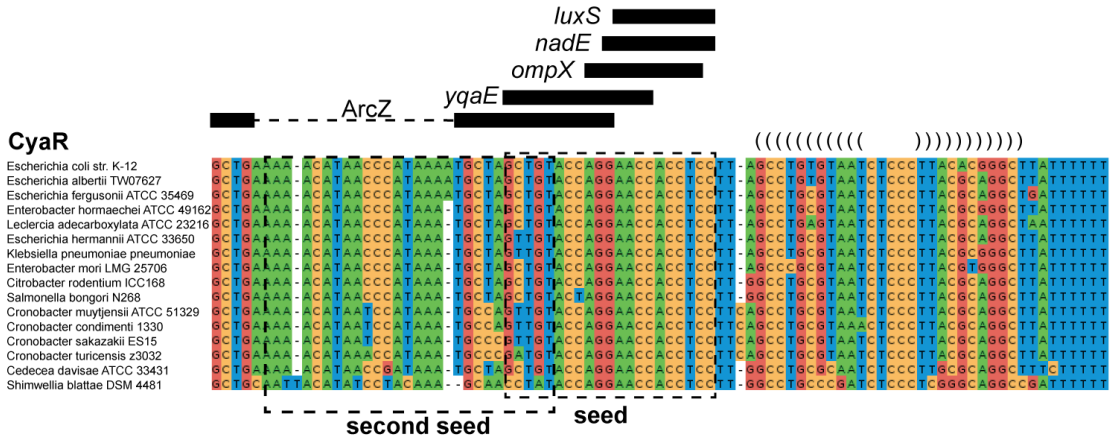
luxS
nadE
ompX
yqaE
ArcZ
CyaR
((((((((((( ))))))))))
Escherichia coli str. K-12
Escherichia albertii TW07627
Escherichia fergusonii ATCC 35469
Enterobacter hormaechei ATCC 49162
Leclercia adecarboxylata ATCC 23216
Escherichia hermannii ATCC 33650
Klebsiella pneumoniae pneumoniae
Enterobacter mori LMG 25706
Citrobacter rodentium ICC168
Salmonella bongori N268
Cronobacter muytjensii ATCC 51329
Cronobacter condimenti 1330
Cronobacter sakazakii ES15
Cronobacter turicensis z3032
Cedecea davisae ATCC 33431
Shimwellia blattae DSM 4481
second seed
seed

A

All chimeras

E-value	sites
5.8e+000	6/9

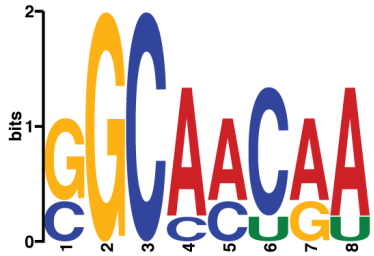

CLASH unique chimeras <4 reads

E-value	sites
5.8e+000	6/9

B

***glnA*-3'UTR**

MAST p-value: 8.7e-4

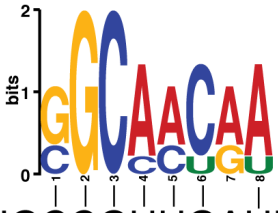

3'- UCCGGACGGUCUCUGUCCGCUUUUCAAAGGUGCCGUUGAUUUUGUG-5'

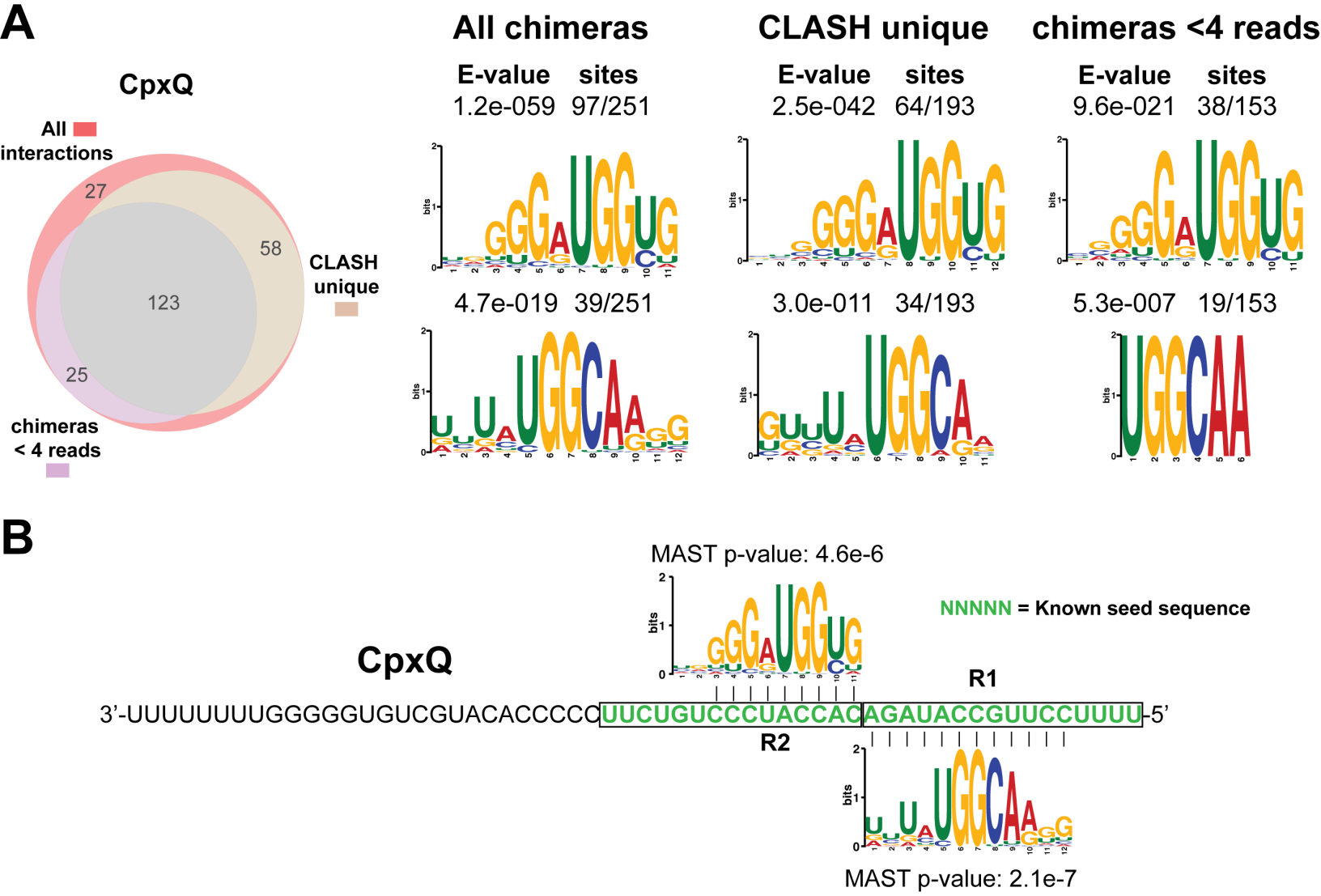
A
CpxQ
All interactions
27
58
123
25
CLASH unique
chimeras < 4 reads
All chimeras
E-value sites
1.2e-059 97/251
4.7e-019 39/251
CLASH unique
E-value sites
2.5e-042 64/193
3.0e-011 34/193
chimeras <4 reads
E-value sites
9.6e-021 38/153
5.3e-007 19/153
B
CpxQ
MAST p-value: 4.6e-6
NNNNN = Known seed sequence
R1
3'-UUUUUUUUGGGGGUGUCGUACACCCCCUUCUGUCCCUACCACAGAUACCGUUCCUUUU-5'
R2
MAST p-value: 2.1e-7

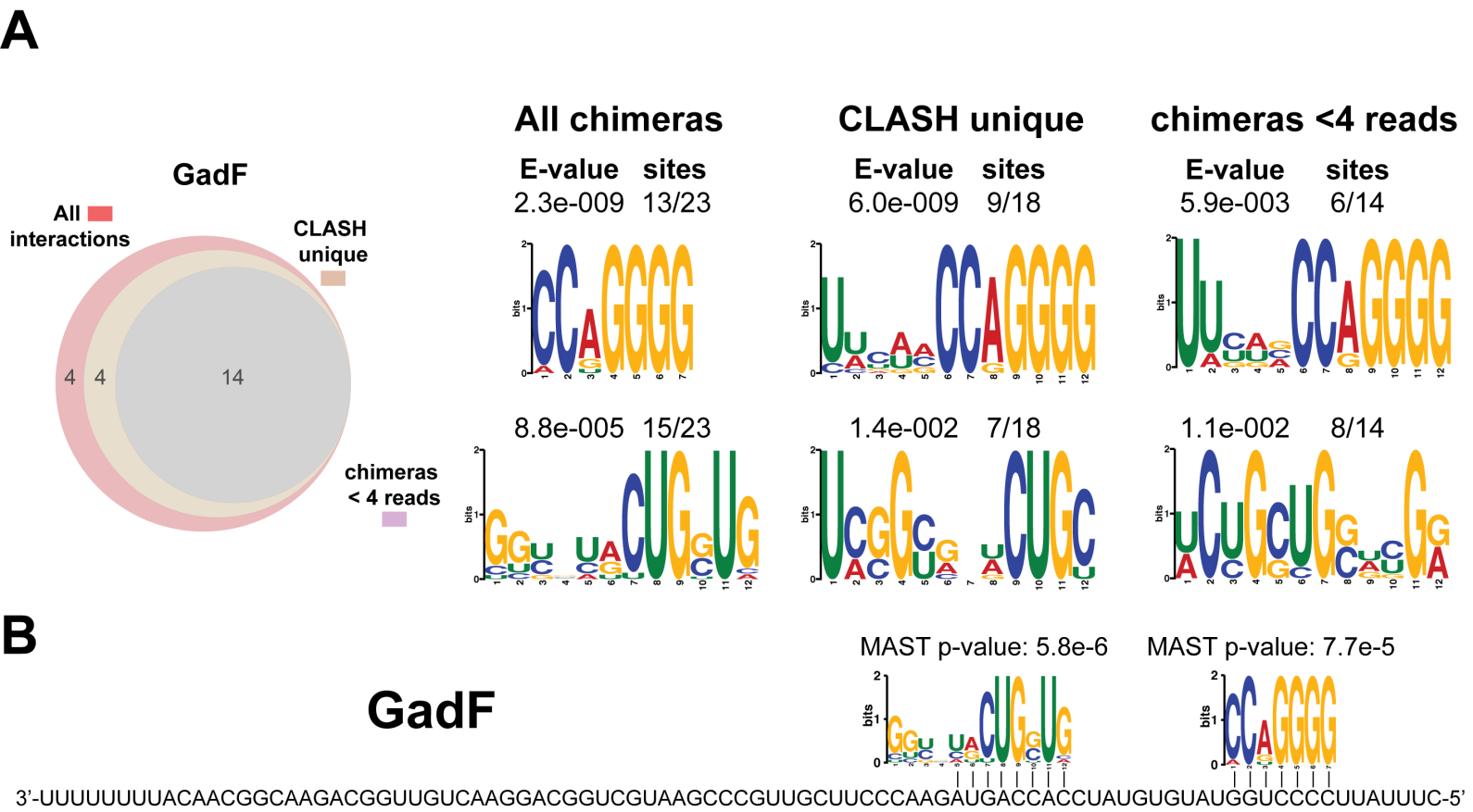
A
GadF
All interactions
CLASH unique
chimeras < 4 reads
4
4
14
All chimeras
E-value sites
2.3e-009 13/23
8.8e-005 15/23
CLASH unique
E-value sites
6.0e-009 9/18
1.4e-002 7/18
chimeras <4 reads
E-value sites
5.9e-003 6/14
1.1e-002 8/14
B
GadF
MAST p-value: 5.8e-6
MAST p-value: 7.7e-5
3'-UUUUUUUUACAACGGCAAGACGGUUGUCAAGGACGGUCGUAAGCCCGUUGCUUCCCAAGAUGACCACCUAUGUGUAUGGUCCCCUUAUUUC-5'

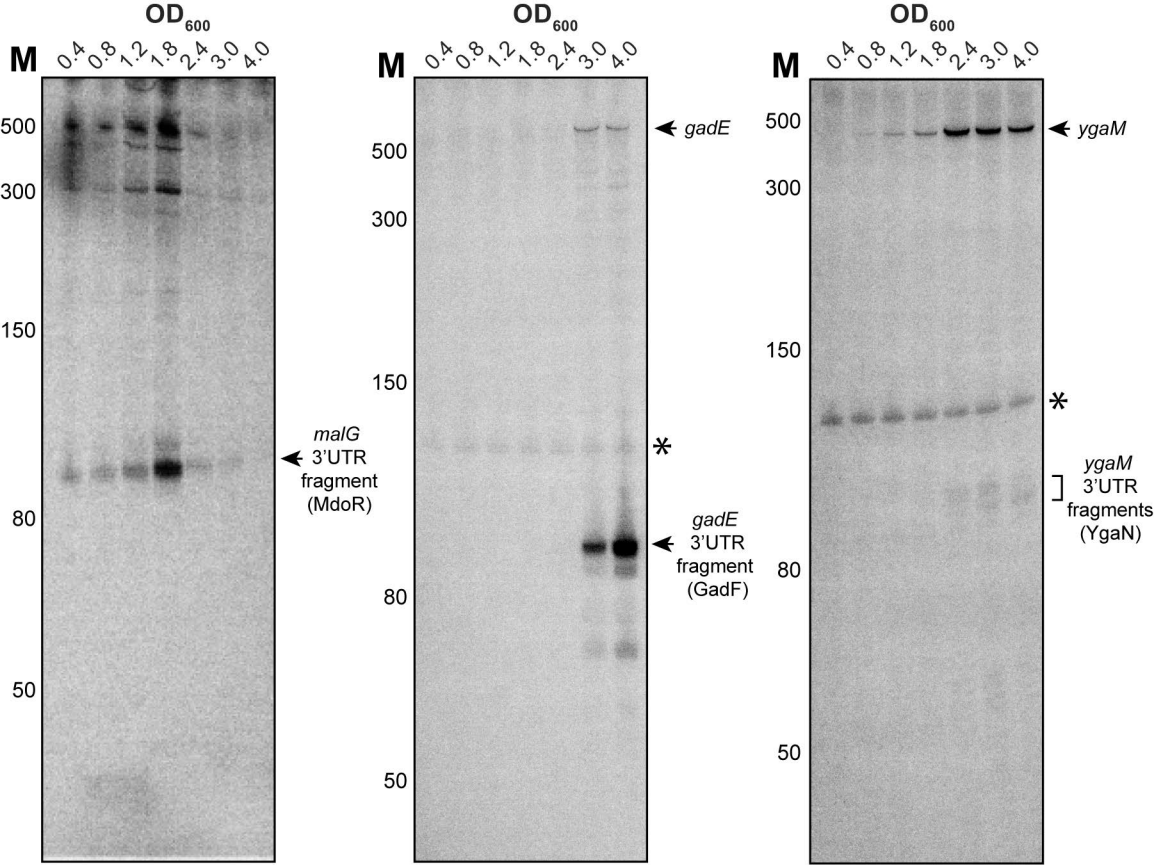
OD600
M
0.4
0.8
1.2
1.8
2.4
3.0
4.0
500
300
150
80
50
malG
3'UTR
fragment
(MdoR)
gadE
gadE
3'UTR
fragment
(GadF)
*
ygaM
ygaM
3'UTR
fragments
(YgaN)

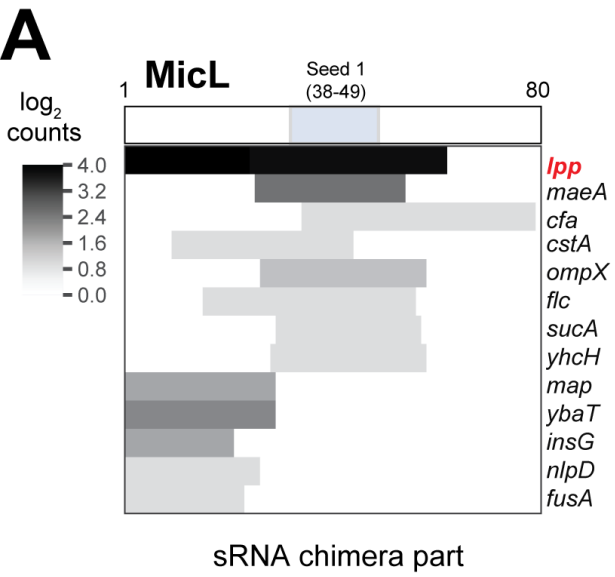
A
MicL
Seed 1
(38-49)
1
80
log2
counts
4.0
3.2
2.4
1.6
0.8
0.0
lpp
maeA
cfa
cstA
ompX
flc
sucA
yhcH
map
ybaT
insG
nlpD
fusA
sRNA chimera part

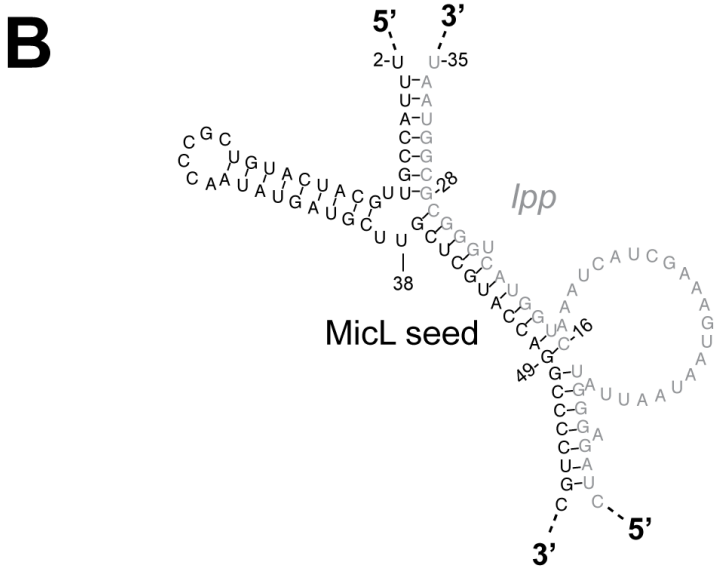
B
5'
3'
2-U
U-35
lpp
MicL seed
38
49
16
3'
5'

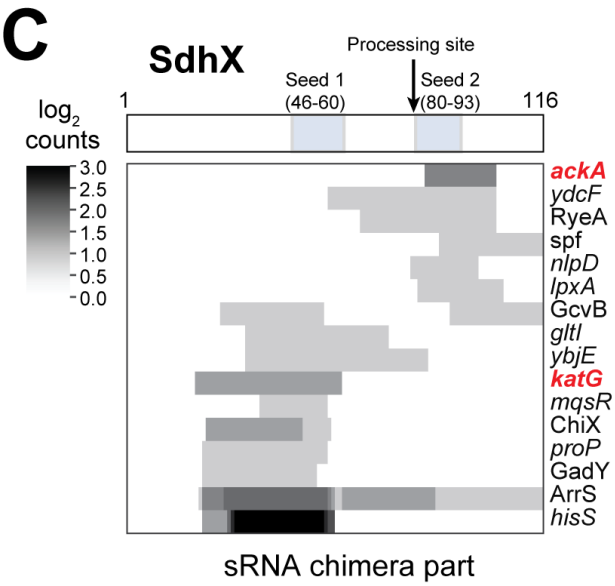
C
SdhX
Processing site
Seed 1
(46-60)
Seed 2
(80-93)
1
116
log2
counts
3.0
2.5
2.0
1.5
1.0
0.5
0.0
ackA
ydcF
RyeA
spf
nlpD
lpxA
GcvB
gltI
ybjE
katG
mqsR
ChiX
proP
GadY
ArrS
hisS
sRNA chimera part

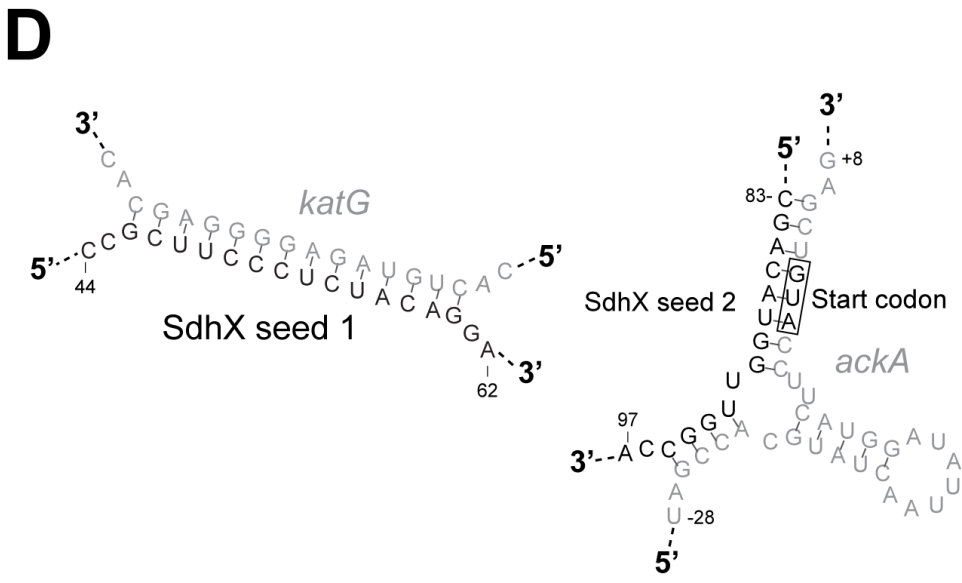
D
3'
5'
katG
5'
44
SdhX seed 1
62
3'
3'
5'
+8
83-
SdhX seed 2
Start codon
ackA
97
3'
-28
5'

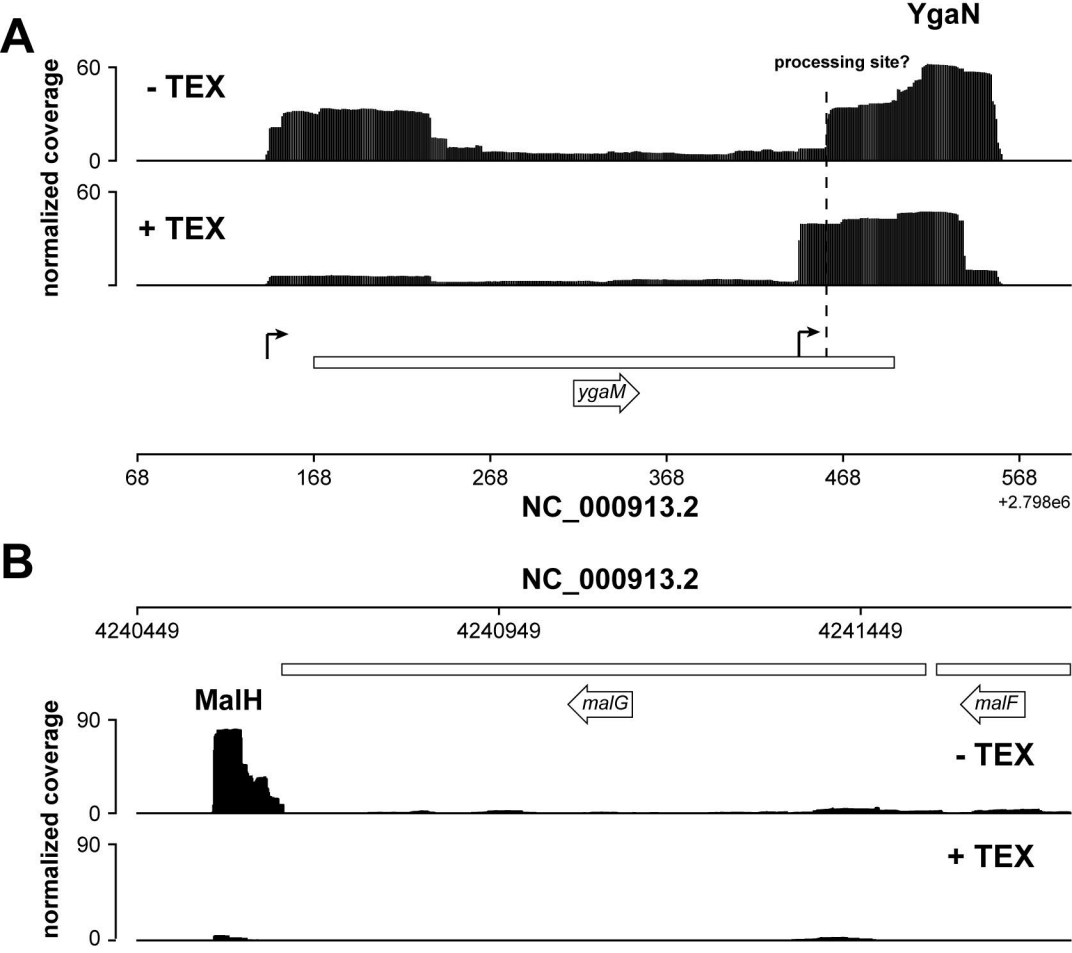
A
YgaN
processing site?
- TEX
+ TEX
normalized coverage
60
0
60
ygaM
68
168
268
368
468
568
+2.798e6
NC_000913.2
B
NC_000913.2
4240449
4240949
4241449
MalH
malG
malF
- TEX
+ TEX
normalized coverage
90
0
90
0